EXCITED-STATE DYNAMICS OF BIOLOGICAL MOLECULES IN SOLUTION: PHOTOINDUCED CHARGE TRANSFER IN OXIDATIVELY DAMAGED DNA AND DEACTIVATION OF VIOLACEIN IN VISCOUS SOLVENTS

by

Ashley Ann Beckstead

A dissertation submitted in partial fulfillment
of the requirements for the degree

of

Doctor of Philosophy

in

Chemistry

MONTANA STATE UNIVERSITY
Bozeman, Montana

May 2017

©COPYRIGHT

by

Ashley Ann Beckstead

2017

All Rights Reserved

DEDICATION

This work is dedicated to…

…my best friend and fiancé, Alex James Bergeron, for always believing in me and for never letting me deny my strengths,

…my late grandfather, Jerry D. Beckstead, for always praising me and thinking my work in science was “so cool”,

…and to my extraordinary family, for loving me unconditionally and for being the reason I come by my characteristics honestly.

ACKNOWLEDGEMENTS

I would like to humbly thank my advisor Professor Bern Kohler for all his guidance, patience, and understanding through the years. His fastidious work ethic and Zen-like nature have been a constant inspiration for me. I thank my committee members, Professors Rob Walker, Patrik R. Callis and Rufus Cone, for all their mentoring and assistance with my research. I also wish to thank my collaborators, Professors Roberto Improta, Cynthia J. Burrows, Spiridoula Matsika, Christine Foreman, Tom A. A. Oliver and their group members that contributed to our work. Thank you to the MSU Mass Spectrometry Facility, including Jonathan Hilmer and Jesse Thomas.

My mentor and friend Tom Zhang taught me everything he knows about ultrafast spectroscopy. Every long night I spent in the lab was made more enjoyable by his company. I cannot thank him enough for sharing his expertise and for always pushing me to work harder. I thank my fellow group members, past and current, Kimberly de La Harpe, Jinquan Chen, Charles Stark, David Skowron, Rebecca Danforth, Jordan Dood, Jacob Remington and Natasha Pettinger, for all their help with experiments, writing and presentations.

I could not have accomplished this goal without the wise encouragement of my father, Todd Beckstead, or the loving care of my mother, Sarah Beckstead, or the listening ears of my dear siblings and extended family and friends through the inevitable frustrations of academic research. Undoubtedly, I never would have finished this degree without the extensive love and support I received from my soon-to-be husband, Alex Bergeron. He alone knows what it really took for me to succeed and to become the person I am today. I will be forever grateful to him for staying by my side through it all.

TABLE OF CONTENTS

1. INTRODUCTION 1

1.1 References 10

2. EXPERIMENTAL METHODS 14

2.1 Transient Absorption Spectroscopy 14
2.1.1 Introduction 14
2.1.2 Single-Wavelength Transient Absorption 17
2.1.2.1 Lock-In Amplifier Phase Check 19
2.1.3 Time-Resolved IR Spectroscopy 21
2.2 Time-Correlated Single-Photon Counting 23
2.2.1 Measurements at 77 K 24
2.3 Sample Handling 25
2.3.1 Buffer Solution and DNA Sample Preparation 25
2.3.2 Violacein Pigment Purification 26
2.3.2.1 HPLC with ESI-MS Detection 26
2.3.2.2 Solid-Phase Extraction 27
2.3.3 Deep Eutectic Solvent Preparation 29
2.3.4 Flow Cell 32
2.4 Steady-State Spectroscopy 32
2.4.1 UV-Visible Absorption 32
2.4.2 FTIR Absorption 33
2.4.3 Fluorescence 33
2.4.4 Circular Dichroism 34
2.5 Data Processing 34
2.5.1 Single-Wavelength Kinetics 34
2.5.1.1 Solvated Electron Signal Subtraction Procedure 35
2.5.2 Broadband Spectra 35
2.5.3 TCSPC Emission Decay Spectra 36
2.6 References 37

3. THE NATURE OF LONG-LIVED TRANSIENT SIGNALS IN UV-EXCITED DNA 39

3.1 Introduction 39
3.2 Experimental 41
3.2.1 Computational Methods 43
3.3 Results 43
3.3.1 8-Oxo-7,8-Dihydro-2’-Deoxyguanosine Photophysics 43
3.3.2 Dinucleotide Containing 8-Oxo-7,8-Dihydroguanine and Adenine 48

TABLE OF CONTENTS CONTINUED

3.4 Discussion 53
3.4.1 Nucleoside Photophysics: Ultrafast S_1 Decay and Vibrational Cooling 53
3.4.2 Dinucleotide Photophysics: Photoinduced ET Dynamics 56
3.4.3 Connections to Long-Lived Transient Signals in Natural DNA 60
3.4.3.1 Photoinduced Charge Transfer in Single Strands 61
3.4.3.2 Proton Transfer and Proton-Coupled ET in Duplexes 63
3.5 Conclusion 65
3.6 References 66

4. PHOTOINDUCED ELECTRON TRANSFER IN OXIDATIVELY DAMAGED PYRIMIDINES 69

4.1 Introduction 69
4.2 Experimental 71
4.3 Results 73
4.3.1 5-Hydroxycytidine and 5-Hydroxyuridine Monomers 75
4.3.1.1 UV Pump / Visible Probe TA and Steady-State Emission 75
4.3.1.2 UV Pump / Mid-IR Probe TRIR 77
4.3.2 Dinucleotides Containing Adenine 80
4.3.2.1 Temperature-Dependent CD and UV Absorption Spectra 80
4.3.2.2 UV Pump / Mid-IR Probe TRIR 82
4.4 Discussion 87
4.4.1 Monomer Photophysics 87
4.4.2 Dinucleotide Photophysics 93
4.4.2.1 Evidence for Photoinduced Electron Transfer 95
4.4.2.2 Driving Force Calculations and Marcus Theory 100
4.5 Conclusion 101
4.6 References 102

5. EXCITED-STATE DEACTIVATION OF VIOLACEIN ISOLATED FROM ANTARCTIC BACTERIA 106

5.1 Introduction 106
5.2 Experimental 109
5.2.1 Pigment Production and Composition 109
5.2.2 Spectroscopic Methods 110
5.3 Results 111
5.3.1 Purification Results 111
5.3.1.1 Violacein vs. Deoxyviolacein Control Measurements 117
5.3.2 Emission and Ultrafast Spectroscopy in Methanol 119

TABLE OF CONTENTS CONTINUED

5.3.3 Emission and Ultrafast Spectroscopy in Viscous Solvents....124
5.3.4 Time-Resolved Emission in an Optical Glass at 77 K....130
5.4 Discussion....133
5.4.1 Violacein Excited-State Deactivation and Dynamics....134
5.4.2 Photostability and Comparison with Other Natural Pigments....142
5.5 Conclusion....144
5.6 References....145

6. CONCLUSION AND OUTLOOK....149

6.1 Summary....149
6.2 Future Directions....152
6.3 References....156

REFERENCES CITED....157

LIST OF TABLES

Table Page

3.1 Global Fit Parameters for d(OA) TRIR GSB Signals.....52

3.2 Fluorescence Data and S_1 Lifetimes of 8-Oxo-dGuo and GMP.....55

4.1 Absorption and Fluorescence Data and S_1 Lifetimes of 5-HC and 5-HU in pD 6 D_2O Phosphate Buffer Solution.....76

4.2 Fit Parameters for TRIR Spectra of 5-HC, 5-HU, and Dinucleotides.....89

5.1 Physical Properties of Solvents Used in Violacein Measurements.....124

5.2 TCSPC Fit Parameters of 310 nm Excited Violacein at 77 K.....131

5.3 Absorption and Emission Spectral Data and Fluorescence Quantum Yields of Violacein in Various Solvents.....133

5.4 Kinetic Fit Parameters of Violacein in Various Solvents.....135

LIST OF FIGURES

Figure Page

1.1 Chemical Structures and UV Absorption Spectra of Canonical Bases.....2

1.2 Absorption Spectra of Bases Compared to Solar Irradiation Spectra.....3

1.3 Transient Decays of AMP, GMP and Dinucleotide Containing A and G Showing Long-Lived Signal 4

1.4 Schematic of Proposed Deactivation in Single-Stranded DNA.....6

2.1 Schematic Showing General Principle of Chirped Pulse Amplification 15

2.2 Schematic of Femtosecond Pump-Probe Instrument Optical Layout.....16

2.3 Schematic Illustrating Method for Setting Phase of Lock-In Amplifier.....20

2.4 Schematic of TCSPC Instrument Optical Layout.....23

2.5 Schematic of SPE Procedure for Violacein Purification 28

2.6 Photographs Showing Efficient and Inefficient Pigment Loading on SPE Columns.....29

3.1 UV Absorption Spectra of 8-Oxo-dGuo and GMP 44

3.2 ESA Kinetics of 8-Oxo-dGuo.....45

3.3 TRIR Spectra and Single-Frequency Kinetics of 8-Oxo-dGuo 46

3.4 Chemical Structure and UV Absorption Spectrum of d(OA).....48

3.5 TRIR Spectra of d(OA) and O Plus A 49

3.6 Single-Frequency Kinetics of d(OA) and 8-Oxo-dGuo After 295 and 265 nm Excitation.....51

3.7 Steady-State Emission Spectra of 8-Oxo-dGuo and GMP 54

3.8 Calculated Vibrational Spectra of 8-Oxo-dGuo, Adenine, O Radical Cation and A Radical Anion 58

LIST OF FIGURES CONTINUED

Figure Page

3.9 Calculated and Experimental Difference Spectra of d(OA) 59

4.1 Chemical Structures and UV Absorption Spectra of 5-HC, 5-HU, and Dinucleotides Containing Adenine 73

4.2 ESA Kinetics and Steady-State Emission Spectra of 5-HC and 5-HU.....75

4.3 TRIR Spectra of 5-HC and 5-HU 77

4.4 Single-Frequency Kinetic Traces of 5-HC and 5-HU After 295 and 265 nm Excitation 78

4.5 Temperature-Dependent CD and Absorption Spectra of d(5-HCA) 81

4.6 Temperature-Dependent CD and Absorption Spectra of d(5-HUA) 82

4.7 TRIR Spectra of d(5-HCA) and d(5-HUA) 83

4.8 Single-Frequency Kinetic Traces of d(5-HCA) and d(5-HUA) Compared to 5-HC and 5-HU 86

4.9 Decay-Associated Difference Spectra of d(5-HCA) and d(5-HUA) Compared to 5-HC and 5-HU 95

4.10 TRIR Spectra of d(5-HCA) Compared to 5-HC Plus A 96

4.11 TRIR Spectra of d(5-HUA) Compared to 5-HU Plus A.....97

4.12 Transient IR Spectra of 5-HC and 5-HU Radical Cations.....99

5.1 Chemical Structures of Violacein and Deoxyviolacein 108

5.2 HPLC Chromatogram and Mass Spectrum of Pigment Extract 112

5.3 HPLC Chromatograms of Pigment Extract Before and After SPE 113

5.4 Mass Spectra of Pigment from Hyper-Producing and WT Strains.....115

LIST OF FIGURES CONTINUED

Figure Page

5.5 UV-Visible Absorption Spectra of Pigment Extract and Fractions Collected During SPE 116

5.6 Absorption Spectra and Decay Kinetics of Violacein and Violacein Plus Deoxyviolacein Mixture 118

5.7 UV-Visible Absorption and Steady-State Emission Spectra of Violacein in Methanol 120

5.8 Stimulated Emission and GSB Kinetics of Violacein in Methanol 121

5.9 UV Pump GSB Kinetics of Violacein in Methanol 122

5.10 UV-Visible Absorption Spectra of Violacein in Methanol Before and After Visible and UV TA Laser Irradiance 123

5.11 UV-Visible Absorption and Steady-State Emission Spectra of Violacein in Acetone, Ethylene Glycol, and Glycerol 125

5.12 Stimulated Emission and GSB Kinetics of Violacein in Acetone, Ethylene Glycol, and Glycerol 126

5.13 UV-Visible Absorption and Steady-State Emission Spectra of Violacein in GlyDES 127

5.14 Stimulated Emission and GSB Kinetics of Violacein in GlyDES 128

5.15 Time-Resolved Emission Decay and Spectra of Violacein at 77 K 130

5.16 Time-Integrated and Steady-State Emission Spectra of Violacein at 77 K 132

5.17 RICC2 Optimized Minimum S_0 and S_1 Geometries of Violacein 141

LIST OF ABBREVIATIONS

A: Adenine; 2’-deoxyadenosine
AMP: Adenosine 3’-Monophosphate
C: Cytosine
CD: Circular Dichroism
CI: Conical Intersection
CPD: Cyclobutane Pyrimidine Dimer
CT: Charge Transfer
DES: Deep Eutectic Solvent
E1: First Elution
E2: Second Elution
ECCD: Exciton-Coupled Circular Dichroism
ESA: Excited-State Absorption
ESI-MS: Electrospray Ionization Mass Spectrometry
ET: Electron Transfer
FAD: Flavin Adenine Dinucleotide
G: Guanine
GMP: Guanosine 5’-Monophosphate
GSB: Ground-State Bleach
5-HC: 5-Hydroxy-2’-Deoxycytidine
5-HI: 5-Hydroxyindole
5-HU: 5-Hydroxy-2’-Deoxyuridine
IRF: Instrument Response Function
M: Molecular Weight
MS: Mass Spectrometry
O: 8-Oxo-7,8-dihydro-2’-deoxyguanosine
OPA: Optical Parametric Amplifier
OX: Oxindole
PCET: Proton-Coupled Electron Transfer
2-PYR: 2-Pyrollidone
SPE: Solid-Phase Extraction
T: Thymine
TA: Transient Absorption
TCSPC: Time-Correlated Single-Photon Counting
TRES: Time-Resolved Emission Spectra
TRIR: Time-Resolved Infrared
U: Uracil
UIC: Ultrafast Internal Conversion
UV: Ultraviolet
VC: Vibrational Cooling
WT: Wild-Type

ABSTRACT

UV radiation from the sun is strongly absorbed by DNA, and the resulting electronic excited states can lead to the formation of mutagenic photoproducts. Decades of research have brought to light the excited-state dynamics of single RNA and DNA nucleobases, but questions remain about the nature of excited states accessed in DNA strands. In this thesis, I present ultrafast spectroscopic observations of photoinduced electron transfer from the oxidatively damaged bases, 8-oxo-7,8-dihydro-2'-deoxyguanosine, 5-hydroxy-2'-deoxycytidine and 5-hydroxy-2'-deoxyuridine, to adenine in three dinucleotides. The results reveal that charge transfer states are formed on a timescale faster than our instrumental resolution (<0.5 ps), and back electron transfer efficiently returns the excited-state population to the ground state on timescales from tens to hundreds of ps. In addition to recent spectroscopic observations of charge transfer state species in DNA by other groups, our results have augmented understanding of the long-lived transient signals observed in DNA strands. The observation of photoinduced electron transfer in these oxidatively damaged nucleobases also supports a recent proposal regarding the role of oxidative products in pre-RNA catalysis. I discuss these observations in the contexts of fundamental DNA excited-state dynamics and prebiotic chemical evolution. In this thesis, I also present the first ultrafast spectroscopic investigation of violacein, a pigment isolated from Antarctic bacteria. Despite claims for the photoprotective role of this pigment, there has never been a spectroscopic analysis of excited-state deactivation in violacein. Emission spectra, fluorescence quantum yields and excited-state lifetimes of violacein in various solvents were measured for the first time. Both the fluorescence quantum yield and excited-state lifetime of violacein increase in increasingly viscous solvents, suggesting a large-scale motion mediates excited-state deactivation. I compare these results to similar observations of viscosity-dependent excited-state decay rates in other molecules. I also consider the relevance of violacein's excited-state properties to the hypothesized sunscreening role of violacein. Overall, the studies presented in this dissertation illustrate how ultrafast spectroscopic techniques can be used to unravel complex biomolecular excited-state dynamics in solution.

CHAPTER ONE

INTRODUCTION

Photophysical processes are ubiquitous in biochemical systems and play central roles in the delicate balance between energy and life. From the earliest chemical mixtures on the prebiotic Earth to advanced modern biochemistry, the study of photophysical chemistry is relevant to many interdisciplinary fields of research. Photophysical processes begin the instant a photon of light is absorbed, and for decades the subsequent fundamental excited-state dynamics could only be presumed from evidence collected on familiar timescales.[1] Relatively recent improvements in the time resolution of spectroscopic instrumentation have facilitated observation of ultrafast excited-state phenomena in real-time and have shed light on molecular excited-state dynamics.[2-3] Many biological molecules have heterocyclic conjugated chemical structures that strongly absorb the visible and ultraviolet (UV) photons capable of promoting electrons to highly energetic excited states. For example, the nucleobases adenine (A), guanine (G), cytosine (C), thymine (T), and uracil (U) exhibit strong UV absorption (Figure 1.1). As light from the sun is a main source of energy for biochemistry, a detailed understanding of the excited-state dynamics of biomolecules can provide crucial insights into light-driven biochemical processes.

Research on the excited-state dynamics of nucleobases has far-reaching applications. We recently published a perspective on the relevance of nucleobase photophysical studies to the field of astrobiology.[4] During the Archean era (when life is predicted to have originated),[5] Earth's atmosphere lacked the ozone essential for filtering

out highly-energetic UVC (100 – 280 nm, wavelength designations shown by horizontal arrows in Figure 1.2) photons, which are energetic enough to break chemical bonds.[6-8] Figure 1.2 shows the solar irradiance spectrum at the Earth's surface in comparison with the spectrum above the atmosphere, which is a rough approximation of the solar irradiance experienced in the absence of ozone.[4] The additional UVC radiation incident on the prebiotic Earth would have limited the geological environments suitable for the formation of life, and would have imposed a selection pressure on prebiotic chemistry.

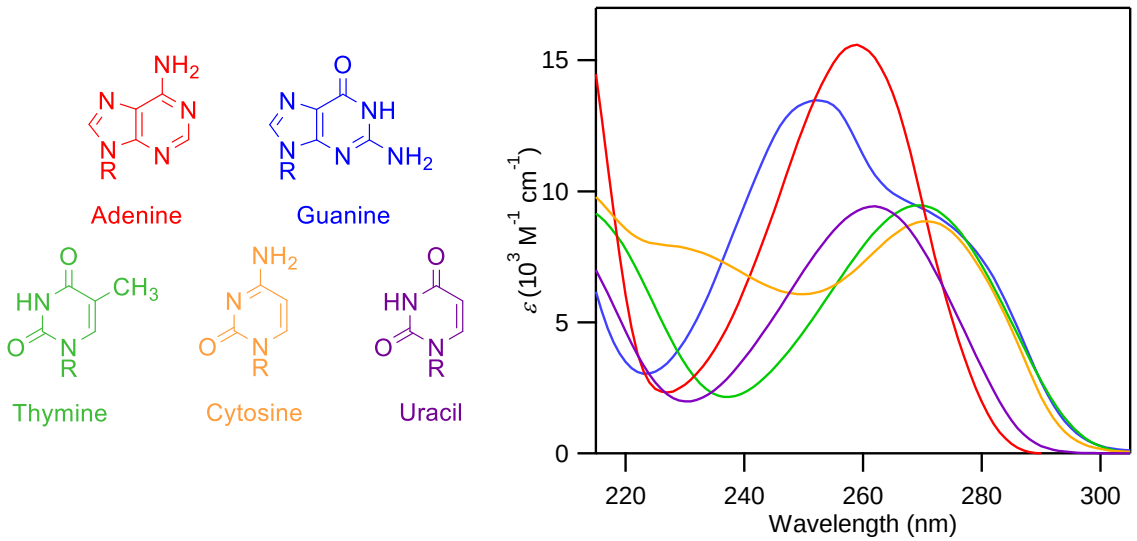


Figure 1.1. Structures of the canonical nucleobases (R = H) found in DNA (A, G, C, and T) and RNA (A, G, C, and U) shown next to their color-coded absorption spectra. Adapted from ref. 21.

As shown in Figure 1.2, the nucleobases that comprise modern RNA and DNA, known as the canonical bases A, G, C, T, and U, absorb precisely in the UVC region.[4] Excited-state dynamics investigations have revealed that the canonical bases have photophysical properties associated with intrinsic photostability, or UV hardiness, differentiating them from many molecularly similar alternative nucleobases. This finding

has led to the hypothesis that the inherent molecular photostability of the canonical bases may have contributed to their selection as life's genetic material in the early stages of chemical evolution.[9] Studying the excited-state dynamics of the nucleobases and other terrestrial biological molecules is thus important for identifying life and possible life-sustaining chemistries on exoplanets.[4]

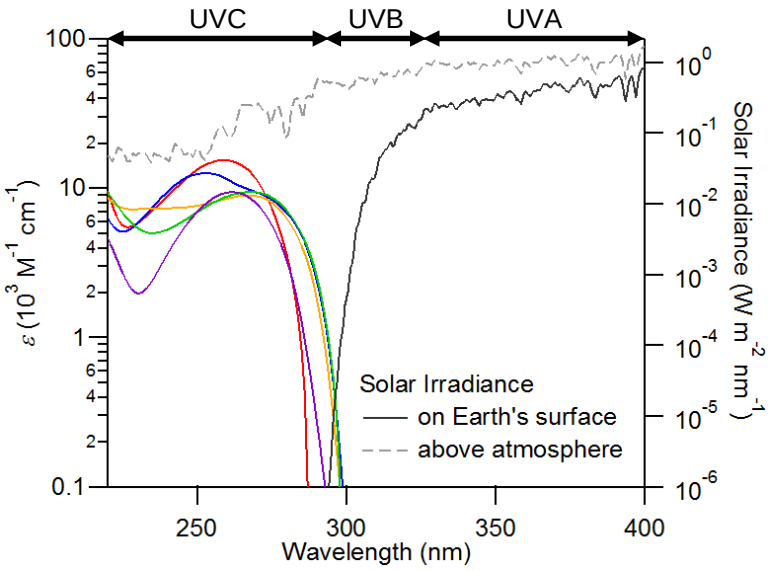


Figure 1.2. UV absorption spectra of the nucleobases color-coded according to Figure 1.1 (left vertical axis). Solar irradiance spectra above the atmosphere (dashed gray trace) and at the surface (black trace) of present-day Earth (right vertical axis), both obtained from data collected at NREL.[10] Note the logarithmic scale of the left and right axes. Adapted from ref 4.

Interest in nucleobase photophysics began with an inquiry into the molecular mechanisms responsible for photochemical damage of modern-day DNA and RNA. The harmful effects of UV radiation on organisms and its correlation with skin cancer have been known for centuries.[11] Skin cancer occurs at rates that exceed those for any other type of cancer even today.[12-13] DNA excited-state dynamics research is largely motivated by the

goal of understanding how UV-induced electronic excited states can lead to the formation of mutagenic DNA photolesions, such as cyclobutane pyrimidine dimers (CPDs).[14-15]

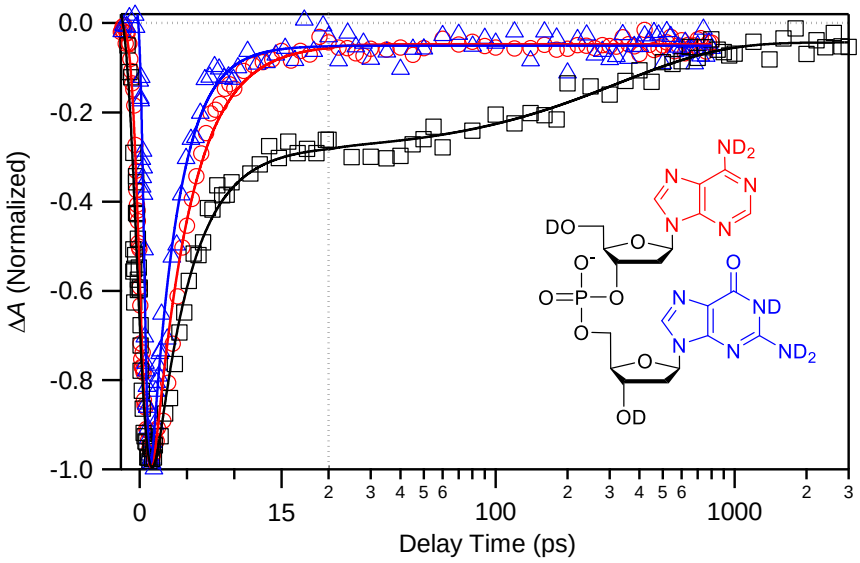


Figure 1.3. Transient signals of the 5'-monophosphate forms of adenosine (red circles) and guanosine (blue triangles) and the dinucleotide (black squares) composed of both bases (structure shown) recorded using UV-pump / broadband mid-IR probe wavelengths. The decay of the base-stacked dinucleotide contains an additional long-lived signal that is not present in the transient signals of the monomer bases. Note that all labile protons on the dinucleotide structure are replaced with deuterons due to mid-IR probing. Adapted from ref 4.

Femtosecond pump-probe transient absorption (TA) spectroscopy is commonly employed to monitor excited-state dynamics on ultrafast timescales. Early studies revealed the quantum yields for UV-induced photoproduct formation in DNA are less than 1%.[16-18] The first ultrafast spectroscopic measurements on the canonical bases in aqueous solution revealed that their UV-induced excited states deactivate non-radiatively on the hundreds of femtoseconds timescale.[19-20] Using ultrafast spectroscopic techniques, research over the last 20 years has achieved a detailed understanding of the excited-state dynamics of

monomer RNA and DNA bases.[1, 3, 21] This foundation was well established when I began my thesis work five years ago. However, the same level of comprehension had not been reached for excited-state processes operative in single- and double-stranded DNA.

In DNA strands, long-lived (tens to hundreds of ps) decay signals are observed in addition to shorter ps and sub-ps lifetimes (Figure 1.3). The shorter lifetimes are comparable to those of the corresponding monomer bases and are thus attributed to deactivation of unstacked bases (Figure 1.4). The long-lived signals have been more difficult to interpret.[22] Among disparate interpretations, the nature of the excited states responsible for these long-lived transient signals has been highly debated.[23-24] Our group hypothesized that the long-lived signals observed in single-stranded DNA reflect charge transfer (CT) excited states, which form when UV-induced excitation of two π-stacked bases in a DNA strand decays to an excimer or exciplex consisting of a radical ion contact pair (Figure 1.4).[25-26] Others maintain that the excited states involve delocalized neutral excitons spanning at least two bases in strands.[27-28] Despite significant experimental and theoretical work over the last decade, consensus in assigning the long-lived excited states in DNA single strands had not been fully reached at the beginning of this thesis work.

One of the main objectives of this thesis is to provide definitive spectroscopic evidence needed to determine the excited states responsible for long-lived transient signals observed in DNA strands. The studies presented in this dissertation resulted in the direct observation of radical ion species generated from photoinduced electron transfer (ET) between stacked nucleobases.[29] Using time-resolved IR (TRIR) TA spectroscopy, we collected ultrafast spectroscopic measurements on DNA dinucleotides containing

oxidatively damaged DNA bases, which were chosen based on their proposed ability to undergo photoinduced ET (see below).[30-31] Our observations of radical ion species suggests that ultrafast intrastrand ET is a principal decay channel in the dinucleotides studied and have added to the evidence supporting assignment of the long-lived excited states in single-stranded DNA to CT states.[29, 32-34]

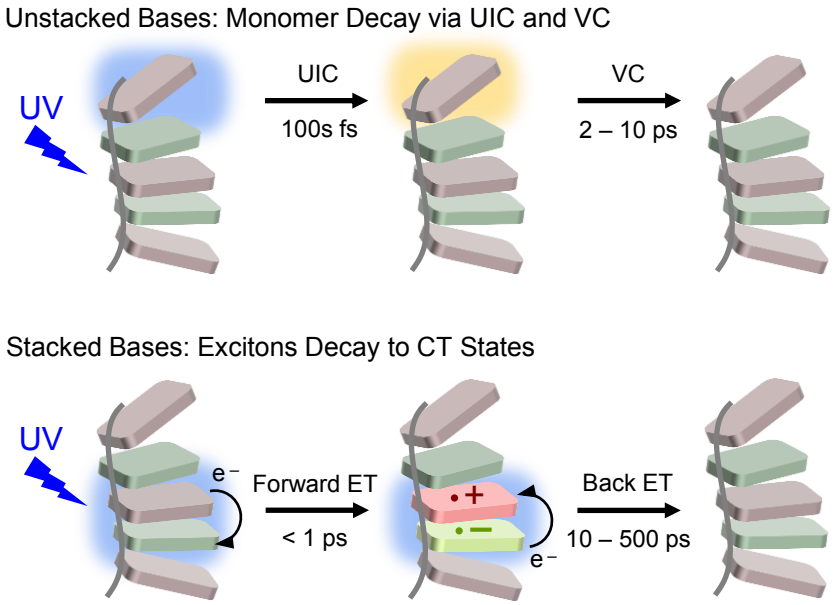


Figure 1.4. Proposed model for UV-induced excited-state deactivation in single-stranded DNA showing the distinct decay pathways of unstacked and stacked bases. Unstacked bases decay via monomeric pathways, i.e., ultrafast internal conversion (UIC) followed by vibrational cooling (VC). Stacked bases initially decay to a charge transfer state formed upon forward electron transfer (ET), and subsequent back ET on a lengthened timescale of tens to hundreds of picoseconds returns the population to the ground state.

In Chapter 3, I present and discuss our published work detecting CT species in a dinucleotide containing the oxidative product 8-oxo-7,8-dihydroguanine and A, along with the impact this and similar observations by others has had on the interpretation of excited-state dynamics in single- and double-stranded DNA.[32-33, 35-36] Disentangling the excited-

state dynamics of DNA is even more complex in double-stranded systems, where bases are both π-stacked and base-paired. Some studies have postulated that the interstrand base-pairing interaction drives DNA excited-state deactivation,[37] whereas there is also evidence suggesting intrastrand base-stacking has the greater influence on the excited-state dynamics.[25] Through the course of my thesis research, we also used TRIR to illuminate the deactivation pathways in DNA duplexes. I conclude Chapter 3 with a summary of the main findings from these DNA duplex studies.[35-36, 38]

Interestingly, the oxidatively damaged bases mentioned above are prebiotically relevant.[31] The canonical bases are susceptible to oxidative damage by endogenous or exogenous oxidizing agents.[39] Upon oxidative damage, the weakly redox-active canonical bases become better electron donors. The one-electron oxidative products of guanine, cytosine, and uracil, 8-oxo-7,8-dihydroguanine, 5-hydroxycytosine, and 5-hydroxyuracil, respectively, are proposed to be flavin precursors based on their enhanced redox properties[31] and their ability to repair CPD photoproducts upon irradiation in a hypothesized photoinduced ET mechanism.[30, 40] In Chapters 3 and 4, I present ultrafast spectroscopic studies of these oxidatively damaged bases, as monomer nucleosides and as dinucleotides with adenine. The results reveal that all three oxidative products undergo photoinduced ET to base-stacked adenine, which supports the proposed mechanism of CPD repair. Furthermore, these results reinforce the hypothesis that oxidatively damaged bases may have functioned as primitive redox cofactors before the advent of modern enzymes.[31, 40]

Another project presented in this dissertation is the first ultrafast spectroscopic investigation of the excited-state properties of the pigment violacein. In collaboration with the Christine Foreman group from Montana State University's Department of Biofilm Engineering, we conducted steady-state and time-resolved measurements of the excited-state deactivation of violacein produced by *Janthinobacterium* sp. CG23_2, an Antarctic bacterial species isolated from supraglacial stream water.[41] Violacein absorbs across the UV and visible regions, giving rise to its deep purple color. Among the many known beneficial properties of violacein,[42] it has been proposed to provide photoprotection for the bacteria that produce it.[43-45] Under UV irradiation, violacein-pigmented bacteria showed increased survival rates compared to non-pigmented bacteria, supporting the putative sunscreening role of violacein.[43-45]

Molecular sunscreens are characterized by high rates of non-radiative excited-state decay.[46] The efficient and ultrafast non-radiative decay observed in DNA nucleobases has led to them being described as natural sunscreens.[4, 20] Presented in Chapter 5, we measured an ultralow fluorescence quantum yield and a ps excited-state lifetime for violacein in methanol. Interestingly, the fluorescence quantum yield and the excited-state lifetime of violacein increase in increasingly viscous solvents and at cryogenic temperature. I discuss these results as they relate to the mechanism of deactivation and the proposed sunscreening ability of violacein. To the best of our knowledge, this is the first ultrafast spectroscopic investigation of violacein's excited-state dynamics in various solvents.

This dissertation is organized as follows. Ultrafast spectroscopic techniques and experimental methods are detailed in Chapter 2. In Chapter 3, I summarize our published

work on the photophysics of the 8-oxo-7,8-dihydroguanine monomer nucleoside and its dinucleotide with adenine. My aim in this chapter is to highlight how our observation of photoinduced ET in a model dinucleotide has aided in resolving the nature of long-lived excited states in DNA strands. In Chapter 4, I present and discuss recent observations of photoinduced ET in two more dinucleotides containing the oxidatively damaged pyrimidines, 5-hydroxycytidine and 5-hydroxyuridine. The photophysics of these 5-hydroxypyrimidine monomer nucleosides have not been evaluated previously, and their excited-state dynamics in aqueous solution are also presented in Chapter 4. The excited-state deactivation dynamics of violacein isolated from Antarctic bacteria are presented in Chapter 5. The photophysics of this bisindolic pigment were investigated in acetone, methanol, ethylene glycol, glycerol, a choline-chloride-based deep eutectic solvent, and in a 5:1 volume ratio ethanol / methanol optical glass at 77 K. Lastly, in Chapter 6, I provide a summary of the key findings presented in this dissertation and offer suggestions for future research directions.

1.1 References

1. Chen, J.; Zhang, Y.; Kohler, B., Excited States in DNA Strands Investigated by Ultrafast Laser Spectroscopy. In *Photoinduced Phenomena in Nucleic Acids II: DNA Fragments and Phenomenological Aspects*; Barbatti, M.; Borin, A. C., Ullrich, S., Eds.; Springer International Publishing Switzerland: New York, **2015**, *356*, pp. 39-87.

2. Berera, R.; van Grondelle, R.; Kennis, J. T. M., Ultrafast Transient Absorption Spectroscopy: Principles and Application to Photosynthetic Systems. *Photosynth. Res.* **2009**, *101*, 105-118.

3. Kohler, B., Excited States of Single-Stranded DNA Revealed by Femtosecond Transient Absorption Spectroscopy. In *Ultrafast Dynamics at the Nanoscale: Biomolecules and Supramolecular Assemblies*; Burghardt, I., Haacke, S., Eds. Pan Stanford Publishing Pte. Ltd.: Singapore, **2017**, pp. 1-31.

4. Beckstead, A. A.; Zhang, Y. Y.; de Vries, M. S.; Kohler, B., Life in the Light: Nucleic Acid Photoproperties as a Legacy of Chemical Evolution. *Phys. Chem. Chem. Phys.* **2016**, *18*, 24228-24238.

5. Dodd, M. S.; Papineau, D.; Grenne, T.; Slack, J. F.; Rittner, M.; Pirajno, F.; O'Neil, J.; Little, C. T. S., Evidence for Early Life in Earth's Oldest Hydrothermal Vent Precipitates. *Nature* **2017**, *543*, 60-64.

6. Canuto, V. M.; Levine, J. S.; Augustsson, T. R.; Imhoff, C. L., Oxygen and Ozone in the Early Earth's Atmosphere. *Precambrian Res.* **1983**, *20*, 109-120.

7. Bekker, A.; Holland, H. D.; Wang, P. L.; Rumble, D.; Stein, H. J.; Hannah, J. L.; Coetzee, L. L.; Beukes, N. J., Dating the Rise of Atmospheric Oxygen. *Nature* **2004**, *427*, 117-120.

8. Cockell, C. S.; Raven, J. A., Ozone and Life on the Archaean Earth. *Philos. Trans. R. Soc. London, Ser. A* **2007**, *365*, 1889-1901.

9. Serrano-Andrés, L.; Merchán, M., Are the Five Natural DNA/RNA Base Monomers a Good Choice from Natural Selection? A Photochemical Perspective. *J. Photochem. Photobiol., C* **2009**, *10*, 21-32.

10. American Society for Testing and Materials Standardized Solar Irradiance Spectra. http://rredc.nrel.gov/solar/spectra (Accessed July 2006).

11. Barbatti, M.; Borin, A. C.; Ullrich, S., Photoinduced Processes in Nucleic Acids. In *Photoinduced Phenomena in Nucleic Acids I: Nucleobases in the Gas Phase and in Solvents*, Barbatti, M., Borin, A. C., Ullrich, S., Eds.; Springer International Publishing Switzerland: New York, **2015**, *355*, pp. 1-32.

12. de Gruijl, F. R., Skin Cancer and Solar UV Radiation. *Eur. J. Cancer* **1999**, *35*, 2003-9.

13. U.S. Department of Health and Human Services. The Surgeon General's Call to Action to Action to Prevent Skin Cancer. Washington, DC: U.S. Department of Health and Human Services, Office of the Surgeon General; 2014.

14. Schreier, W. J.; Gilch, P.; Zinth, W., Early Events of DNA Photodamage. *Annu. Rev. Phys. Chem.* **2015**, *66*, 497-519.

15. Pfeifer, G. P.; You, Y.-H.; Besaratinia, A., Mutations Induced by Ultraviolet Light. *Mutation Research* **2005**, *571*, 19-31.

16. Cadet, J.; Vigny, P., The Photochemistry of Nucleic Acids. In *Bioorganic Photochemistry*, Morrison, H., Ed.; Wiley: New York, **1990**, *1*, pp. 1-272.

17. Lemaire, D. G. E.; Ruzsicska, B. P., Quantum Yields and Secondary Photoreactions of the Photoproducts of dTpdT, dTpdC and dTpdU. *Photochem. Photobiol.* **1993**, *57*, 755-69.

18. Görner, H., Photochemistry of DNA and Related Biomolecules - Quantum Yields and Consequences of Photoionization. *J. Photochem. Photobiol., B* **1994**, *26*, 117-139.

19. Pecourt, J.-M. L.; Peon, J.; Kohler, B., Ultrafast Internal Conversion of Electronically Excited RNA and DNA Nucleosides in Water. *J. Am. Chem. Soc.* **2000**, *122*, 9348-9349.

20. Pecourt, J.-M. L.; Peon, J.; Kohler, B., DNA Excited-State Dynamics: Ultrafast Internal Conversion and Vibrational Cooling in a Series of Nucleosides. *J. Am. Chem. Soc.* **2001**, *123*, 10370-10378..

21. Middleton, C. T.; de La Harpe, K.; Su, C.; Law, Y. K.; Crespo-Hernández, C. E.; Kohler, B., DNA Excited-State Dynamics: From Single Bases to the Double Helix. *Annu. Rev. Phys. Chem.* **2009**, *60*, 217-239.

22. Kohler, B., Nonradiative Decay Mechanisms in DNA Model Systems. *J. Phys. Chem. Lett.* **2010**, *1*, 2047-2053.

23. Markovitsi, D.; Talbot, F.; Gustavsson, T.; Onidas, D.; Lazzarotto, E.; Marguet, S., Molecular Spectroscopy: Complexity of Excited-State Dynamics in DNA. *Nature* **2006**, *441*, E7.

24. Crespo-Hernández, C. E.; Cohen, B.; Kohler, B., Molecular Spectroscopy: Complexity of Excited-State Dynamics in DNA (Reply). *Nature* **2006**, *441*, E8.

25. Crespo-Hernández, C. E.; Cohen, B.; Kohler, B., Base Stacking Controls Excited-State Dynamics in A·T DNA. *Nature* **2005**, *436*, 1141-1144.

26. Su, C.; Middleton, C. T.; Kohler, B., Base-Stacking Disorder and Excited-State Dynamics in Single-Stranded Adenine Homo-oligonucleotides. *J. Phys. Chem. B* **2012**, *116*, 10266-10274.

27. Buchvarov, I.; Wang, Q.; Raytchev, M.; Trifonov, A.; Fiebig, T., Electronic Energy Delocalization and Dissipation in Single- and Double-Stranded DNA. *Proc. Natl. Acad. Sci. USA* **2007**, *104*, 4794-4797.

28. Emanuele, E.; Markovitsi, D.; Millie, P.; Zakrzewska, K., UV Spectra and Excitation Delocalization in DNA: Influence of the Spectral Width. *ChemPhysChem* **2005**, *6*, 1387-1393.

29. Zhang, Y.; Dood, J.; Beckstead, A. A.; Li, X.-B.; Nguyen, K. V.; Burrows, C. J.; Improta, R.; Kohler, B., Efficient UV-Induced Charge Separation and Recombination in an 8-Oxoguanine-Containing Dinucleotide. *Proc. Natl. Acad. Sci. USA* **2014**, *111*, 11612-11617.

30. Nguyen, K. V.; Burrows, C. J., A Prebiotic Role for 8-Oxoguanosine as a Flavin Mimic in Pyrimidine Dimer Photorepair. *J. Am. Chem. Soc.* **2011**, *133*, 14586-14589.

31. Nguyen, K. V.; Burrows, C. J., Whence Flavins? Redox-Active Ribonucleotides Link Metabolism and Genome Repair to the RNA World. *Acc. Chem. Res.* **2012**, *45*, 2151-2159..

32. Doorley, G. W.; Wojdyla, M.; Watson, G. W.; Towrie, M.; Parker, A. W.; Kelly, J. M.; Quinn, S. J., Tracking DNA Excited States by Picosecond-Time-Resolved Infrared Spectroscopy: Signature Band for a Charge-Transfer Excited State in Stacked Adenine-Thymine Systems. *J. Phys. Chem. Lett.* **2013**, *4*, 2739-2744.

33. Bucher, D. B.; Pilles, B. M.; Carell, T.; Zinth, W., Charge Separation and Charge Delocalization Identified in Long-Living States of Photoexcited DNA. *Proc. Natl. Acad. Sci. USA* **2014**, *111*, 4369-4374.

34. Pilles, B. M.; Bucher, D. B.; Liu, L.; Gilch, P.; Zinth, W.; Schreier, W. J., Identification of Charge Separated States in Thymine Single Strands. *Chem. Commun.* **2014**, *50*, 15623-15626.

35. Zhang, Y.; de La Harpe, K.; Beckstead, A. A.; Improta, R.; Kohler, B., UV-Induced Proton Transfer between DNA Strands. *J. Am. Chem. Soc.* **2015**, *137*, 7059-7062.

36. Zhang, Y.; de La Harpe, K.; Beckstead, A. A.; Martinez-Fernandez, L.; Improta, R.; Kohler, B., Excited-State Dynamics of DNA Duplexes with Different H-Bonding Motifs. *J. Phys. Chem. Lett.* **2016**, *7*, 950-954.

37. Bucher, D. B.; Schlueter, A.; Carell, T.; Zinth, W., Watson-Crick Base Pairing Controls Excited-State Decay in Natural DNA. *Angew. Chem. Int. Ed.* **2014**, *53*, 11366-11369.

38. Zhang, Y.; Li, X.-B.; Fleming, A. M.; Dood, J.; Beckstead, A. A.; Orendt, A. M.; Burrows, C. J.; Kohler, B., UV-Induced Proton-Coupled Electron Transfer in Cyclic DNA Miniduplexes. *J. Am. Chem. Soc.* **2016**, *138*, 7395-7401.

39. Burrows, C. J.; Muller, J. G., Oxidative Nucleobase Modifications Leading to Strand Scission. *Chem. Rev.* **1998**, *98*, 1109-1151.

40. Nguyen, K. V.; Burrows, C. J., Photorepair of Cyclobutane Pyrimidine Dimers by 8-Oxopurine Nucleosides. *J. Phys. Org. Chem.* **2012**, *25*, 574-577.

41. Smith, H. J.; Foreman, C. M.; Akiyama, T.; Franklin, M. J.; Devitt, N. P.; Ramaraj, T., Genome Sequence of Janthinobacterium sp. CG23_2, a Violacein-Producing Isolate from an Antarctic Supraglacial Stream. *Genome Announcements* **2016**, *4*, 1-2.

42. Choi, S. Y.; Yoon, K. H.; Lee, J. I.; Mitchell, R. J., Violacein: Properties and Production of a Versatile Bacterial Pigment. *Biomed Research International* **2015**, article no. 465056.

43. Jiang, P.-X.; Wang, H.-S.; Xiao, S.; Fang, M.-Y.; Zhang, R.-P.; He, S.-Y.; Lou, K.; Xing, X.-H., Pathway Redesign for Deoxyviolacein Biosynthesis in Citrobacter Freundii and Characterization of This Pigment. *Appl. Microbiol. Biotechnol.* **2012**, *94*, 1521-1532.

44. Mojib, N.; Farhoomand, A.; Andersen, D. T.; Bej, A. K., UV and Cold Tolerance of a Pigment-Producing Antarctic Janthinobacterium sp Ant5-2. *Extremophiles* **2013**, *17*, 367-378.

45. Suryawanshi, R. K.; Patil, C. D.; Borase, H. P.; Narkhede, C. P.; Stevenson, A.; Hallsworth, J. E.; Patil, S. V., Towards an Understanding of Bacterial Metabolites Prodigiosin and Violacein and Their Potential for Use in Commercial Sunscreens. *International Journal of Cosmetic Science* **2015**, *37*, 98-107.

46. Pickett, J. E.; Moore, J. E., Photodegradation of UV Screeners. *Polym. Degrad. Stab.* **1993**, *42*, 231-244.

CHAPTER TWO

EXPERIMENTAL METHODS

2.1 Transient Absorption Spectroscopy

2.1.1 Introduction

Femtosecond pump-probe TA spectroscopy is well-suited for studying photophysical processes of biomolecules in solution because it enables one to directly monitor ultrafast (sub-picosecond) excited-state transitions, including those that involve non-emissive states.[2] At the heart of the femtosecond pump-probe TA technique is the ultrafast pulse-generating laser. Obtaining laser pulses that are both ultrafast and energetic enough for studying electronic transitions is not trivial. The development of the chirped-pulse amplification (CPA) technique has greatly increased spectroscopic time resolution, which is determined by the duration of the laser pulse. In this section, the general theory behind CPA and the femtosecond pump-probe technique is briefly described.

CPA is responsible for generating the femtosecond pulses used in TA and works essentially as its name describes. An initial weak pulse with short duration is stretched, or *chirped*, which decreases its peak power. The chirped *pulse* is then amplified to increase its peak power, and after *amplification* the pulse is recompressed to almost its original temporal width.[47] The basic principle behind CPA is shown in Figure 2.1. In practice, pulse shaping is achieved by diffraction gratings, which delay certain wavelengths with respect to others, thereby slowing their relative arrival time to a given point in space and effectively broadening the pulse temporally. After amplifying the energy of the pulse with a pump

laser, a second, but oppositely acting, diffraction grating is used to compress the amplified-pulse duration. The result is a laser pulse that has both high energy, which is necessary to promote excited-state transitions in molecules of interest, and ultrashort temporal resolution, which is necessary to observe ultrafast excited-state processes as they are occurring.

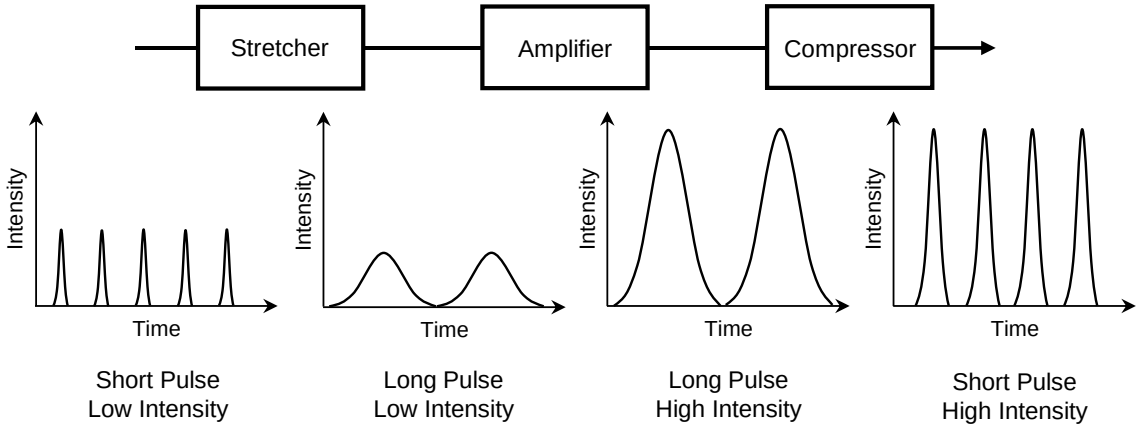


Figure 2.1. Schematic illustrating the general principle of the chirped-pulse amplification technique used to generate the ultrashort, high-energy pulses used in femtosecond pump-probe spectroscopy.

In femtosecond pump-probe spectroscopy, an initial UV or visible pulse (pump) promotes a portion of the ground state population to an excited state. Over time, the excited-state population decays, which is monitored by observing changes in the transmission (or absorption) of a second pulse (probe). The relative arrival time between the pump and probe pulses, or delay time, is determined by the difference of the two travelling path lengths, which is controlled using an optical delay stage (Figure 2.2). Throughout this thesis, TA data is plotted as the change in absorption of the probe versus the delay time. Exponential functions are used to fit the resulting kinetics, and produce

time components that can be attributed to excited-state lifetimes or other processes that occur on the excited state.

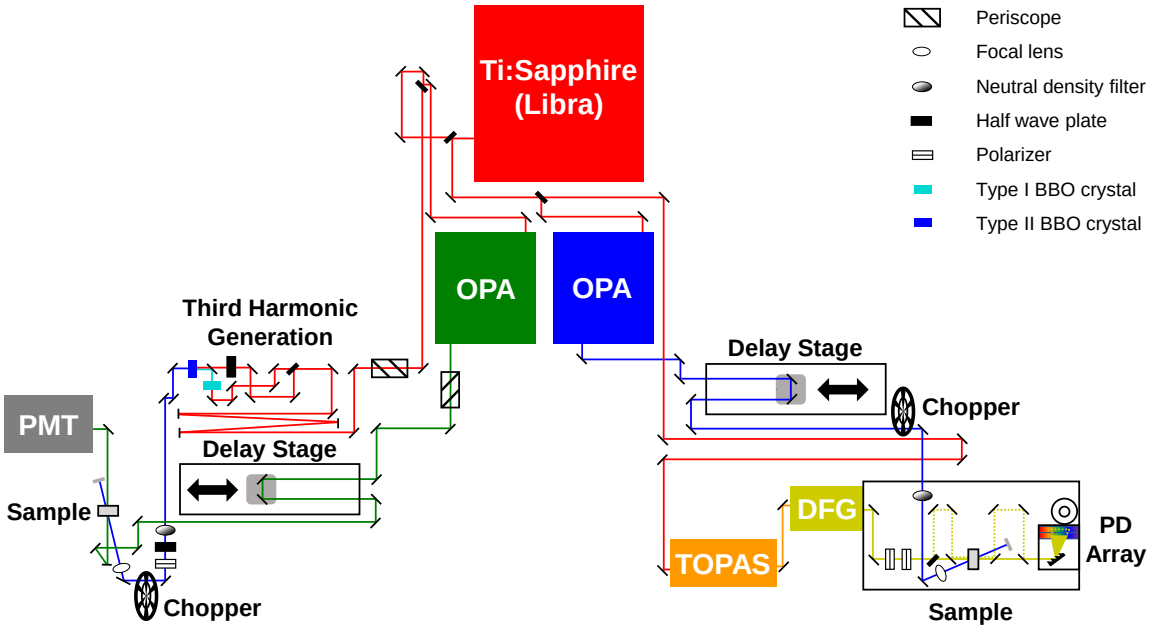


Figure 2.2. Optical layout of the femtosecond pump-probe techniques used, with UV pump (third harmonic generation) / visible probe (green OPA) TA set-up shown on the left and the UV pump (blue OPA) / broadband mid-IR probe (DFG) TRIR set-up shown on the right. The 800 nm fundamental (red beam) is produced in the Ti:sapphire oscillator (Libra).

Pump wavelengths are selected based on the ground-state electronic absorption spectrum of the molecule of interest. For instance, a 265 nm pump beam excites the canonical nucleobases to their first $\pi\pi^*$ excited state. Different probe wavelengths can be used to interrogate different excited-state events to provide a more detailed understanding of the excited-state dynamics. Using nucleobases as an example again, a 250 nm probe

beam monitors repopulation of the ground state, known as ground-state bleaching (GSB), whereas a 570 nm probe beam captures excited-state absorption (ESA).

UV and visible wavelengths probe electronic transitions. However, in solution electronic transitions result in bands that are broad and often overlapping. Consequently, spectra obtained from UV/visible probing can be difficult or ambiguous to interpret. In broadband TRIR spectroscopy, mid-IR probe beams are used to monitor vibrational transitions, which produce narrower spectral bands that can be easier to interpret than electronic bands.[48] Another advantage of TRIR is that mid-IR beams are spectrally broad (($\Delta t \Delta \nu = 0.44$) for Gaussian-shaped pulses), spanning about 200 cm^{-1} in our instrument. As a result, a single mid-IR probe beam provides a range of spectral data and can measure GSB and ESA kinetics simultaneously.

Both TA and TRIR spectroscopies were utilized in the research presented in this dissertation. In our lab, ultrashort pulses were generated using CPA in a 1 kHz titanium sapphire (Ti:Sapphire) regenerative amplifier (Libra HE, Coherent), which produced 3.5 W of 800 nm fundamental laser pulses with 80 fs duration. The optical layout is shown in Figure 2.2. One side of the laboratory was set up for single-wavelength UV/visible TA spectroscopy, and the other side was set up for broadband TRIR spectroscopy. In the remainder of this section, the experimental methods pertaining to ultrafast spectroscopic measurements are given.

2.1.2. Single-Wavelength Transient Absorption

UV and visible beams were generally produced using a white-light-seeded, two-stage optical parametric amplifier (OPA, OPerA Solo, Coherent), which was pumped by

approximately 1 W of the 800 nm fundamental. The UV pump beam centered at 266 nm was produced by third harmonic generation of about 20% of the 800 nm fundamental. First, a type I BBO crystal was used to produced 400 nm by doubling the 800 nm fundamental. Next, a type II BBO was used for sum frequency generation of the 400 and 800 nm beams to produce the 266 nm laser beam (Figure 2.2).

The probe beam was delayed with respect to the pump beam in all TA experiments described in this dissertation. A computer-controlled motorized translation state (Newport Inc.) was used to control the optical path length of the probe, giving ~4 ns of total delay time at ~8 fs resolution. A mechanical optical chopper (New Focus) operating at 333 Hz let through every third pump pulse. The pump beam was attenuated to about 0.3 mW using a neutral density filter, and focused to a defined spot size, ranging from ~300 – 600 μm. The specific values are given in the experimental sections in each of the following chapters. In all experiments, the relative linear polarizations of the pump and probe beams were set to the magic angle (54.7˚) to eliminate signal contribution from molecular reorientation.

The pump and probe beams were spatially and temporally overlapped at the sample, which was recirculated through a flow cell (Harrick), unless otherwise indicated. Previously in the Kohler group, it was determined that flowing the irradiated samples decreased the amount of photodegradation or photodamage occurrence in the samples.[21, 49] In all TA experiments, steady-state UV-visible absorption spectra measurements of the sample were taken before and after laser exposure to monitor photodegradation and determine if photoproducts had formed through the course of the experiment.

After the sample, the pump beam was blocked and the probe beam was guided into a double-grating monochromator equipped with a photomultiplier tube (PMT). The small change in the probe signal in the presence of the pump was detected by a lock-in amplifier (Stanford Research Systems Inc.) referenced to the modulation frequency of the optical chopper, and recorded by our LabVIEW-based data collection program. TA signals were recorded as the change in absorbance (ΔA) calculated from the detected intensity (I) of the probe with the pump on and off using the equation

$$\Delta A = \log\left(\frac{I_{\text{pump off}}}{I_{\text{pump on}}}\right) \tag{2.1}$$

According to this equation, when $I_{\text{pump off}} < I_{\text{pump on}}$, $\Delta A < 0$, and the resulting transient signal is negative. Signals are positive in the opposite case.

2.1.2.1 Lock-In Amplifier Phase Check. In practice, the sign of the TA signal depends on the phase setting on the lock-in amplifier. In most experiments, the lock-in phase was set according to the transient signal of a sample that has been well-described before, i.e., the phase was set to give a negative signal when using probe wavelengths that were known to probe GSB. In some experiments described in this thesis (Chapter 5), the electronic transition being probed was unknown. A positive "spike" due to coherent two-photon absorption of the solvent could aid in determining the correct lock-in phase, however this signal is not observed when both pump and probe wavelengths are in the visible region, such as those used in Chapter 5, because the two-photon absorption cross section of water or alcohol is extremely small. Although a reasonable solution to this problem could be to first check that the lock-in phase is set correctly by observing a sample

with a known TA signal before the sample in question. However, out of concern for obtaining a more universally applied procedure, we devised a method for accurately determining the lock-in amplifier phase for any pump/probe wavelength combination.

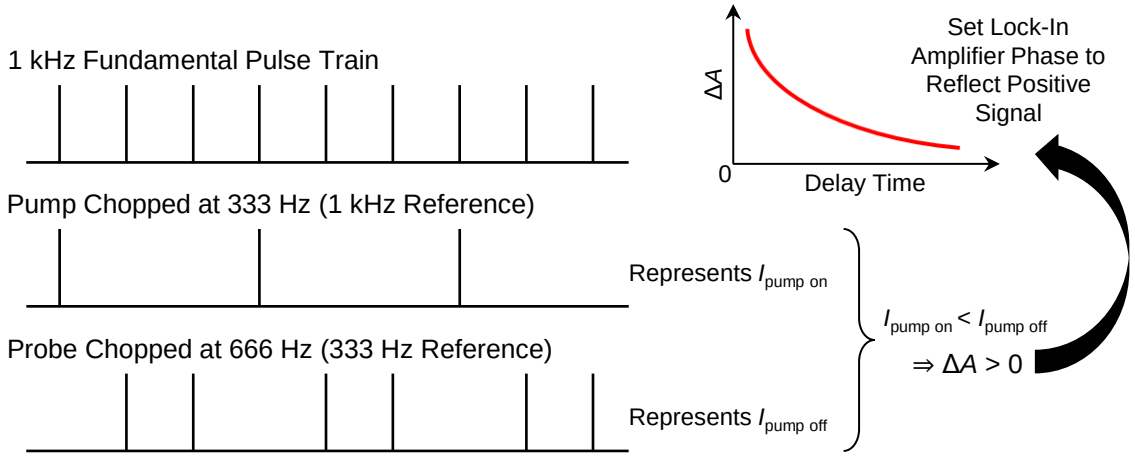


Figure 2.3. Schematic illustrating method developed for correctly determining the phase of the lock-in amplifier for any pump/probe wavelengths used.

The main idea is to simulate a large positive signal ($I_{pump\ off} > I_{pump\ on}$) without using an actual sample that can be interpreted according to eqn. (2.1). The phase of the lock-in amplifier is set to reflect the positive sign of this simulated signal. As illustrated in Figure 2.3, the method requires the use of a second optical chopper wheel, which is set to block 1 out of 3 probe pulses that have the same repetition rate as the 1 kHz fundamental. This setting is the reverse of the chopper used for the pump beam, which is set to pass 1 out of every 3 pump pulses. The former probe chopper is referenced to the 333 Hz frequency of the latter pump. The relative phase of the probe chopper must be offset by 120° with respect to the pump chopper, so that the first passed pulses do not overlap with one another (Figure 2.3). By setting the phase relation in this way, the pump pulses represent the simulated

positive signal ($I_{\text{pump on}}$), and the probe pulses represent the signal when the pump is off ($I_{\text{pump off}}$). After setting the lock-in phase to reflect the correct sign of the positive transient signal, the second chopper is removed from the probe line and the experiment is carried out as normal using the determined lock-in phase.

We tested this method by using it to set the lock-in phase before flowing in a sample with a known TA signal sign. Using this method resulted in the correct TA signal sign, as expected. It was also determined that the method works for any probe wavelength, as the method accurately predicted the lock-in phase to produce known transient signals using several other probe wavelengths. We also confirmed that, when the choppers are set correctly, the exact placement of the second probe chopper on the laser table is not crucial to interpreting the correct lock-in phase.

2.1.3 Time-Resolved IR Spectroscopy

An OPA was used to produce the UV pump beams used in TRIR experiments. The pump beam was delayed using a motorized translation stage and chopped at 500 Hz to block every other pulse. As in the TA measurements, the pump energy was attenuated and the beam was focused to a defined spot size at the sample, as detailed in the experimental sections of each chapter. A second OPA (TOPAS-C, Light Conversion) was pumped with 800 mW of the laser fundamental to produce signal and idler pulses, which were subsequently mixed non-collinearly in a GaSe crystal for difference frequency generation (NDFG, Light Conversion) to produce about 8 – 10 mW of mid-IR pulses with a bandwidth of 150 – 200 cm^{-1}. The pump and probe polarizations were set to the magic angle (54.7˚)

by rotating the probe beam using a CaF_2 holographic wire-grid polarizer. The power of the probe beam was controlled by a second polarizer of this type.

The mid-IR beam was split into two portions, "signal" and "reference" using a 3 mm Zn Se beam splitter. Both beams were passed through the sample, and the signal beam was overlapped with the pump beam while the reference beam, vertically displaced by 7.5 mm below the signal, was used to reduce pulse-to-pulse noise. The signal and reference beams were recollimated and focused into a spectrograph (Triax, Horiba) with a 0.75 mm entrance slit. A 100 lines/mm grating blazed at 6000 nm projected both beams onto a dual-row, 64-element mercury-cadmium-telluride diode array (Infrared Systems Development), which was cooled by liquid nitrogen. The signal was detected by the bottom row, and the reference was detected by the top row. The intensity (I) of the mid-IR beam was recorded at each diode and the spectrum was calculated as the change in absorbance (ΔA) according to eqn. (2.2).

$$\Delta A = \log\left(\frac{I_{\text{signal, pump off}} / I_{\text{reference, pump off}}}{I_{\text{signal, pump on}} / I_{\text{reference, pump on}}}\right) \tag{2.2}$$

At each delay time in the TRIR data, the plotted spectrum is the average of 5,000 spectra. As in the TA experiments, the samples were recirculated through a flow cell. D_2O (Cambridge Isotope Laboratories) was used for all TRIR experiments to increase optical transparency in the mid-IR probe regions of interest, which was the double-bond stretching "fingerprint" region in all experiments presented here. Steady-state UV-visible and FTIR absorption spectra were measured before and after laser exposure to monitor sample degradation and any photoproduct formation.

2.2 Time-Correlated Single-Photon Counting

TA is useful for studying excited-state dynamics involving dark states that cannot be easily detected in emission experiments.[21] If the sample is emissive, however, time-resolved emission techniques are also commonly employed in solution-phase experiments. Another useful technique is time-correlated single-photon counting (TCSPC), which provides time-dependent emission decay measurements. This technique can detect very weak emission, but its high sensitivity is obtained at the expense of time resolution (approximately 50 ps). As discussed in Chapter 5, time-resolved emission measurements were collected at 77 K using TCSPC. In this section, the instrument is briefly described, followed by the preparation method of the optical glass used at cryogenic temperatures.

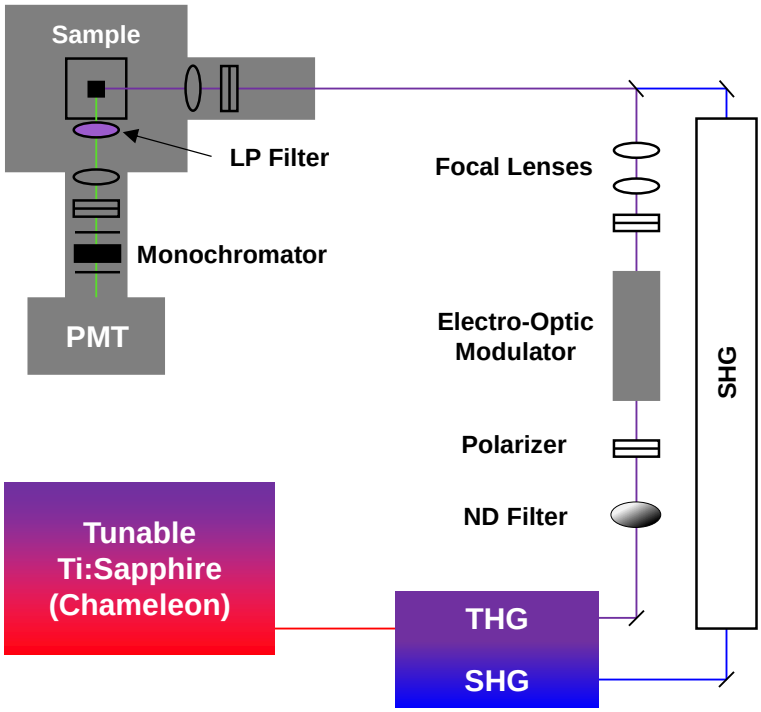


Figure 2.4. Schematic of the optical layout of the TCSPC instrument used to collect time-resolved emission measurements.

Figure 2.4 displays the optical layout of our TCSPC instrument. A tunable Ti:Sapphire laser (Chameleon Ultra II, Coherent Inc.) produced 795 and 930 nm laser fundamental pulses (180 fs, 80 MHz), which were converted into 265 and 310 nm using a harmonics generator (Coherent Inc.). An electro-optic modulator (M350-80, Conoptics) reduced the repetition rate to 4 MHz. The TCSPC setup consists of a fluorescence lifetime spectrometer (Picoquant model FluoTime 200 with Picoharp 300 timing electronics) and a microchannel plate photomultiplier (MCP-PMT, Hamamatsu) detector set at the right-angle geometry. Excitation beams were linearly polarized using a Glan-Thompson polarizer. The excitation pulses were filtered using a 300 nm long pass filter (Ashai), and the emission from the sample was passed through a polarizer set to the magic angle (54.7°) relative to the polarization of the excitation beam. The instrument response function (IRF) was determined from the scattering of a solution of dilute Ludox® HS-40 colloidal silica (Sigma Aldrich) at 265 nm. The IRF fwhm was approximately 50 ps. A bin width of 8.0 ps was used for each TCSPC measurement.

2.2.1 Measurements at 77 K

Prof. Kimberly de La Harpe from the U.S. Air Force Academy in Colorado Springs kindly provided a finger-Dewar cryogenic sample holder (Thorlabs) from her lab for TCSPC measurements at 77 K at MSU. Various solvents and solvent combinations were tested for their ability to form an optically transparent glass, i.e., a solid that does not crack or form "snow" at 77 K.[50-51] The solutions were held in a quartz EPR tube, which does not crack at 77 K, and submerged into the liquid-nitrogen filled finger-Dewar sample holder. Some solutions cracked every time, whereas others cracked much less frequently. Care

must be taken not to place the EPR tube into the liquid nitrogen too quickly or to bump the side of the tube when doing so. For the TCSPC measurements of violacein emission at 77 K presented in Chapter 5, an ethanol / methanol solvent mixture in a 5:1 volume ratio was used because it formed an optical glass when submerged with a frequency of 8 out of 10 to 9 out of 10 times.[50] Methanol, another solvent used for violacein studies in Chapter 5, instantly cracked throughout at 77 K making it unusable for cryogenic spectroscopic measurements.

2.3 Sample Handling

2.3.1 Buffer Solution and DNA Sample Preparation

Unless otherwise indicated, all DNA samples were dissolved in a phosphate buffer solution with 50 mM phosphate ($H_2PO_4^-$ / HPO_4^{2-}) buffer and 100 mM NaCl. Generally, the buffer was prepared by dissolving 0.034 g KH_2PO_4, 0.067 g Na_2HPO_4 and 0.054 g NaCl in 10 mL of H_2O or D_2O using a volumetric flask.

The DNA samples studied in this dissertation were dissolved as received in the phosphate buffer solution. Specific sample concentrations were prepared by weighing out the proper amount of solid, or in the case that the amount required was too low to weigh out, the exact concentration was determined from the UV-visible absorption spectrum using the Beer-Lambert Law. In the samples where the extinction coefficient (ε) was unknown, it was calculated by $\varepsilon = A/L \cdot c$, where A is the measured absorbance of the sample, L is the optical path length, and c is the sample concentration.

In Chapter 4, the D_2O solution pD was adjusted by adding dropwise DCl or NaOD (40 wt % in D_2O, 99.5 atom % D, Sigma-Aldrich) per the standard conversion pD = pH + 0.4, where pH was measured using a calibrated pH electrode. After experiments, all DNA samples were adjusted back to neutral pH and stored in a freezer to minimize degradation.

2.3.2 Violacein Pigment Purification

The relative amount of impurities and the ratio of violacein and deoxyviolacein compounds present in the pigment extracts from both wild-type (WT) and hyper-producing mutant *Janthinobacterium* sp. CG23_2 strains (see Chapter 5 for details) were determined using high-performance liquid chromatography (HPLC) with electrospray ionization mass spectrometry (ESI-MS) detection in the Mass Spectrometry (MS) facility at Montana State University. From these results, MS Facility coordinator Jonathan Hilmer devised a method for further pigment purification using solid-phase extraction (SPE).

2.3.2.1 HPLC with ESI-MS Detection. The crude pigment extract was diluted 100-fold using acetonitrile with 0.1% formic acid for HPLC. Formic acid was used to aid the ionization of the analyte for MS detection (see below). About 100 μL of the dilute solution was placed into an auto-collection sample vial and injected into a reverse-phase HPLC column. Analytes were eluted using water with 0.1% formic acid (solvent A) and acetonitrile with 0.1% formic acid (solvent B) mixtures (denoted as % B) with a gradient of 50% B – 95% B at 600 μL/min over a course of 1 – 5 minutes. Eluted products were detected using ESI-MS, which provides molecular weight information with each eluted species enabling accurate molecule identification. The resulting HPLC chromatograms

thus include weight assignments, designated as $[M + H]^+$, or the analyte molecular weight (M) plus the weight of a proton. Note that the superscript refers to the overall positive charge of the analyte plus ESI-added proton.

2.3.2.2 Solid-Phase Extraction. Based on the mobile-phase gradient used in the HPLC separations of the crude pigment extract solution, Jonathan Hilmer developed a purification method using disposable C18 packed SPE columns (Sep-Pak Vac C18 6cc, Waters) and HPLC grade acetonitrile / water mobile phases, which are designated in the procedure below by the percent of organic solvent (% ACN) in H_2O.

The crude pigment extract solutions from WT *Janthinobacterium* sp. CG23_2 were typically very dilute. Although the solutions from the hyper-producing mutants had much higher concentrations of violacein, all extract solutions were in 50 – 100 mL of methanol. To decrease solution volume the samples were dried and reconstituted in a smaller volume. The methanol was evaporated using a water-pressurized rotary-evaporator with water-bath heating (MP > 290°C for both violacein and deoxyviolacein).[52] The dried pigment was dissolved in 2 mL of DMSO and 2 mL of methanol, a solvent mixture that was expected to help the pigment molecules adsorb onto the C18 solid phase. The 4 mL solutions were diluted by half with pure H_2O, and SPE was carried out on these 8 mL total volume solutions.

The 6 mL SPE columns were primed by washing with 3 column volumes of 50% ACN, followed by 3 column volumes of 100% ACN, and finally, 1 column volume of 25% ACN. The first step in the purification procedure, summarized in Figure 2.5, is to load the pigment solution prepared, as described above. The flow through solution (FT) was

transparent if the all pigment was completely loaded onto the column (see Figure 2.6(a)). Next the loaded pigment was washed with 5 mL of 25% ACN to remove impurities, and the solution was collected (W). The pigment was eluted using two different organic solutions. First, 2 mL of 35% ACN was used to elute violacein (E1) and second, 6 mL 50% ACN was used to elute the remainder of pigment, which consisted of a mixture of the violacein and deoxyviolacein forms (E2). Each separation (FT, W, E1 and E2) was collected for analysis by HPLC with ESI-MS detection.

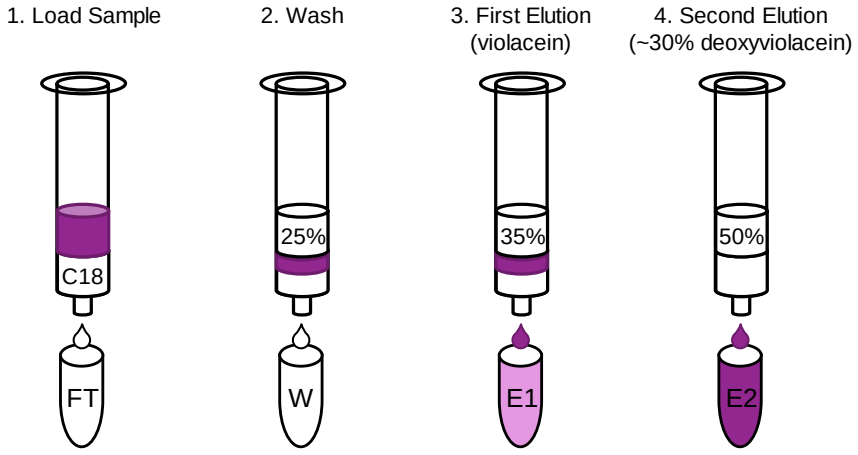


Figure 2.5. Schematic of the solid-phase extraction purification procedure developed to purify violacein (E1) and the violacein and deoxyviolacein mixture (E2) using disposable C18 columns. The percentages indicate the percent acetonitrile in water used as the mobile phases.

After elution of E2, almost no purple pigment was visible on the column, which was subsequently cleaned using 100% ACN and primed for re-use. Each 6 mL column was re-used up to three times without noticeable changes in efficiency of retaining the loaded pigment, i.e., the FT solution was not transparent after about three uses (Figure 2.6(b)).

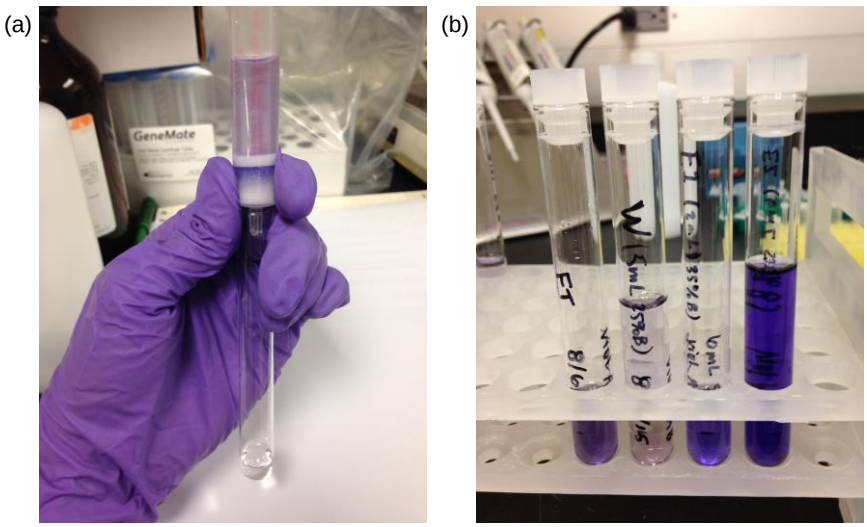


Figure 2.6. Photographs of (a) efficient pigment loading (transparent flow through solution) and (b) inefficient pigment loading (purple pigment in the flow through and wash solutions).

2.3.3 Deep Eutectic Solvent Preparation

Deep Eutectic solvents (DESs) are novel non-aqueous ionic solvents consist of an ammonium salt and a hydrogen bond donor in a 1:2 molar ratio. DESs can be made with a variety of compositions providing a range of viscosities at room temperature.[53] We have prepared DESs using anhydrous choline chloride (Sigma Aldrich) as the ammonium salt and urea, glycerol and ethylene glycol as the hydrogen bond donors, which produce DESs with viscosities in decreasing order: UreaDES > GlyDES > EgDES. The Kohler group began using DESs because DNA strands dissolved in DESs have been shown to maintain their secondary structure enabling spectroscopic study of the oligomers in non-aqueous environments.[54-55] In this section, the general DES preparation procedure is described, including suggestions for avoiding frustrating pitfalls while preparing this finicky solvent, followed by procedures for incorporating DNA and non-DNA solutes.

DESs are prepared by heating a 1:2 molar ratio of ammonium salt and hydrogen bond donor in a secured round bottom flask at 100°C until all solid is dissolved. Although the solid(s) may dissolve in about an hour, it is recommended to continue heating for about 3 hours total. We observed that the solid precipitated after the solution cooled to room temperature if the mixture is heated for an insufficient amount of time. Conversely, over-heating the solution, either by heating for too long or heating at higher temperatures, resulted in the solution turning faintly brown in color. Using a round-bottom flask minimizes the portion of the vessel in direct contact with the hot plate. It is important to closely monitor the solution as it is heating to maintain the temperature at 100°C. The mixture should be heated under a chemical hood because the vapor is caustic. Clamping a fractional distillation column into the opening of the round bottom flask helps the caustic vapor to condense or to be guided upward into the fume hood. Unless the heating apparatus has a temperature controller, the best way to monitor the temperature is to place a clamped-down thermometer in a beaker filled with a low boiling point liquid, such as ethylene glycol, and place this beaker on the heating plate alongside the round bottom flask. It is not advised to directly place a thermometer into the round bottom flask because the DES solution is very sensitive to contaminants.

All glassware must be thoroughly cleaned before use as even trace contaminants appeared to compromise the quality of the solvent, either by causing it to crystallize at room temperature or by causing the otherwise transparent solvent to become cloudy. On this note, cleaning the glassware an hour or more before preparing the solution is recommended to ensure it is completely dry before use. Because choline chloride is an

ionic compound, it can absorb a substantial amount of water over time. Care must be taken to reduce the amount of exposure to air and to store it in a dry environment or wrapped tightly with parafilm between use.

After the mixture has been heated for a sufficient amount of time, it should be allowed to equilibrate with room temperature before proceeding. In order to ensure that the DES is water-free, especially if the experimental application specifically aims at investigating non-aqueous solvent effects, the DES should be lyophilized over-night. Due to its low freezing temperature, for best results the DES must be frozen in a -80°C freezer before placing it in the lyophilizer. It is not advised to leave the solvent on the lyophilizer for more than 24 hours, as doing so will cause it to crystallize completely and become unusable.

Some solutes can be dissolved directly into the DES. For example, the violacein pigment investigated in Chapter 5 was directly added to a 1 ChoCl : 2 Gly DES and dissolved by gentle heating. DNA samples do not dissolve in DESs easily. To prepare DNA samples using DES, the sample must be dissolved in a small amount of pure water (or D_2O) before mixing the solution into the DES. If the DNA sample requires salt, which can help stabilize the DNA secondary structure, 100 millimolal salt can be dissolved with the DNA sample and added to the DES at the same time. The salt KCl is recommended over NaCl, as once again, it was observed that using NaCl resulted in DES crystallization. When making DNA samples, it is best to add the DNA before lyophilizing the sample over-night to remove the water used to dissolve the DNA.

2.3.4 Flow Cell

Unless otherwise indicated, samples were recirculated in a flow cell (Harrick) during laser experiments to minimize re-excitation of relaxing chromophores. The cell is assembled with two CaF_2 windows clamped together with either a 1 mm path length (TA experiments) or a 100 μm path length (TRIR experiments) spacer. The front window is 1 mm thick and the back window is 2 mm thick, which was intended to minimize broadening of the pump pulses. Sample solutions contained in 2 mL vials were pulled through PTFE septa caps (Fischer Scientific) with tubing connected to the pump drawing the solution through the flow cell at linear flow rate of 0.1 m/s.

2.4 Steady-State Spectroscopy

2.4.1 UV-Visible Absorption

UV-visible absorption spectra were recorded using a table-top UV-visible spectrophotometer (Lambda 25, Perkin-Elmer). The spectrum of a holmium oxide standard was collected to ensure proper instrument calibration. Generally, cells with the following path lengths were used for absorption measurements of the indicated sample concentrations: 1 cm quartz cuvette (Starna) for fluorescence concentrations (~0.02 mM), 1 mm quartz cuvette (Starna) for TA concentrations (1 mM) and 100 μm home-built cell with CaF_2 windows for TRIR concentrations (10 mM). Background subtractions were made using solvent-only measurements. Spectra were collected using 1 nm increments at room temperature (20 ± 2°C).

2.4.2 FTIR Absorption

Ground-state vibrational absorption spectra were recorded using a table-top FTIR spectrophotometer (FTIR 4200, Jasco, Inc.). The sample chamber was purged with dry air from a generator for ten minutes before recording FTIR spectra. The spectra were collected from 5000 – 500 cm^{-1} with 4.0 cm^{-1} resolution after 16 accumulations. Background spectra for automatic background subtraction were recorded with the chamber empty, and solvent-only spectra were recorded as sample scans for manual baseline subtractions. By doing this the solvent spectrum could be saved and checked to ensure proper baseline subtraction. Samples (10 mM) were held in the 100 μm spin cell with CaF_2 windows. Note that as the samples accumulate H_2O by contact with the atmosphere or surfaces (vial, flow tube, etc.) over time. To lessen this accumulation and to obtain clearer FTIR spectra, free from interference from water absorption, it is recommended to thoroughly rinse the CaF_2 windows with pure D_2O before using them to record a sample FTIR spectrum.

2.4.3 Fluorescence

Steady-state emission spectra were recorded using a commercial fluorometer (FluoroLog 3 FL3-11, Jobin-Yvon Horiba), which contains a 450 W xenon arc lamp as the excitation source. Spectra were collected at the right-angle geometry, and were corrected for spectral sensitivity of the instrument by multiplication with a wavelength-dependent correction factor determined from a series of standards. All samples were held in a 1 cm path length quartz cuvette, and all spectra were collected at room temperature (20 ± 2°C).

In Chapters 3 and 4, the DNA samples studied were in D_2O phosphate buffer solution during TA or TRIR experiments. However, the emission spectra of these samples

were collected in pure deionized H_2O because the D_2O, phosphate buffer salts, and NaCl exhibit substantial background emissions compared to the weakly emissive DNA samples. This results in an imperfect baseline subtraction from the emission spectrum of the analyte, and introduced significant error in the fluorescence quantum yield measurements. Subtraction of a neat H_2O background emission spectrum resulted in more accurate fluorescence measurements in comparison with literature values.

2.4.4 Circular Dichroism

Circular dichroism (CD) spectra were collected using a spectropolarimeter (Model J-815, Jasco, Inc.). Reported spectra are the average of two accumulations. Temperature-controlled CD spectra were collected using a 1 mm quartz cell with a tight-fitting stopper to prevent the solvent from evaporating and to prevent degassing and the introduction of spectral noise from air bubbles in the solution. The temperature of the sample holder was controlled by a Peltier mini water circulation bath (MCB-100, Jasco, Inc.). CD spectra were recorded from 10°C – 80°C at 10°C intervals.

2.5 Data Processing

All data was plotted and processed using the IGOR Pro 6.37 program (Wavemetrics Inc.), unless otherwise indicated.

2.5.1 Single-Wavelength Kinetics

Kinetic signals obtained from either TA or single-frequency TRIR signals were fit using a sum of exponentials as given in the equation

$$\sum_i A_i \exp(-t/\tau_i) \quad (2.3)$$

where A_i is the amplitude of the i^{th} exponential component, which decays with the time constant τ_i. All uncertainties are reported as 2σ.

2.5.1.1 Solvated Electron Signal Subtraction Procedure. In Chapters 3 and 4, solvated electron signals were observed in the 265 nm pump / 570 nm probe TA measurements.[56-57] These signals interfere with the kinetics pertaining to the analyte in these experiments and were removed using a subtraction procedure described previously.[20, 58] Briefly, the solvated electron signal from a solvent-only TA kinetic trace is scaled to tail-match with the kinetic trace of another solute with a known signal and lifetime with the same solvent and pump / probe wavelengths. These solutes must be prepared to match the optical density of the analyte at the excitation wavelength. The scaled solvent kinetic trace is subtracted from the solute kinetic trace. If the remaining solute signal can be fit using its known lifetime, the scaling factor is used to subtract the solvated electron signal from that of the analyte. For the experiments described in Chapters 3 and 4, we used adenosine 3'-monophosphate (AMP) in D_2O[20] and caffeine in methanol[59] as the known solutes, respectively.

2.5.2 Broadband Spectra

The broadband spectra collected in TRIR experiments were processed by setting a boxcar average and subtracting the pre-time zero offset. This was done using either the LabVIEW program developed for our TRIR instrument (TAP, Tom's Awesome Program), or using the MatLab commands developed by Dr. Tom Zhang. The former data processing

procedure produces a 123 × 64 matrix. To plot the spectra (ΔA vs. frequency) from this file type (.ProcSpec), the matrix minus the first column, which contains the delay time points, must be transposed. The 64 × 122 matrix produced using MatLab does not require transposing and also does not contain the delay time points. TRIR spectra were globally analyzed using the Glotaran program.[60-61] Note that the uncertainties produced in Glotaran are 1σ, and the reported values were multiplied by 2. Single-frequency kinetic data was obtained from the row in the 64 × 122 matrix pertaining to the frequency of interest. The data was transposed into column-form so it could be plotted against the delay time points given in the first column of the 123 × 64 matrix (.ProcSpec file type). The kinetics were fit with a sum of exponentials as described in Section 2.5.1 above.

2.5.3 TCSPC Emission Decay Spectra

Emission decays collected using the TCSPC instrument were fit using a model function in the FluoFit Version 4.5 (PicoQuant) global analysis program. The function (eqn. 2.4), formally described previously,[62] consists of a sum of exponentials convoluted with the normalized IRF, collected as described in Section 2.2.

$$S(t) = \int_{-\infty}^{t} \mathrm{IRF}(t' - t_s) \sum_{i=1}^{n} A_i e^{-\frac{t-t^i}{\tau_i}} dt' + N_0 \Delta t \cdot \mathrm{IRF}(t - t_s) \qquad (2.4)$$

Where A_i is the amplitude of the i^{th} decay lifetime component (τ), Δt is the bin width (0.008 ns), and t_s is an adjustable parameter that accounts for temporal offset between emission decays and the IRF. The N_0 factor is included to account for the emitted photons that account for emission decay components not detected within the 50 ps temporal resolution of the instrument.

2.6 References

47. Maine, P.; Strickland, D.; Bado, P.; Pessot, M.; Mourou, G., Generation of Ultrahigh Peak Power Pulses by Chirped Pulse Amplification. *IEEE Journal of Quantum Electronics* **1988**, *24*, 398.

48. Zhang, Y.; Chen, J.; Kohler, B., Hydrogen Bond Donors Accelerate Vibrational Cooling of Photoexcited Purine Derivatives in Heavy Water. *J. Phys. Chem. A* **2013**, *117*, 6771-6780.

49. Chen, J.; Kohler, B., Base Stacking in Adenosine Dimers Revealed by Femtosecond Transient Absorption Spectroscopy. *J. Am. Chem. Soc.* **2014**, *136*, 6362-6372.

50. Winefordner, J. D.; Stjohn, P. A., Solvents for Phosphorimetry. *Anal. Chem.* **1963**, *35*, 2211-2212.

51. Scott, D. R.; Allison, J. B., Solvent Glasses for Low Temperature Spectroscopic Studies. *J. Phys. Chem.* **1962**, *66*, 561-562.

52. Laatsch, H.; Thomson, R. H.; Cox, P. J., Spectroscopic Properties of Violacein and Related Compounds: Crystal Structure of Tetramethylviolacein. *J. Chem. Soc. Perkin Trans. II* **1984**, *8*, 1331-1339.

53. Abbott, A. P.; Harris, R. C.; Ryder, K. S., Application of Hole Theory to Define Ionic Liquids by Their Transport Properties. *J. Phys. Chem. B* **2007**, *111*, 4910-4913.

54. Mamajanov, I.; Engelhart, A. E.; Bean, H. D.; Hud, N. V., DNA and RNA in Anhydrous Media: Duplex, Triplex, and G-Quadruplex Secondary Structures in a Deep Eutectic Solvent. *Angew. Chem. Int. Ed.* **2010**, *49*, 6310-6314.

55. Lannan, F. M.; Mamajanov, I.; Hud, N. V., Human Telomere Sequence DNA in Water-Free and High-Viscosity Solvents: G-Quadruplex Folding Governed by Kramers Rate Theory. *J. Am. Chem. Soc.* **2012**, *134*, 15324-15330.

56. Jou, F.-Y.; Freeman, G. R., Temperature and Isotope Effects on the Shape of the Optical Absorption Spectrum of Solvated Electrons in Water. *J. Phys. Chem.* **1979**, *83*, 2383-2387.

57. Elkins, M. H.; Williams, H. L.; Neumark, D. M., Dynamics of Electron Solvation in Methanol: Excited State Relaxation and Generation by Charge-Transfer-to-Solvent. *J. Chem. Phys.* **2015**, *142*, article no. 234501.

58. Crespo-Hernández, C. E.; Kohler, B., Influence of Secondary Structure on Electronic Energy Relaxation in Adenine Homopolymers. *J. Phys. Chem. B* **2004**, *108*, 11182-11188.

59. Chen, J.; Kohler, B., Ultrafast Nonradiative Decay by Hypoxanthine and Several Methylxanthines in Aqueous and Acetonitrile Solution. *Phys. Chem. Chem. Phys.* **2012**, *14*, 10677-10682.

60. van Stokkum, I. H. M.; Larsen, D. S.; van Grondelle, R., Global and Target Analysis of Time-Resolved Spectra. *Biochim. Biophys. Acta Bioenergetics* **2004**, *1657*, 82-104.

61. Snellenburg, J. J.; Laptenok, S. P.; Seger, R.; Mullen, K. M.; van Stokkum, I. H. M., Glotaran: A Java-Based Graphical User Interface for the R Package TIMP. *Journal of Statistical Software* **2012**, *49*, 1-22.

62. Skowron, D. J.; Zhang, Y.; Beckstead, A. A.; Remington, J. M.; Strawn, M.; Kohler, B., Subnanosecond Emission Dynamics of AT DNA Oligonucleotides. *ChemPhysChem* **2016**, *17*, 3558-3569.

CHAPTER THREE

THE NATURE OF LONG-LIVED TRANSIENT SIGNALS IN UV-EXCITED DNA

3.1 Introduction

Understanding the mechanisms by which DNA dissipates excess electronic energy deposited by solar UV radiation is crucial because the efficiency of this process is directly responsible for the integrity of genetic information. In the single monomers, non-radiative decay channels provide access to the electronic ground state on a sub-picosecond timescale in aqueous solution.[63] However, femtosecond studies on DNA single and double strands in aqueous solution reveal new lifetime components on the order of tens to hundreds of picoseconds.[25, 37] The appearance of these long-lived signals suggests that fundamentally different deactivation channels are accessed in higher-order systems. Covalently linked bases are within 3.4 Å of each other within strands, and the close arrangements of bases alter the electrostatic and steric environments of the individual chromophores. Noncovalent interactions, including base stacking and pairing, modify the DNA electronic structure and could provide access to new photophysical pathways not available in the monomer bases. Using the reductionist approach, researchers have worked to delineate excited-state deactivation pathways in single oligonucleotide strands to better interpret duplex excited states.

Over the last decade, the nature of the excited states that give rise to long-lived transient signals in DNA strands has been highly debated.[23-24] Some attribute the new signals to delocalized excitons spanning several bases.[23, 27] In 2005, our group proposed

that the long-lived signals are due to CT states formed by photoinduced ET between two π-stacked bases.[25, 64] In our model, UV excitation of oligonucleotide strands initially generates delocalized excited states that rapidly (<0.5 ps) decay to CT states.[64] The resulting radical ion contact pair (Figure 1.4) subsequently undergoes back ET, which restores the electronic ground state of the participating bases. The timescales of CT state deactivation are thus dependent on ET rates, and Takaya et al. showed that the observed lifetimes in a series of dinucleotides are consistent with calculated thermodynamic driving forces for forward and back ET.[64]

Although significant experimental support exists for this model,[25-26, 49] the direct spectroscopic observation of photoinduced ET in DNA strands was lacking until recently. In this chapter, I present our observation of photoinduced ET in a model DNA dinucleotide consisting of the oxidatively damaged product of guanine, 8-oxo-7,8-dihydro-2'-deoxyguanosine (O), at the 5'-position and 2'-deoxyadenosine (A) at the 3'-position (d(OA)). Oxidation results in the lower reduction potential of O compared to G (0.74 V compared to 1.29 V vs. NHE).[65-66] It was previously shown that O can mediate photoinduced repair of CPD photoproducts via a proposed ET mechanism.[30, 40] With its enhanced photo-redox properties, O is a useful modified base for investigating photoinduced ET processes in single-stranded DNA. Incorporating the oxidative product into a dinucleotide with A also enables the advantage of selective excitation, as O has a significantly red-shifted absorption band compared to its canonical form (Figure 3.1).

After selectively exciting O within d(OA), we monitored the dynamics using TRIR spectroscopy. We observed transient vibrational bands assigned to radical ion species

generated by UV-induced ET from O to base-stacked A. Global fitting analysis of the broadband TRIR spectra produced two lifetimes, one corresponding to that of the O monomer and a long-lived lifetime on the order of tens of picoseconds. By comparing the time- and frequency-resolved TRIR spectra with time-dependent DFT calculations, the radical ion marker bands were unambiguously identified and the long-lived lifetime was assigned to the rate of back ET between A and O.[29]

Observing O undergo excited-state ET provides physical basis for the proposed photoinduced ET CPD repair mechanism, which is reminiscent of the CPD repair mechanism identified in the flavin adenine dinucleotide (FAD) redox cofactor of photolyase.[67] The significance of this connection is more thoroughly discussed in Chapter 4. Here, I focus more on the implications of our results for interpreting long-lived transient signals in time-resolved DNA excited-state measurements. By drawing on recent experimental work, undertaken by our group and others, I conclude this chapter with a discussion of several new developments in the field of DNA excited-state dynamics to emphasize how the results obtained for a modified dinucleotide apply to natural DNA systems.

3.2 Experimental

Monomer O (≥ 97%, Berry and Associates, Inc.) samples were prepared by dissolving the solid as received in 2 mL of D_2O phosphate buffer solution (buffer recipe given in Chapter 2). The d(OA) dinucleotide was synthesized, characterized, and generously donated by Dr. Xi-Bo Li from the Cynthia J. Burrows research group at the

University of Utah in Salt Lake City. The full synthesis and characterization procedure has been reported previously.[29] Dr. Li sent 10 μmol of dried d(OA) sample. A mixture of O and AMP was prepared using 5 μmol of each base to match the concentrations of O and A in the d(OA) sample. The d(OA) and equimolar mixture samples were each dissolved in 2 mL of the D_2O phosphate buffer solution. All sample concentrations were 1 mM for UV pump / visible probe TA and 10 mM for UV pump / broadband mid-IR probe TRIR measurements.

Steady-state UV absorption and FTIR spectra were collected as described in Chapter 2 before and after laser irradiation for all samples. Steady-state emission spectra were collected for O and guanosine 5'-monophosphate (GMP) samples dissolved in pure deionized H_2O without buffer or NaCl (see Chapter 2). The samples were adjusted to have optical densities of 0.2 at the excitation wavelength (285 nm) to avoid reabsorption of emitted photons. Emission intensity was recorded every 2.5 nm with 20.0 s integration time using 5.0 nm bandpass slit widths. Temperature-dependent CD spectra were collected using 1 mM solutions in a 1 mm path length capped quartz cell.

Details of the UV pump / visible probe TA and UV pump / broadband mid-IR probe TRIR spectroscopy experiments are given in Chapter 2, whereas the methods pertinent to the measurements reported in this chapter are outlined here. For the UV pump / visible probe TA experiments, the 266 nm pump beam was produced by third harmonic generation of the 800 nm laser fundamental, and the 570 nm probe beam was generated by an OPA with about 1 W of the fundamental. The pump beam was focused to 220 μm (fwhm) at the sample with a pulse energy of 0.9 μJ. For the UV pump / broadband mid-IR probe TRIR

experiments, the 265 and 295 nm pump beams were produced by an OPA and the broadband mid-IR probe beam centered at 1626 cm^{-1} (200 cm^{-1} bandwidth) was produced using the TOPAS. The 265 nm pulse energy was 3.2 μJ (470 μm spot size at fwhm) and the 295 nm pulse energy was 1.5 μJ (370 μm spot size at fwhm) at the sample.

3.2.1 Computational Methods. Prof. Roberto Improta at IBB-CNR in Naples performed geometry optimizations and calculated the vibrational frequencies of the O and A monomer nucleobases and their radical ionic forms using TD-DFT with the PBE0[68] functional and the 6-31+G(d,p) basis set. Deuterium atoms were used in place of all labile hydrogen atoms. The 2'-deoxyribose groups and five explicit D_2O molecules were included, and the bulk solvent was approximated using a polarizable continuum model.[69] The ground-state geometry and vibrational frequencies of the dinucleoside monophosphate were calculated using PBE0 and M052X[70] functionals. The excited-state geometry and vibrational frequencies were estimated by their time-dependent extensions,[71] using the smaller 6-31G(d) basis set without including explicit D_2O molecules due to high computational costs. A scaling factor of 0.972 was applied to the vibrational frequencies to account for anharmonicities of the vibrational potentials and for better comparison with experimental spectra.

3.3 Results

3.3.1. 8-Oxo-7,8-Dihydro-2'-Deoxyguanosine Photophysics

One-electron oxidation of G results in carbonyl substitution at the C8 position on the imidazole ring. O has a pK_a value at 8.6 corresponding to the N1 proton.[72] At

physiological pH the N1 position is predominantly protonated, and the most stable tautomer is the 6,8-diketo form shown in Figure 3.1.[72] The UV absorption spectrum of O in neutral aqueous buffer solution, shown by the red trace in Figure 3.1, is consistent with its previously reported spectrum.[72] The spectrum exhibits two distinct transitions centered at 293 and 247 nm, corresponding to the first and second $^1\pi\pi^*$ transitions.[73] The first transition is significantly red-shifted in O compared to GMP (green trace in Figure 3.1), in

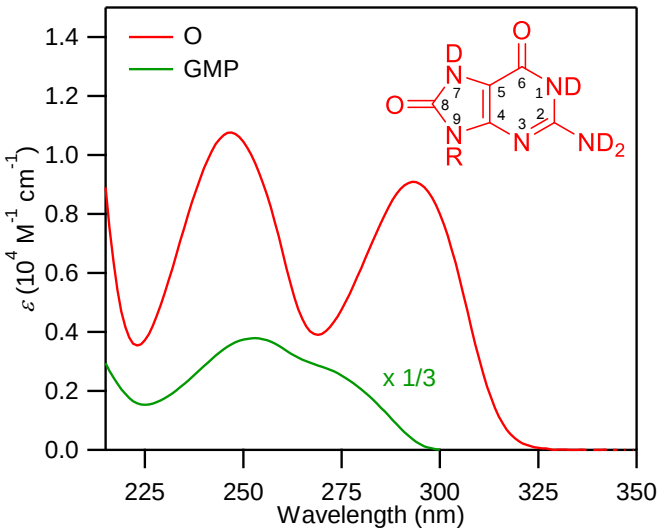


Figure 3.1. UV absorption spectra of 8-oxo-7,8-dihydro-2'-deoxyguanosine (O) at neutral pD (red trace) and guanosine 5'-monophosphate (GMP, green structure) in D_2O phosphate buffer solution. Note that the spectrum of GMP is scaled by a factor of 1/3 for better comparison of its long-wavelength shoulder with the long-wavelength band of O. Inset is the chemical structure of O. Adapted from ref 75.

which this transition is merely a shoulder on the red-edge of the stronger band centered at 252 nm. Theoretical calculations attribute the long-wavelength shoulder of the G absorption spectrum (green trace in Figure 3.1) to the LUMO ← HOMO transition, with the LUMO localized on the imidazole ring.[74] Upon C8 carbonyl substitution at the imidazole, the energy of the LUMO ← HOMO transition decreases and the electronic

structure of G shifts to longer wavelengths. This is consistent with the theoretical calculations of the first couple electronic energy levels of O provided by our collaborator Spiridoula Matsika from Temple University in Philadelphia.[75] Thus, the transition is significantly red-shifted upon C8 carbonyl addition, and the shoulder on the red edge of UV absorption in GMP becomes a discrete second absorption band centered at 293 nm in O. By scaling the absorption spectrum of GMP in Figure 3.1 by a factor of 1/3, this band shifting effect is clearly shown.

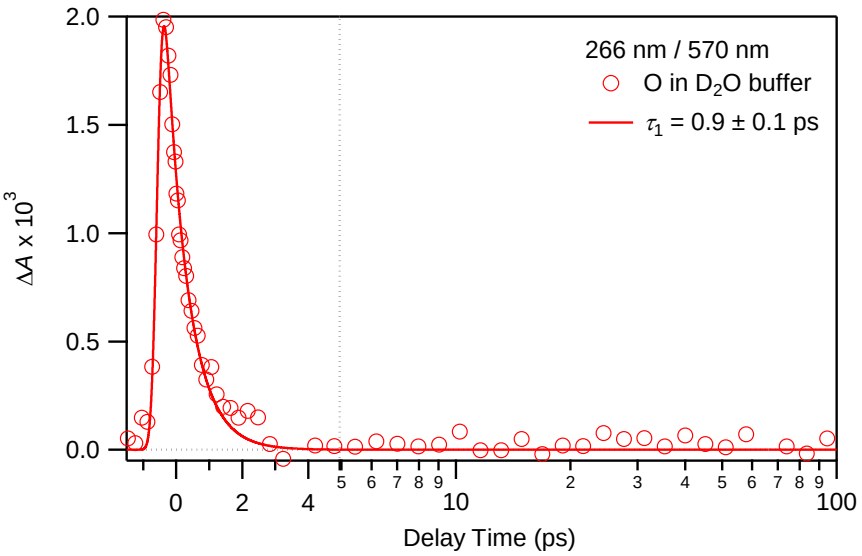


Figure 3.2. Excited-state absorption kinetics of 8-oxo-7,8-dihydro-2'-deoxyguanosine (O) in D_2O phosphate buffer solution (red circles) collected with 266 nm pump and 570 nm probe wavelengths. The decay was fit using a monoexponential function (red trace), which produced the lifetime indicated. Note the break in linear and logarithmic scales of the x-axis at 5 ps. Adapted from ref 75.

The excited-state lifetime of O in D_2O phosphate buffer solution was measured using 266 nm pump / 570 nm probe TA. This probe wavelength is often used to monitor ESA without contributions from VC,[76] which is observed when probing the ground state

using wavelengths that monitor GSB transitions. However, this pump / probe wavelength combination generates solvated electrons by two-photon ionization of the aqueous solvent.[56] The ESA kinetics of O shown in Figure 3.2 were corrected by subtraction of the solvated electron signal using the procedure described in Chapter 2. The excited-state kinetics of O decay monoexponentially with complete ground-state recovery, i.e., all transient signals return to the $\Delta A = 0$ baseline. A single exponential fitting function, with deconvolution of the instrument response (~0.2 ps), produced a lifetime of $\tau = 0.9 \pm 0.1$ ps.

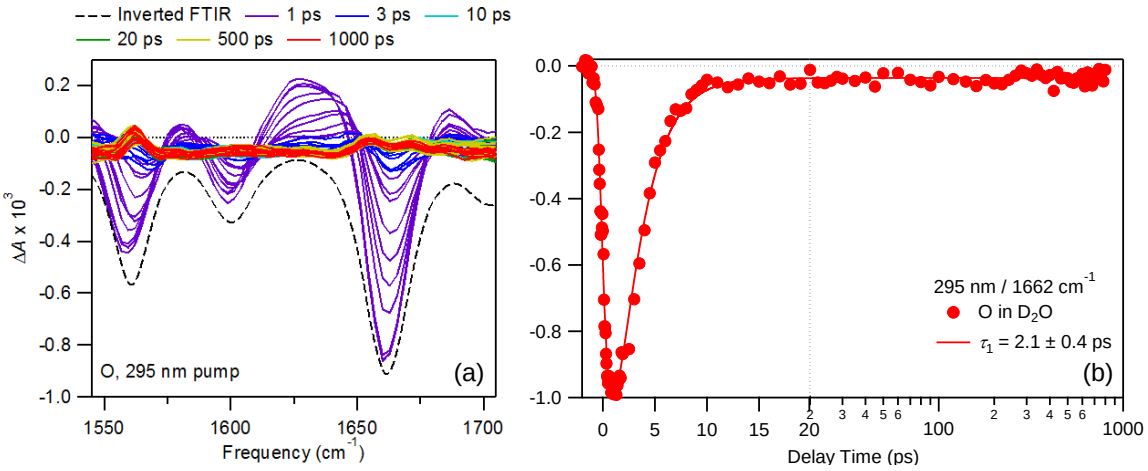


Figure 3.3. TRIR spectra of 8-oxo-7,8-dihydro-2'-deoxyguanosine (O) in D_2O phosphate buffer solution collected using 295 nm pump and 1626 cm^{-1} center-frequency broadband probe with overlaid inverted FTIR spectrum (dashed black trace) (a). The delay times are indicated in the legend above panel (a). Single-frequency kinetics from the 1662 cm^{-1} ground-state bleach band (solid red circles) fit with a single exponential, producing the indicated lifetime (b). Note the break in linear and logarithmic scales of the x-axis at 20 ps. Adapted from ref 75.

Figure 3.3(a) displays the 295 nm pump / 1626 cm^{-1} center-frequency broadband mid-IR probe TRIR spectra of O in D_2O phosphate buffer solution plotted at delay times from 1 – 1000 ps. Note the horizontal dotted line at $\Delta A = 0$, which was included to differentiate negative signals from positive signals. After excitation of the first $^1\pi\pi^*$

transition using the 295 nm pump beam, negative and positive features arise by 1 ps and decrease in signal amplitude ($\Delta A \rightarrow 0$) as they decay completely by 10 ps to a featureless negative offset that extends out to 1 ns. The negative offset is due to altered absorption of the solvent after heating by the 295 nm pump pulses.[59]

The inverted FTIR of O in the same D_2O phosphate buffer solution (dashed black trace) is overlaid for comparison with the TRIR spectra in Figure 3.3(a). Four distinct vibrational modes of O are observed in the mid-IR region shown. Jayanth et al. assigned these IR bands, from highest to lowest frequencies, to C8=O and C6=O carbonyl stretching modes and pyrimidine and pyrimidine + imidazole ring stretches.[73] Importantly, the bands observed at 1702 and 1662 cm^{-1}, due to the C8=O and C6=O stretching modes, respectively, confirm that O is predominantly present in the 6,8-diketo form in neutral solution. The C6=O carbonyl stretching mode at 1662 cm^{-1} is observed at the same frequency in the FTIR spectrum of GMP,[77] which further suggests that the additional C8=O carbonyl in O more greatly affects the energy associated with the imidazole ring in GMP, and does not affect the vibrational energy of the pyrimidine ring C6 carbonyl.

The negative TRIR spectral features align with the ground-state IR absorption bands, and are thus due to GSB. Single-frequency kinetics taken at the 1662 cm^{-1} GSB band (Figure 3.3(b)) were fit using a single exponential function with a negative offset to account for the solvent heating. The monoexponential fit gave a lifetime of $\tau = 2.1 \pm 0.4$ ps. The positive band at 1631 cm^{-1} decays on the same timescale.[75] TRIR spectra of O were also collected with 265 nm excitation, but are not shown here because they were indistinguishable from those obtained after 295 nm excitation. A monoexponential fit of

the 265 nm pump, 1662 cm^{-1} GSB band also produced identical kinetics within experimental error, as shown in the published article.[75]

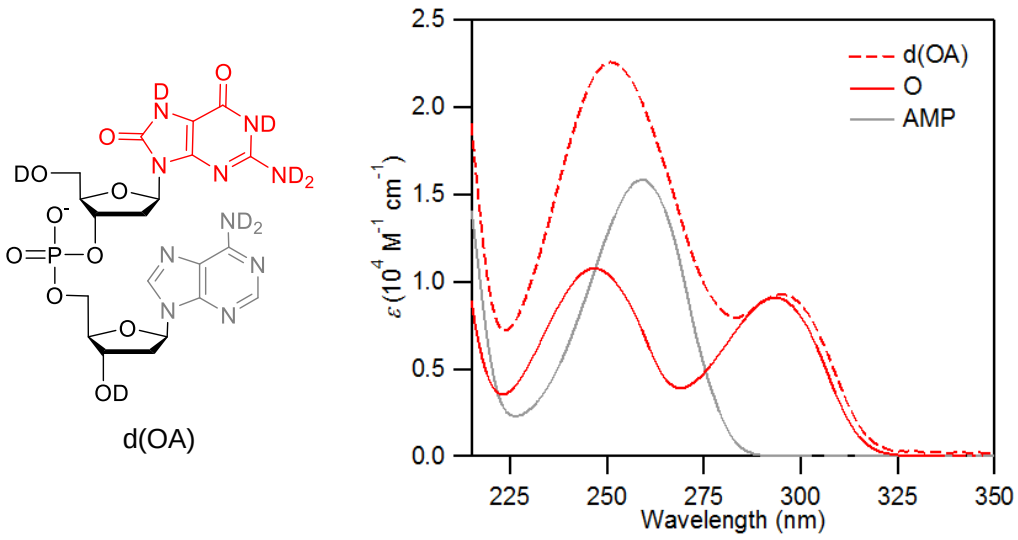


Figure 3.4. Chemical structure of d(OA) and its UV absorption spectrum (dashed red trace) overlaid with the absorption spectra of 8-oxo-7,8-dihydro-2'-deoxyguanosine (O, solid red trace) and adenosine 3'-monophosphate (AMP, gray trace). Adapted from ref 29.

3.3.2 Dinucleotide Containing 8-Oxo-7,8-Dihydro-2'-deoxyguanosine and Adenine

Figure 3.4 shows the chemical structure of the d(OA) dinucleotide alongside its UV absorption spectrum in D_2O phosphate buffer solution (dashed red trace) overlaid with the UV absorption spectra of O (sold red trace) and AMP (gray trace). The dinucleotide spectrum roughly consists of the sum of contributions from its component chromophores. Due to the red-shifted first absorption band of O compared to its canonical form, almost 40 nm of the d(OA) absorption spectrum corresponds to the absorption of only one of its two chromophores. This enables selective excitation of O in d(OA) using longer wavelengths. We used 295 nm pump to excite O only and 265 nm pump to excite both chromophores for comparison.

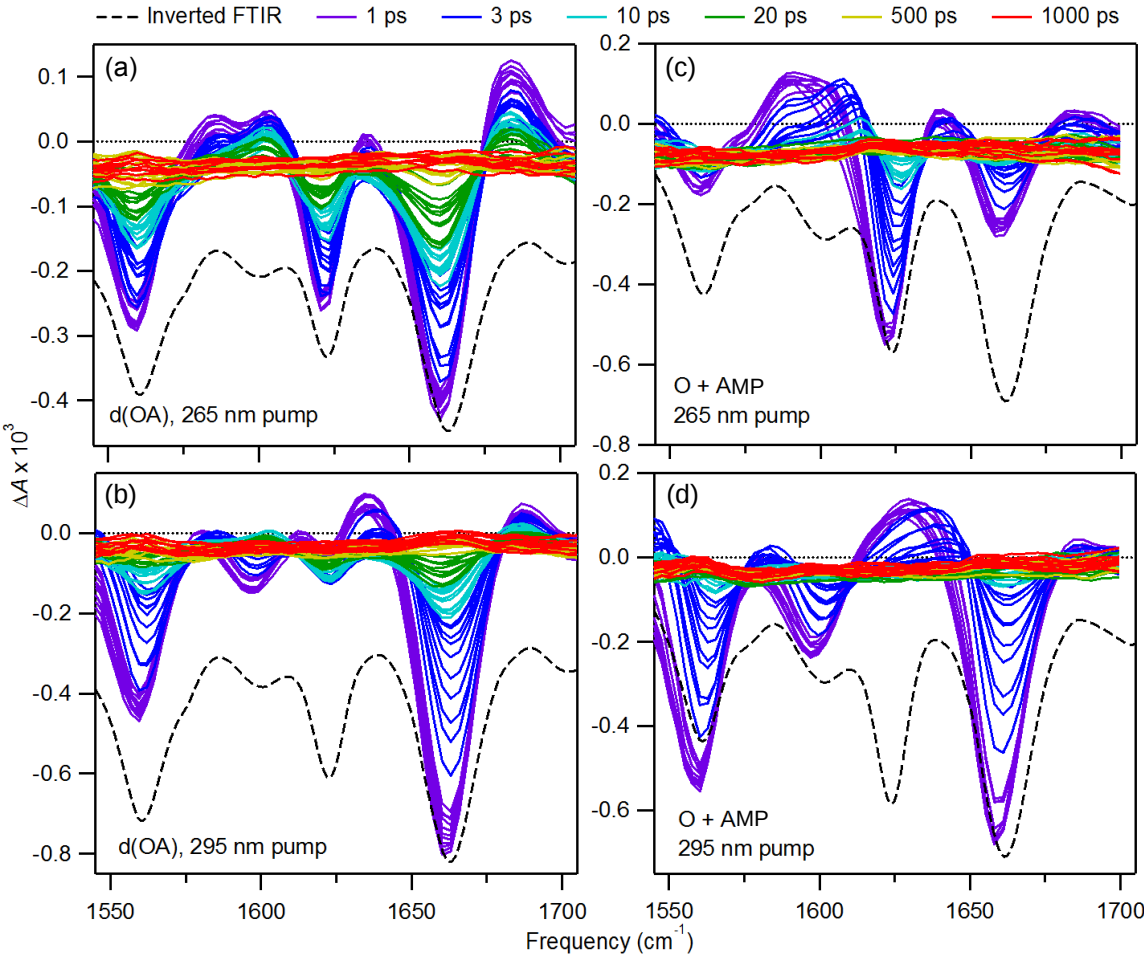


Figure 3.5. TRIR spectra of d(OA) in D_2O phosphate buffer solution collected after 265 (a) and 295 nm (b) excitation with the inverted d(OA) FTIR spectrum (dashed black traces). TRIR spectra of an equimolar mixture of 8-oxo-7,8-dihydro-2'-deoxyguanosine (O) and adenosine 3'-monophosphate (AMP) in D_2O phosphate buffer solution collected after 265 (c) and 295 nm (d) excitation, overlaid with the inverted FTIR spectrum of the mixture (dashed black traces). Adapted from ref 29.

Figures 3.5(a) and (b) include the inverted FTIR spectrum of d(OA) in neutral D_2O phosphate buffer solution. The normal mode calculations provided by Prof. Improta (see Section 3.3.2) aided in our assignments of the d(OA) ground-state vibrational spectrum. The band at 1662 cm^{-1} is due to the C6=O carbonyl stretch of O. The 1626 cm^{-1} band is due to the in-plane ring vibrational mode of A. Bands at 1601 and 1562 cm^{-1} arise from the

ring vibrational modes of O localized on the C4=C5 double bond and on the C2 amino group, respectively. The character and positions of the O vibrational bands are consistent with those assigned previously.[73]

TRIR data for d(OA) in the D_2O solution measured after 265 and 295 nm excitation at delay times from 1 – 1000 ps are shown in Figures 3.5(a) and (b). After excitation with both pump wavelengths, the positive and negative features reach maximum signal by 1 ps and decay completely by 300 ps to a featureless negative offset extending out to 1 ns. The negative bands are centered with the ground-state vibrational transitions shown in the inverted FTIR spectrum of d(OA), indicating that they correspond to GSB. The TRIR spectra show positive bands at 1602 and 1684 cm^{-1} in both sets of data, but these bands are more intense in the 265 nm pump spectra. The GSB signal at 1626 cm^{-1}, due to the A ring vibrational mode, is also much stronger in the 265 nm pump TRIR. As shown in the 295 nm pump TRIR (Figure 3.5(b)), the A vibrational band doesn't reach maximum until about 10 ps.

In contrast with the O monomer TRIR bands (Figure 3.3), the d(OA) TRIR features recover on a lengthened timescale and exhibit biexponential kinetics. Figure 3.6 displays single-frequency decays at 1662 cm^{-1} after 295 and 265 nm of d(OA) compared to O. The dinucleotide TRIR positive and negative signals can be globally linked using the same time constants, a shorter one of about 4 ps and a longer one of about 60 ps. This is the case for both 265 and 295 nm pump TRIR spectra. Despite the identical kinetics at both pump wavelengths, the amplitude of the 60 ps component is lower in the 295 nm pump kinetics.

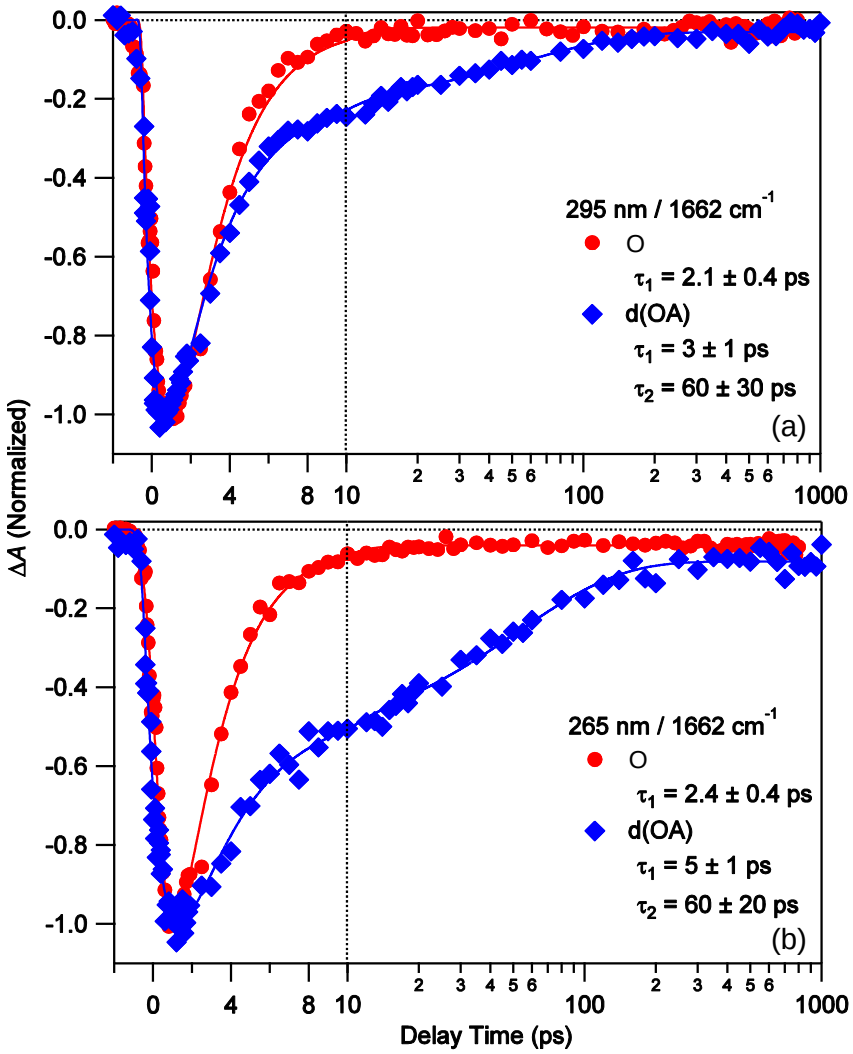


Figure 3.6. Normalized kinetic decay traces of 8-oxo-7,8-dihydro-2'-deoxyguanosine (O, solid red circles) and d(OA) (solid blue diamonds) from TRIR ground-state bleach bands at 1662 cm^{-1} after 295 (a) and 265 nm (b) excitation. O and d(OA) kinetics were fit using monoexponential and biexponential functions with negative offsets (solid traces), respectively, which produced the time constants indicated. Note the break in linear and logarithmic scales of the x-axis at 10 ps. Adapted from ref 29.

As shown in Figure 3.6(a), the amplitude of the long-lived decay component is about 40% decreased compared to that shown in Figure 3.6(b). The lifetimes and signal amplitudes generated from global fitting are listed in Table 3.1. No additional spectral features are

present after the 60 ps component fully decays, indicating that the excited state decays directly to the ground state.

Table 3.1. Global fit parameters for d(OA) TRIR GSB signals at the two pump wavelengths. Normalized traces were fit with $A_1e^{-t/\tau 1} + A_2e^{-t/\tau 2}$ after subtracting the long-lived offset due to D_2O heating.

λ_{pump} (nm)	A_1	τ_1 (ps)	A_2	τ_2 (ps)
265[a]	0.6 ± 0.1	4 ± 1	0.4 ± 0.1	60 ± 20
295[b]	0.9 ± 0.4	3 ± 1	0.10 ± 0.05	60 ± 30

[a]Fit of O GSB signals at 1662 and 1562 cm^{-1}, and A GSB at 1623 cm^{-1}. [b]Fit of O GSB signals at 1662 and 1562 cm^{-1}. Adapted from ref 29.

To determine if the long-lived lifetime component is only observed in the dinucleotide, we collected TRIR spectra of solutions containing equimolar amounts of the individual chromophores, O and AMP. Figures 3.5(c) and (d) display the spectra for this equimolar mixture after 265 and 295 nm excitation, respectively. The negative features align well with the inverted FTIR spectrum of the equimolar mixture, and are due to GSB. Compared to the dinucleotide TRIR spectra (Figures 3.5 (a) and (b)), the relative intensities of the GSB bands in the equimolar mixture TRIR spectra (Figures 3.5 (c) and (d)) are noticeably different. With 265 nm excitation, the A band at 1626 cm^{-1} is the most intense of the three GSB bands present, whereas this band is completely absent in the spectra collected after 295 nm excitation. This observation is consistent with the greater molar absorptivity of A than O at 265 nm, and confirms that A does not absorb 295 nm photons.

The TRIR spectra of the equimolar mixture decay on a faster timescale than d(OA). Single-frequency kinetics and global fits reveal that the equimolar mixture excited states deactivate on a timescale of 2 – 3 picoseconds.[29] No long-lived time component is observed. The short lifetimes and the presence of "rise-blue-shift-decay" VC signatures in

the TRIR spectra at 1600 and 1630 cm^{-1} in Figures 3.5(c) and (d), respectively, imply monomer-like deactivation in the equimolar mixture. Based on these observations, the 60 ps lifetime is unique to the dinucleotide, where the chromophores are covalently connected by the phosphate backbone.

3.4 Discussion

3.4.1 Nucleoside Photophysics: Ultrafast S_1 Decay and Vibrational Cooling

The ESA kinetics of O (Figure 3.2) decay monoexponetially with a time constant of τ = 0.9 ± 0.1 ps, and the transient signal fully recovers to the baseline at ΔA = 0. The absence of a second decay feature or a long-lived offset indicates that the excited state observed in 266 nm pump / 570 nm probe TA does not lead to the population of $n\pi^*$ or triplet states. The same conclusion is drawn from the 295 nm pump TRIR spectra in Figure 3.3, as the single-frequency kinetics at 1662 cm^{-1} decay to the long-lived negative offset that is attributed to absorption of the heated D_2O solvent. The kinetics of this band are also monoexponential and decay on a timescale of about 2 ps. Note that identical spectra and kinetics were observed after 265 nm excitation of O,[75] confirming that long-lived dark states are not populated after either pump wavelength.

From the TA and TRIR measurements, O excited-state deactivation occurs on two timescales, about 0.9 and 2 ps. It was previously shown that the 570 nm probe wavelength interrogates the S_1 excited state in nucleobases.[21, 76] To investigate whether the 0.9 ps lifetime recorded using 266 nm pump / 570 nm probe TA is due to deactivation of an emissive singlet excited state, we collected the steady-state emission spectrum of O and

calculated its fluorescence quantum yield. Figure 3.7 shows the emission spectrum of O compared to that of GMP, both in ultrapure deionized H_2O. The spectra were corrected by

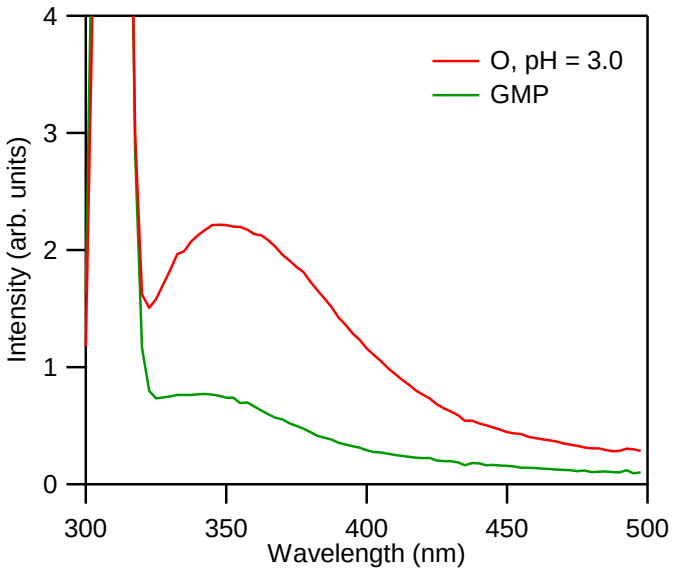


Figure 3.7. Steady-state emission spectra of 8-oxo-7,8-dihydro-2'-deoxyguanosine (O) at pH = 3.0 (red trace) and GMP (green trace) in deionized H_2O collected after 285 nm excitation with 5.0 nm bandwidth slit widths and 20.0 s integration. Adapted from ref 78.

subtraction of the solvent background emission everywhere except in the region of the Raman peak of water at 309 nm. We determined that the deprotonated form of O at pH = 10.5 (pK_a = 8.6)[72] is about 13 times more fluorescent than the neutral form.[78] Although the protonated species is dominant at neutral pH, even a small fraction of the deprotonated form present was found to influence emission measurements of the weakly emissive protonated form. Due to this the emission spectrum of O was collected at pH = 3.0 where the protonated form is present in about 400,000-fold higher concentration than the deprotonated form.[78]

Table 3.2. Wavelengths of maximum emission (λ_{max}^{fl}), fluorescence quantum yields (ϕ_{fl}), and S_1 excited-state lifetimes (τ) of O and GMP.

	λ_{max}^{fl} (nm)	$\phi_{fl} \times 10^4$	τ_1 (ps)
O[a]	350	2.91	0.9 ± 0.1
GMP[b]	342	1.09	0.46 ± 0.04[c]

[a]Measured in this work. [b]From reference 79. [c]From ref 78.

The relative emission intensities of O and GMP in Figure 3.7 suggest that the modified base is slightly more emissive. To quantify this observation, the fluorescence quantum yield (ϕ_{fl}) of O was calculated using eqn. (3.1)

$$\frac{f_A}{f_B} = \frac{I_A\left(1 - 10^{-\mathrm{OD}_A}\right)n_A^2}{I_B\left(1 - 10^{-\mathrm{OD}_B}\right)n_B^2} \tag{3.1}$$

where the subscripts *A* and *B* refer to the solute and reference standard, respectively, *I* is the integrated emission intensity, OD is the optical density at the excitation wavelength, and *n* is the refractive index of the solution. In the measurement for O, the refractive index was assumed to be the same in both dilute solutions and equal to that of water. GMP served as the reference standard.[79] Our calculations revealed that the fluorescence quantum yield of O is roughly three times greater than that of GMP (Table 3.2), which is consistent with values reported previously.[80] Theoretical calculations by Lu et al. indicate that the potential energy surface of O is characterized by a very steep pathway from the initial excitation region leading to a conical intersection (CI) with the ground state.[78] These characteristics of the S_1 excited state explain the weak emission from O. Similar observations were made in calculations of the weakly emitting canonical bases.[81] Changenet-Barret et al. explained that the slightly greater emissions from O compared to GMP could be due to a subtle plateau on the S_1 surface of the former compound.[80]

These results indicate that the 0.9 ps lifetime of O is due to a bright excited state, which is most likely a $\pi\pi^*$ state.[78] The S_1 state of O is slightly more emissive with a proportionately longer-lived lifetime than that of GMP (Table 3.2).[20] Singlet excited states of the canonical nucleobases deactivate via UIC followed by efficient VC to the thermally equilibrated ground state (Figure 1.4).[20] After deactivation via UIC, the excess electronic energy is deposited into the vibrational modes of the ground state, and is subsequently dissipated into the solvent as heat. As the VC occurs on the electronic ground-state potential, these dynamics can be observed by probing with wavelengths that monitor GSB. The negative GSB signals in the O TRIR spectra (Figure 3.3) thus provide a measurement of the VC lifetime, which is about 2 ps in O. The positive band at 1630 cm^{-1} in Figure 3.3 further validates our assignment, as it exhibits the "rise-blue-shift-decay" pattern characteristic of VC.[75] It is noteworthy that the 2 ps VC lifetime of O is one of the fastest observed in purine nucleobases.[48]

3.4.2 Dinucleotide Photophysics: Charge Recombination Dynamics

The dinucleotide kinetics shown in Figure 3.6 decay on two timescales (Table 3.1). The shorter lifetime of about 2 – 3 ps is identical to the lifetime measured for O. The longer-lived lifetime of about 60 ps was not observed in the kinetics of either the monomer (Figure 3.3) or the equimolar mixture (Figures 3.5(c) and (d)). The difference between the dinucleotide and equimolar mixture samples is that the nucleobases are covalently linked in d(OA). Consequently, the bases are held at a defined distance from one another, and are more likely to be base-stacked than the free bases in solution. Base-stacking was previously shown to be an essential requirement for the observation of long-lived lifetimes in

dinucleotides and longer DNA single strands.[26, 49] Nucleobases that are π-π stacked often give rise to exciton-coupled CD (ECCD) signals, which can be diagnostic of base stacking.[49] The temperature-dependent CD spectra of d(OA) indeed have ECCD signals, verifying that a fraction of the bases in d(OA) are stacked (see SI of ref 29).

Based on our proposed model, base-stacked regions in UV-excited single-stranded DNAs decay to exciplex, or CT states, formed by ET from one base to another. Based on standard reduction potentials, O is a better electron donor than A ($E°$ = 1.17 and −2.45 V vs. SHE, respectively).[29] Thus, it is more likely that photoinduced ET occurs from O to base-stacked A. This would generate an O radical cation and an A radical anion. Photoinduced ET in d(OA) is further supported by the Gibbs energy ($\Delta G°_{ET}$) for ET. We estimated the thermodynamic driving forces for forward (FET) and back ET (BET) using the Rehm-Weller equation[82] given by

$$\Delta G°_{FET} = e[E°(D^{\bullet+}/D) - E°(A/A^{\bullet-})] - E_{photon} \quad (3.2)$$

$$\Delta G°_{BET} = e[E°(A/A^{\bullet-}) - E°(D^{\bullet+}/D)] \quad (3.3)$$

where e is the elementary charge, $E°$ is the standard reduction potential for the donor (D) and acceptor (A) couples shown, and E_{photon} is the photon energy of the pump wavelength. With O as the donor and A as the acceptor, this calculation predicts favorable FET with both 265 (4.68 eV) and 295 nm (4.20 eV) excitation.[29] These considerations led us to obtain TD-DFT calculations for the vibrational transitions of the O radical cation, A radical anion, and the lowest couple electronic excited-states in d(OA).

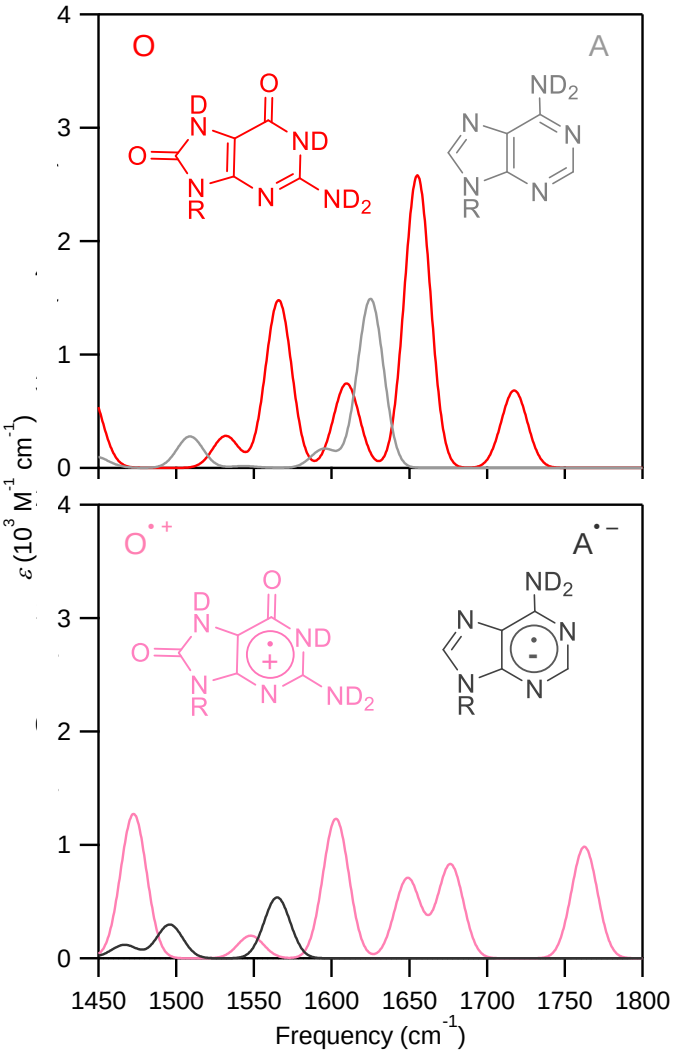


Figure 3.8. Calculated vibrational spectra obtained using PCM/PBE0/6-31+G(d,p) and the harmonic approximation for the monomer species illustrated by inset chemical structures. The frequency is scaled by a factor of 0.972. Note that the calculations were performed on the structures shown (R = 2'-deoxyribose) including 5 explicit D_2O molecules not shown. Adapted from ref 29.

Time-dependent calculations located an excited state with well-defined CT character in d(OA) that lies close in energy with the optically accessed excited states of O and A.[29] Optimization of this state led to a minimum with strong CT character and a small interbase separation. The calculated vibrational transitions of the O radical cation and A

radical anion are compared with the calculated ground-state vibrational transitions of O and A in Figure 3.8. The theoretical difference spectrum, obtained by subtracting the sum

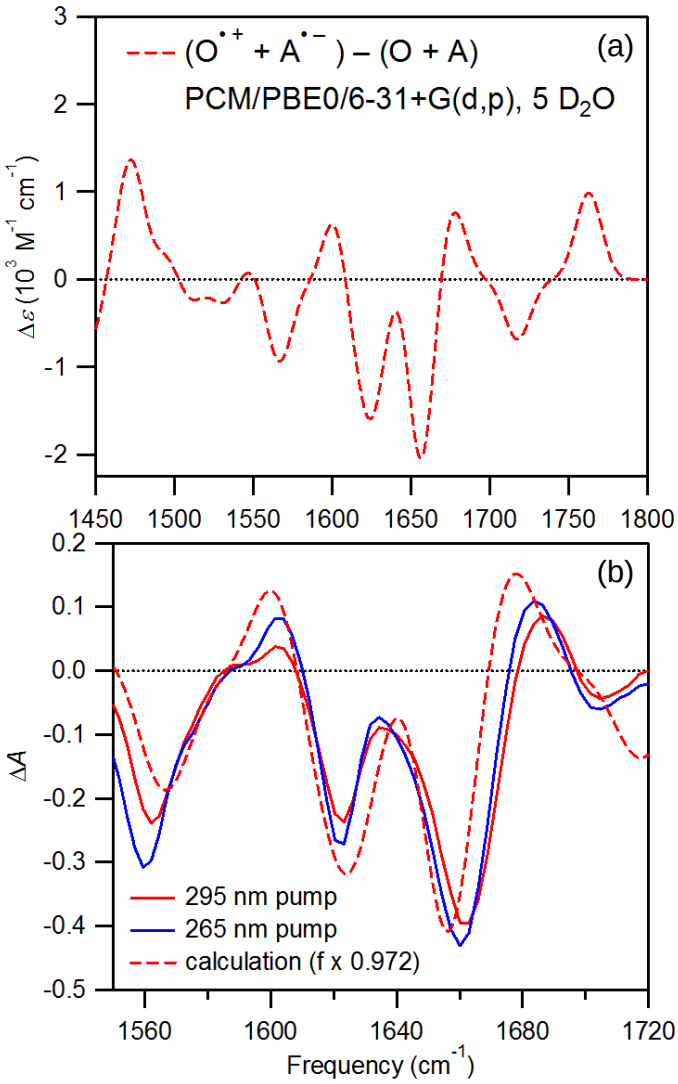


Figure 3.9. Theoretically calculated difference spectrum obtained by subtracting the sum of the calculated radical ion spectra from the sum of the calculated ground-state spectra. The lower panel shows the calculated difference spectrum compared to the experimental difference spectra after 295 (red trace) and 265 nm (blue trace) excitation. Adapted from ref 29.

of the radical ion spectra from the sum of the ground-state spectra (Figure 3.9(a)), is overlaid with the 265 and 295 nm experimental difference spectra of d(OA) at 60 ps in Figure 3.9(b). The excellent agreement between the calculated and experimental spectra indicates that the ESA signals observed in the d(OA) TRIR spectra are due to absorption by the radical ion species generated upon photoinduced ET from O to A.

The radical ion absorption signals reach maximum at the earliest delay times in Figure 3.5, suggesting that forward ET occurs on a timescale <1 ps and that the 60 ps decay lifetime corresponds to back ET. Based on the our estimates for the thermodynamic driving forces for forward and back ET, the latter is the more exergonic process, with $\Delta G°_{BET} = -3.62$ eV compared to $\Delta G°_{FET} = -1.06$ and -0.58 eV at 265 and 295 nm, respectively.[29] These Gibbs energies predict that back ET should be the faster process. However, the Gibbs energy for forward ET is nearly equal to the reorganization energy,[29] and would be a barrierless, and thus ultrafast, process.[29] We propose that forward ET occurs in d(OA) on a timescale faster than the time resolution of our instrument (<0.5 ps) because we do not observe the corresponding ultrafast lifetime component. The more exergonic BET process exhibits the longer lifetime (slower rate) because it is predicted to occur in the Marcus inverted region, where the rates for CT processes decrease as the exergonicity increases.[83]

3.4.3 Connections to Long-Lived Transient Signals in Natural DNA

Within higher-order DNA structures, noncovalent interactions alter the electrostatic and steric environments of the monomer bases when they are linked together. Experimentally isolating the individual effects these noncovalent interactions have on DNA excited-state dynamics in solution is complicated by several factors.[22] In addition to

ambiguous interpretations of the data, there are unavoidable physical limitations. Base-stacking dynamics remain unclear due to the structural heterogeneity of single strands and uncertainty in the number of stacked bases in each strand.[26, 84] Single base pairs do not form in aqueous solution without the bases stacking. Thus, determining the influence solely due to hydrogen bonding on DNA excited-state deactivation is difficult, if not impossible, to determine in water. Despite these challenges, extensive experimental and theoretical work over the last 5 years has led to a more detailed understanding of the nature of long-lived excited states accessed in DNA strands.

3.4.3.1 Photoinduced Charge Transfer in Single DNA Strands. The excited-state dynamics of d(OA) provide strong evidence that the long-lived 60 ps transient signal observed is due to decay from a CT state composed of an O radical cation and an A radical anion. Figure 3.6 and Table 3.1 show that the amplitude of the 60 ps component is 4-times greater after 265 nm excitation. Because the excited-state population fully returns to the ground state, the amplitudes of this decay component represent rough approximations of the excited-state population of the CT state after each pump wavelength. The greater amplitude of the 60 ps component after 265 nm excitation indicates that the quantum yield for CT state population is higher at the shorter excitation wavelength.

The natural bases absorb more strongly near 265 nm, exhibit similar excited-state kinetics in long-lived transient signals, and are thermodynamically capable of undergoing photoinduced ET.[29, 64] Given these considerations, and the results presented in this chapter, photoinduced population of CT states may occur with relatively high efficiency in natural DNA base stacks, in addition to the oxidatively damaged DNA presented here. Other

groups have spectroscopically identified species generated from photoinduced ET in DNA and also attribute the long-lived transient signals to CT states.[32-34] Doorley et al. observed vibrational signatures of A radical cation and T radical anion generated by photoinduced ET from A to T in a dinucleotide containing the two bases.[32] Another group identified CT states in single DNA strands by observing characteristic absorption bands of radical cations and anions.[33]

These studies have initiated a growing agreement among researchers that the long-lived TA signals in DNA are due to CT states, but there is still uncertainty regarding the spatial extent of the CT state.[23, 33] For instance, Buchvarov et al. attributed their observation of length-dependent ESA signals in single- and double-stranded DNA to exciton delocalization.[27] Other groups, including ours, do not observe any evidence to suggest charge delocalization in DNA strands.[34, 64, 85-86] Identical long-lived TA signals were observed in a series of A-containing oligonucleotide strands ranging in length from 2 – 18 bases, indicating that the same excited state is accessed between a minimum of two stacked bases.[26] Theoretical calculations revealed a minimum CT state geometry consisting of only two stacked bases in 9-methyladenine trimers.[87]

The base-stacked architecture of DNA strands enables deactivation via the formation of CT states, and this same structural feature may inhibit charge delocalization. Long-lived excited states that result from intrastrand ET are only observed when bases in single-stranded DNA are π-stacked. ET rates decrease exponentially with distance so it is only when the bases are in van der Waals contact (3.4 Å) that this channel can compete with the non-radiative decay channels in single bases (Figure 1.4). Disrupting base-

stacking by means of repulsion[26] or by adding a denaturant[49] completely eliminates the ET decay channel, demonstrating its short-range character. Consequently, the charge-separated state consists of closely-spaced oppositely charged nucleobase ions. The Coulombic binding energy of the opposite charges is generally much greater than thermal energy, making separation of the nascent charges very unlikely. The opposite charges would need about 20-times thermal energy at room temperature to overcome the Coulombic attraction and dissociate from one another. In addition, the long-lived lifetimes attributed to CT states in single and double strands fully decay to the ground state.[25-26, 88] The absence of additional decay signals indicates that the vast majority of CT states deactivate via back ET. If delocalization does occur, the percentage of charges that separate from one another is so small we do not detect this channel within our instrumental resolution.

3.4.3.2 Proton Transfer and Proton-Coupled Electron Transfer in Duplexes. Presently, the nature of excited states in double strands remains unclear. There is evidence indicating that the base-pairing interaction can have a profound influence on the excited-state dynamics. Theoretical studies have identified proton-transfer coordinates in the deactivation of single base pairs,[89-90] and lifetime measurements of single base pairs in the gas phase and chloroform solution suggest that interbase proton transfer aids in UIC.[91-94] Despite this evidence, a precise understanding of the relative influences of base-stacking and base-pairing on duplex DNA excited-state deactivation in solution is lacking, which has led to different interpretations.

One viewpoint holds that the deactivation rates are more dependent on the base-

pairing interaction.[37] Conversely, deactivation via the base-stacking interaction could be rate-limiting in DNA excited-state deactivation.[25] Our group presented femtosecond TA measurements of DNA showing that the same long-lived transient signals were present in both single and double strands, leading us to propose that base-stacking predominantly drives DNA excited-state deactivation.[25]

Recently, we revisited the defined-sequence DNA duplexes investigated in ref 25 using TRIR spectroscopy, which provides data that can be easier to interpret (see Chapter 2). Duplex isomers containing the same number of A and T base pairs but with alternating or non-alternating A-T base stacking patterns showed strikingly different TRIR spectra and corresponding kinetics.[35] In light of the new TRIR results and our previous findings in d(OA), we obtained calculations for the different possible transient species that could be formed via intrastrand ET, interstrand ET or proton-coupled ET (PCET), as determined by our estimated thermodynamic driving forces for the various forms of ET. Agreement between the calculated and experimental vibrational marker bands confirmed that intrastrand ET and PCET are responsible for excited-state deactivation of the alternating and non-alternating A-T duplexes, respectively.[35]

Our conclusions were validated by conducting TRIR spectroscopic studies on several other DNA double strands, including G-C-containing DNA duplexes with different base-pairing interactions (Hoogsteen vs. Watson-Crick (W-C) base pairing) and duplexes with different base-stacking interactions (B- vs. Z-form base stacking).[35-36, 38] Our investigation of these duplexes revealed that, although the deactivation mechanisms are different in Hoogsteen vs. W-C and B- vs. Z-form duplexes, the lifetimes are the same in

each set.[36] This observation explains why an earlier TA spectroscopic study of the same duplexes showed no difference in deactivation lifetimes between the compared forms,[95] and indicates that intrastrand ET is the rate-determining step in the deactivation mechanism in these G-C-based duplexes.[36]

3.5 Conclusion

The excited-state dynamics of O, as a monomer nucleoside and in a dinucleotide with A, were studied using ultrafast spectroscopic techniques. To investigate to possibility of photoinduced ET, the dynamics were monitored using TRIR spectroscopy after selective excitation of O. Our results reveal the photoinduced generation of an O radical cation and an A radical anion in d(OA). This CT state decays via back ET on a timescale of about 60 ps. The rates of forward and back ET are consistent with those predicted by nonadiabatic Marcus theory. Our observation of vibrational marker bands for radical ion species generated by photoinduced ET has validated that O can undergo excited-state ET and has helped to resolve a decades-long debate over the nature of long-lived excited states in DNA.

3.6 References

63. Crespo-Hernández, C. E.; Cohen, B.; Hare, P. M.; Kohler, B., Ultrafast Excited-State Dynamics in Nucleic Acids. *Chem. Rev.* **2004**, *104*, 1977-2019.

64. Takaya, T.; Su, C.; de La Harpe, K.; Crespo-Hernández, C. E.; Kohler, B., UV Excitation of Single DNA and RNA Strands Produces High Yields of Exciplex States Between Two Stacked Bases. *Proc. Natl. Acad. Sci. U.S.A.* **2008**, *105*, 10285-10290.

65. Steenken, S.; Jovanovic, S. V.; Bietti, M.; Bernhard, K., The Trap Depth (in DNA) of 8-Oxo-7,8-dihydro-2'-deoxyguanosine as Derived from Electron-Transfer Equilibria in Aqueous Solution. *J. Am. Chem. Soc.* **2000**, *122*, 2373-2374.

66. Steenken, S.; Jovanovic, S. V., How Easily Oxidizable is DNA? One-Electron Reduction Potentials of Adenosine and Guanosine Radicals in Aqueous Solution. *J. Am. Chem. Soc.* **1997**, *119*, 617-618.

67. Liu, Z.; Tan, C.; Guo, X.; Kao, Y.-T.; Li, J.; Wang, L.; Sancar, A.; Zhong, D., Dynamics and Mechanism of Cyclobutane Pyrimidine Dimer Repair by DNA Photolyase. *Proc. Natl. Acad. Sci. USA* **2011**, *108*, 14831-14836.

68. Adamo, C.; Barone, V., Toward Reliable Density Functional Methods Without Adjustable Parameters: The PBE0 Model. *J. Chem. Phys.* **1999**, *110*, 6158-6170.

69. Tomasi, J.; Mennucci, B.; Cammi, R., Quantum Mechanical Continuum Solvation Models. *Chem. Rev.* **2005**, *105*, 2999-3093.

70. Zhao, Y.; Truhlar, D. G., Density Functionals with Broad Applicability in Chemistry. *Acc. Chem. Res.* **2008**, *41*, 157-167.

71. Scalmani, G.; Frisch, M. J.; Mennucci, B.; Tomasi, J.; Cammi, R.; Barone, V., Geometries and Properties of Excited States in the Gas Phase and in Solution: Theory and Application of a Time-Dependent Density Functional Theory Polarizable Continuum Model. *J. Chem. Phys.* **2006**, *124*, article no. 94107.

72. Culp, S. J.; Cho, B. P.; Kadlubar, F. F.; Evans, F. E., Structural and Conformational Analyses of 8-Hydroxy-2'-Deoxyguanosine. *Chem. Res. Toxicol.* **1989**, *2*, 416-422.

73. Jayanth, N.; Ramachandran, S.; Puranik, M., Solution Structure of the DNA Damage Lesion 8-Oxoguanosine from Ultraviolet Resonance Raman Spectroscopy. *J. Phys. Chem. A* **2009**, *113*, 1459-1471.

74. Karunakaran, V.; Kleinermanns, K.; Improta, R.; Kovalenko, S. A., Photoinduced Dynamics of Guanosine Monophosphate in Water from Broad-Band Transient Absorption Spectroscopy and Quantum-Chemical Calculations. *J. Am. Chem. Soc.* **2009**, *131*, 5839-5850.

75. Zhang, Y.; Dood, J.; Beckstead, A.; Chen, J.; Li, X.-B.; Burrows, C. J.; Lu, Z.; Matsika, S.; Kohler, B., Ultrafast Excited-State Dynamics and Vibrational Cooling of 8-Oxo-7,8-dihydro-2 '-deoxyguanosine in D2O. *J. Phys. Chem. A* **2013**, *117*, 12851-12857.

76. Cohen, B.; Hare, P. M.; Kohler, B., Ultrafast Excited-State Dynamics of Adenine and Monomethylated Adenines in Solution: Implications for the Nonradiative Decay Mechanism. *J. Am. Chem. Soc.* **2003**, *125*, 13594-13601.

77. Zhang, Y.; Improta, R.; Kohler, B., Mode-Specific Vibrational Relaxation of Photoexcited Guanosine 5 '-Monophosphate and its Acid Form: a Femtosecond Broadband Mid-IR Transient Absorption and Theoretical Study. *Phys. Chem. Chem. Phys.* **2014**, *16*, 1487-1499.

78. Lu, Z.; Beckstead, A. A.; Kohler, B.; Matsika, S., Excited State Relaxation of Neutral and Basic 8-Oxoguanine. *J. Phys. Chem. B* **2015**, *119*, 8293-8301.

79. Onidas, D.; Markovitsi, D.; Marguet, S.; Sharonov, A.; Gustavsson, T., Fluorescence Properties of DNA Nucleosides and Nucleotides: A Refined Steady-State and Femtosecond Investigation. *J. Phys. Chem. B* **2002**, *106*, 11367-11374.

80. Changenet-Barret, P.; Gustavsson, T.; Improta, R.; Markovitsi, D., Ultrafast Excited-State Deactivation of 8-Hydroxy-2 '-deoxyguanosine Studied by Femtosecond Fluorescence Spectroscopy and Quantum-Chemical Calculations. *J. Phys. Chem. A* **2015**, *119*, 6131-6139.

81. Shukla, M. K.; Leszczynski, J., Electronic Spectra, Excited State Structures and Interactions of Nucleic Acid Bases and Base Assemblies: a Review. *J. Biomol. Struct. Dyn.* **2007**, *25*, 93-118.

82. Zhang, Y.; Dood, J.; Beckstead, A. A.; Li, X.-B.; Nguyen, K. V.; Burrows, C. J.; Improta, R.; Kohler, B., Photoinduced Electron Transfer in DNA: Charge Shift Dynamics Between 8-Oxo-Guanine Anion and Adenine. *J. Phys. Chem. B* **2015**, *119*, 7491-7502.

83. Gould, I. R.; Moser, J. E.; Armitage, B.; Farid, S., Electron-Transfer Reactions in the Marcus Inverted Region: Charge Recombination vs. Charge Shift Reactions. *J. Am. Chem. Soc.* **1989**, *111*, 1917-1919.

84. Remington, J. M.; Philip, A. M.; Hariharan, M.; Kohler, B., On the Origin of Multiexponential Fluorescence Decays from 2-Aminopurine-Labeled Dinucleotides. *J. Chem. Phys.* **2016**, *145*, article no. 155101.

85. Wan, C.; Fiebig, T.; Schiemann, O.; Barton, J. K.; Zewail, A. H., Femtosecond Direct Observation of Charge Transfer Between Bases in DNA. *Proc. Natl. Acad. Sci. U. S. A.* **2000**, *97*, 14052-14055.

86. Kuimova, M. K.; Dyer, J.; George, M. W.; Grills, D. C.; Kelly, J. M.; Matousek, P.; Parker, A. W.; Sun, X. Z.; Towrie, M.; Whelan, A. M., Monitoring the Effect of Ultrafast Deactivation of the Electronic Excited States of DNA Bases and Polynucleotides Following

267 nm Laser Excitation Using Picosecond Time-Resolved Infrared Spectroscopy. *Chem. Commun.* **2005**, *9*, 1182-1184.

87. Santoro, F.; Barone, V.; Improta, R., Influence of Base Stacking on Excited-State Behavior of Polyadenine in Water, Based on Time-Dependent Density Functional Calculations. *Proc. Natl. Acad. Sci. USA* **2007**, *104*, 9931-9936.

88. de La Harpe, K.; Crespo-Hernández, C. E.; Kohler, B., Deuterium Isotope Effect on Excited-State Dynamics in an Alternating GC Oligonucleotide. *J. Am. Chem. Soc.* **2009**, *131*, 17557-17559.

89. Sobolewski, A. L.; Domcke, W., Ab Initio Studies on the Photophysics of the Guanine-Cytosine Base Pair. *Phys. Chem. Chem. Phys.* **2004**, *6*, 2763-2771.

90. Perun, S.; Sobolewski, A. L.; Domcke, W., Role of Electron-Driven Proton-Transfer Processes in the Excited-State Deactivation Adenine-Thymine Base Pair. *J. Phys. Chem. A* **2006**, *110*, 9031-9038.

91. Abo-Riziq, A.; Grace, L.; Nir, E.; Kabelac, M.; Hobza, P.; de Vries, M. S., Photochemical Selectivity in Guanine-Cytosine Base-Pair Structures. *Proc. Natl. Acad. Sci. USA* **2005**, *102*, 20-23.

92. Schwalb, N. K.; Temps, F., Ultrafast Electronic Relaxation in Guanosine is Promoted by Hydrogen Bonding with Cytidine. *J. Am. Chem. Soc.* **2007**, *129*, 9272-9273.

93. Schwalb, N. K.; Michalak, T.; Temps, F., Ultrashort Fluorescence Lifetimes of Hydrogen-Bonded Base Pairs of Guanosine and Cytidine in Solution. *J. Phys. Chem. B* **2009**, *113*, 16365-16376.

94. Roettger, K.; Marroux, H. J. B.; Grubb, M. P.; Coulter, P. M.; Boehnke, H.; Henderson, A. S.; Galan, M. C.; Temps, F.; Orr-Ewing, A. J.; Roberts, G. M., Ultraviolet Absorption Induces Hydrogen-Atom Transfer in G center dot C Watson-Crick DNA Base Pairs in Solution. *Angew. Chem. Int. Ed.* **2015**, *54*, 14719-14722.

95. de La Harpe, K.; Crespo-Hernández, C. E.; Kohler, B., The Excited-State Lifetimes in a G•C DNA Duplex are Nearly Independent of Helix Conformation and Base-Pairing Motif. *ChemPhysChem* **2009**, *10*, 1421-1425.

CHAPTER FOUR

PHOTOINDUCED ELECTRON TRANSFER IN OXIDATIVELY DAMAGED PYRIMIDINES

4.1 Introduction

Oxidative stress is one of the primary detriments to maintaining genetic integrity in biological systems. In oxidizing environments, the electron-rich nucleobases that comprise RNA and DNA undergo one-electron oxidation reactions to form stable degradation products.[39] Oxidatively damaged products can be formed either endogenously by reactions with hydroxyl radicals generated through aerobic metabolism,[96] or exogenously by ionizing radiation. 5-hydroxy-2'-deoxycytidine (5-HC) and 5-hydroxy-2'-deoxyuridine (5-HU), oxidative products of C and U, have been detected in significant quantities in oxidatively damaged DNA.[96-98] 5-HC and 5-HU are highly mutagenic because they can base pair with more than one partner.[99-101] In addition, 5-HC and 5-HU have lower reduction potentials than their canonical counterparts (0.78 and 0.80 V compared to 1.6 and 1.7 V vs, NHE, respectively),[66, 98] making them more redox active and thus more susceptible to undergoing further reactions, including those that may lead to strand scission.[39]

Lower levels of ozone in the Archean atmosphere resulted in higher levels of solar UV radiation reaching the Earth's surface than present-day.[102] The excess UV radiation may have produced an environment rich with hydrogen peroxide, which under further high-energy UV irradiation would have continually degraded into hydroxyl radicals via

photolysis.[103] Consequently, oxidatively damaged nucleobases may have accumulated at higher concentrations than their canonical forms on the prebiotic Earth.[4, 31] Their enhanced redox activity may have enabled oxidatively damaged nucleobases to participate in catalytic functions during prebiotic chemical evolution.[29-31]

A remaining question in origin of life theories stems from the RNA world hypothesis, which proposes that RNA genetic material preceded modern DNA.[104] Based on the known catalytic functions of modern RNA,[105] primitive RNA oligonucleotides could have driven the earliest replication and catalytic functions prior to the advent of protein synthesis.[106-107] However, it remains unclear how UV-vulnerable RNA strands were repaired after being oxidized and photodamaged without the use of intricate repair enzymes. For instance, the flavin in the flavin adenine dinucleotide (FAD) redox cofactor in modern-day photolyase is synthesized through a series of complex mechanistic steps that were presumably not available to prebiotic chemistry.[31] 8-Oxo-7,8-dihydro-2'-deoxyguanosine (O), an oxidatively damaged product of guanine, has been proposed to be a prebiotic flavin mimic as it can repair cyclobutane pyrimidine dimers by donating an electron to the photoproducts upon absorption of UV radiation.[30-31] We demonstrated that O can indeed donate an electron to its π-stacked neighbor after UV excitation (Chapter 3), confirming its photoinduced electron-donating ability.[29, 82]

The reduction potentials of 5-HC and 5-HU are remarkably similar in magnitude with that of O (0.74 V vs. NHE).[65] Their ability to facilitate ET has previously been inferred by their catalysis of the coupled oxidoreductive reaction of NADH with $K_3Fe(CN)_6$,[97-98] but their excited-state properties in aqueous solution have yet to be evaluated. Presented in

this chapter is an ultrafast spectroscopic investigation of the aqueous excited-state dynamics of 5-HC and 5-HU as monomer nucleosides and as dinucleotides with A, d(5-HCA) and d(5-HUA) (structures in Figure 4.1). We characterized the photophysics of the monomer nucleosides using steady-state absorption and fluorescence, then UV pump / visible probe TA and UV pump / broadband mid-IR probe TRIR spectroscopies. The excited-state lifetimes and fluorescence quantum yields of 5-HC and 5-HU in aqueous solution are reported for the first time. After selective excitation of the C5-hydroxylated pyrimidines within the dinucleotides, we observed photoinduced ET from the 5-hydroxypyrimidine electron donors to the A electron acceptors using TRIR. The observed rates reflect the asymmetry typical of ET kinetics in the Marcus inverted region.[29, 82]

4.2 Experimental

5-HC and 5-HU (≥ 95%) were purchased from Berry and Associates, Inc. The dinucleotides d(5-HCA) and d(5-HUA) were synthesized and characterized by Dr. Xi-Bo Li from the Cynthia J. Burrows research group at The University of Utah in Salt Lake City according to the full synthesis and characterization procedure described previously.[29] The 5-HC / AMP and 5-HU / AMP samples were prepared by mixing equimolar amounts of 5-HC and 5-HU with AMP to match the amount of each nucleoside in d(5-HCA) and d(5-HUA), which were donated in amounts of 14 μmol and 24 μmol, respectively. All samples were dissolved as received in 2 mL D_2O phosphate buffer solutions in concentrations pertaining to the different spectroscopic measurements, as described in Chapter 2. As 5-HC and 5-HU have pK_a values near neutral pH,[108] all experiments were conducted in pD 6

buffered solutions to ensure the solutes were in their uncharged, deuterated forms. Solutions were adjusted to pD = 6, as described in Chapter 2.

UV absorption and FTIR spectra were recorded before and after laser irradiation. Steady-state emission spectra were measured using solutions of 5-HC and 5-HU in pH = 6 deionized H_2O without buffer or salt (see Chapter 2). The optical densities of the solutions were kept at 0.2 at the excitation wavelength (285 nm) to avoid reabsorption of emitted photons. Emission intensity was collected every 2.5 nm after 20.0 s integration with 3.0 nm bandpass slit widths. Temperature-dependent CD spectra were collected using 1 mM solutions in a 1 mm path length quartz capped cuvette.

TA and TRIR instrumentation are thoroughly discussed in Chapter 2 of this thesis. Specifically, the 266 nm pump beam used in UV pump / visible probe TA experiments was produced by third harmonic generation of the 800 nm laser fundamental. The pump energy at the sample was attenuated to 0.9 μJ with a spot size of 250 μm (fwhm). An OPA was used to generate the probe beam at 570 nm. An OPA was used to generate the 265 nm and 295 nm pump pulses used in the TRIR experiments. The pump pulse energy was attenuated to 3.0 μJ with a spot size of 640 μm (fwhm) for 265 nm and to 1.5 μJ with a spot size of 310 μm (fwhm) for 295 nm. About 8-10 mW of mid-IR probe pulses centered at either 1626 or 1470 cm^{-1} with approximately 200 cm^{-1} bandwidth were produced using the TOPAS amplifier described in Chapter 2.

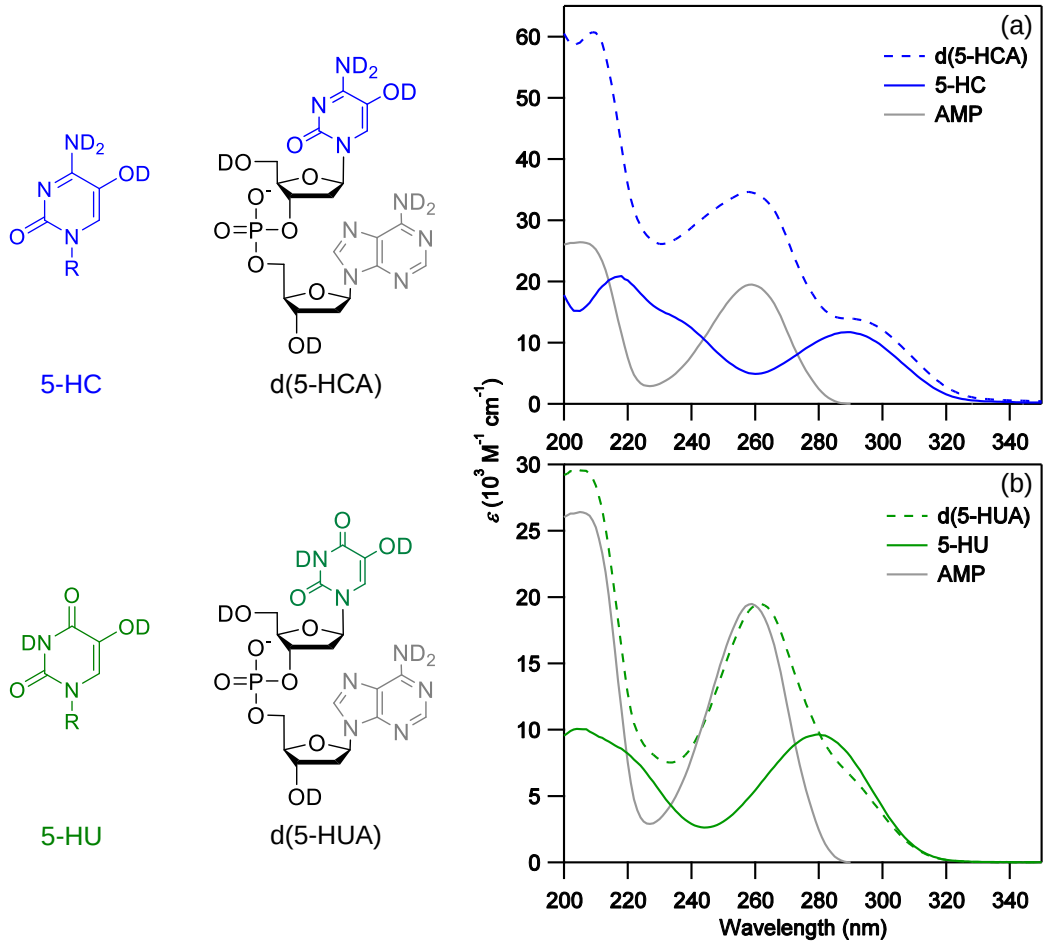


Figure 4.1. Chemical structures of 5-hydroxy-2'-deoxycytidine (5-HC), 5-hydroxy-2'-deoxyuridine (5-HU) with R = 2'-deoxyribose and dinucleotides with adenine, d(5-HCA) and d(5-HUA) are shown on the left. All labile protons have been substituted with deuterons. UV absorption spectra of d(5-HCA) (a) and d(5-HUA) (b) dinucleotides. The UV absorption spectra of their monomer constituents, including adenosine 3'-monophosphate (AMP), are also shown in solid lines.

4.3 Results

Both 5-hydroxypyrimidines have pK_a values near neutral pH (pK_a = 7.4 for 5-HC and 7.7 for 5-HU).[108] Our experiments were carried out at pD = 6.0, where the C5 hydroxyl group is predominantly protonated in both 5-hydroxypyrimidines (96% and 98% for 5-HC

and 5-HU, respectively). It is important to note that 5-HC has a lower pK_a at 3.8.[108] Caution was taken to ensure that the pD value was not too low to protonate the N3 position. In the dinucleotides, only the 5-hydroxypyrimidines are protonated at pD = 6 as protonation of adenine at the N1 position also occurs at lower pH (pK_a = 3.5).[109]

In DMSO, amino 5-HC and diketo 5-HU are the dominant tautomeric forms.[110] It is reasonable to assume that these are also the dominant forms of 5-HC and 5-HU in low pH aqueous solutions, in which the C5 hydroxyls are fully protonated. Hydroxyl group substitutions are electron-withdrawing, and electron-donating when deprotonated. At high pH, the deprotonated C5 hydroxyl renders the N3 of 5-HC more basic than the N4, and when the latter donates an electron to the former the imino tautomer becomes dominant.[111] Thus, in the case of 5-HC, the amino tautomeric form is likely dominant due to the protonated C5-hydroxyl. Furthermore, theoretical calculations have predicted that C5 substitutions, including C5 hydroxyl substitutions, do not appreciably alter the dominant tautomeric forms of aqueous cytosine and uracil, which are the amino and diketo forms, respectively.[112-113]

Panels (a) and (b) in Figure 4.1 show the UV absorption spectra of the 5-hydroxypyrimidine monomers and dinucleotides in pD = 6 D_2O phosphate buffer solutions superimposed with the absorption spectrum of AMP in D_2O phosphate buffer solution. The first absorption bands of 5-HC in Figure 4.1(a) and of 5-HU in Figure 4.1(b) have maxima (λ_{max}^{abs}) at 289 and 280 nm, respectively, as listed in Table 4.1. Our measured spectra are consistent with the pH-dependent absorption spectra observed previously for 5-HC and 5-HU in aqueous solution.[108, 111] The dinucleotide spectra (dashed lines in Figures 4.1(a) and

(b)) are approximately the sum of the absorption spectra of the monomeric 5-hydroxypyrimidine and AMP. Only the 5-hydroxypyrimidines absorb when the dinucleotides are excited at 295 nm, whereas 265 nm excites predominantly the adenine chromophore.

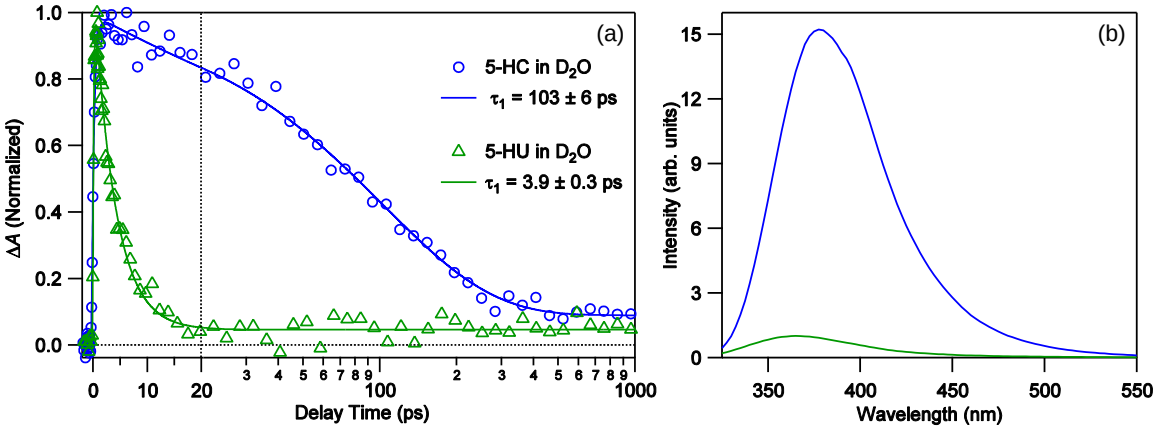


Figure 4.2. Normalized 266 nm pump / 570 nm probe TA kinetics of 5-HC (blue circles) and 5-HU (green triangles) in pD = 6 D_2O phosphate buffer solution (a). Monoexponential kinetic fits are shown as the solid lines. Steady-state fluorescence spectra of 5-HC (blue trace) and 5-HU (green trace) in pH = 6 deionized H_2O (b).

4.3.1 5-Hydroxycytidine and 5-Hydroxyuridine Monomers

4.3.1.1 UV Pump / Visible Probe TA and Steady-State Emission. Figure 4.2(a) displays the ESA kinetics of the monomer 5-hydroxypyrimidines monitored at 570 nm after 266 nm excitation. This probe wavelength interrogates the S_1 excited-state lifetimes of nucleobases[21] without complication from vibrational cooling (VC), which is often observed when monitoring GSB and hot ground-state absorption. The latter is red-shifted with respect to the absorption by the thermally equilibrated ground state (UV absorption spectrum). Solvated electron signal generated from two-photon ionization of the D_2O

solvent was determined by a sequential experiment and was subtracted from the transient absorption signals shown in Figure 4.2(a) using the subtraction procedure described in Chapter 2. The kinetics for both 5-HC (open blue circles) and 5-HU (open green triangles) decay monoexponentially to weak positive offsets. Monoexponential fits (solid lines in Figure 4.2(a)) yield time constants of τ = 103 ± 6 ps for 5-HC and τ = 3.9 ± 0.3 ps for 5-HU, with respective offsets consisting of 9% and 4% of the total signal amplitudes.

Figure 4.2(b) shows corrected steady-state emission spectra for 5-HC and 5-HU in deionized H_2O at pH = 6 (see Experimental). 5-HC is significantly more emissive than 5-HU. Using GMP as a reference standard,[79] fluorescence quantum yields were calculated using eqn. (3.1) and the comparative method after excitation of 5-HC, 5-HU and GMP at 285 nm.[78, 114] Listed in Table 4.1, the measured fluorescence quantum yields (ϕ_{fl}) are 70 × 10^{-4} and 4.6 × 10^{-4} and the maximum emission wavelengths (λ_{max}^{fl}) are 378 and 365 nm for 5-HC and 5-HU, respectively. The Stokes shifts ($\Delta\tilde{\nu}$), defined as the absorption maximum minus the emission maximum in wavenumbers, are 8147 cm^{-1} for 5-HC and 8317 cm^{-1} for 5-HU.

Table 4.1. Maximum wavelengths of the first absorption (abs) and fluorescence (fl) bands, Stokes shifts ($\Delta\tilde{\nu}$), fluorescence quantum yields (ϕ_{fl}) and ESA lifetimes (τ) of 5-HC and 5-HU compared to C and U.

	λ_{max}^{abs} [a] (nm)	λ_{max}^{fl} [a] (nm)	$\Delta\tilde{\nu}$ [b] (cm^{-1})	$\phi_{fl} \times 10^4$ [a]	τ_1 [a] (ps)
5-HC	289	378	8147	70	103 ± 6
C[e]	272[c]	328[c]	6277	1.2[c]	0.720[d]
5-HU	280	365	8317	4.6	3.9 ± 0.3
U[e]	262[d]	317[d]	6622	0.3[d]	0.210[d]

[a]Experimental values from this work unless otherwise indicated. [b]Stokes shifts calculated as the difference of absorption and fluorescence maxima in wavenumbers. [c]From ref 79. [d]From ref 118. [e]Experimental values for C and U in nucleoside form.

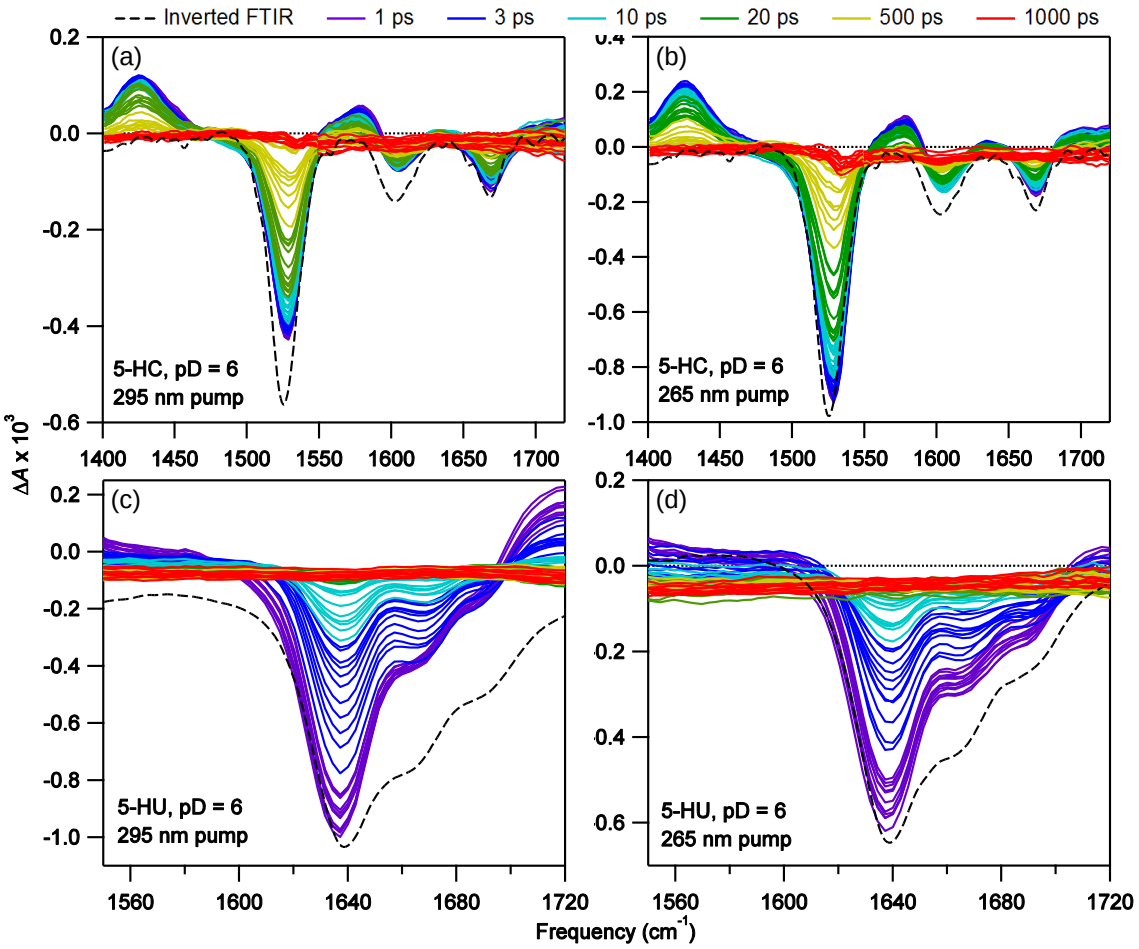


Figure 4.3. TRIR spectra of 10 mM 5-HC (a,b) and 5-HU (c, d) in pD = 6 D_2O phosphate buffer solution after 295 (a,c) and 265 nm (b,d) excitation. The baseline is indicated by the dotted horizontal lines at $\Delta A = 0$. Ground-state IR absorption of 5-HC and 5-HU are shown in the inverted FTIR spectra (dashed traces).

4.3.1.2 UV Pump / Mid-IR Probe TRIR. Broadband TRIR spectra at various delay times of the 5-hydroxyprimidine monomers in pD = 6 D_2O phosphate buffer solution are displayed in Figure 4.3. 5-HC and 5-HU spectra were collected after 295 and 265 nm excitation with broadband mid-IR probing in the ring in-plane vibration and carbonyl stretching regions of the vibrational spectrum. Note that the spectra for 5-HC (Figures 4.3(a) and (b)) are a composite of two spectral regions centered at 1626 and 1470 cm^{-1},

whereas the spectra for 5-HU (Figures 4.3(c) and (d)) were collected in one region centered at 1626 cm^{-1}. All spectra are shown from 1 ps delay time (first purple trace), when the positive and negative signals are at maximum amplitude, to 1 ns (last red trace), when all signals recover to a featureless negative offset arising from D_2O heating.[48, 115] The dotted horizontal lines at the $\Delta A = 0$ are included to indicate the ground-state baseline.

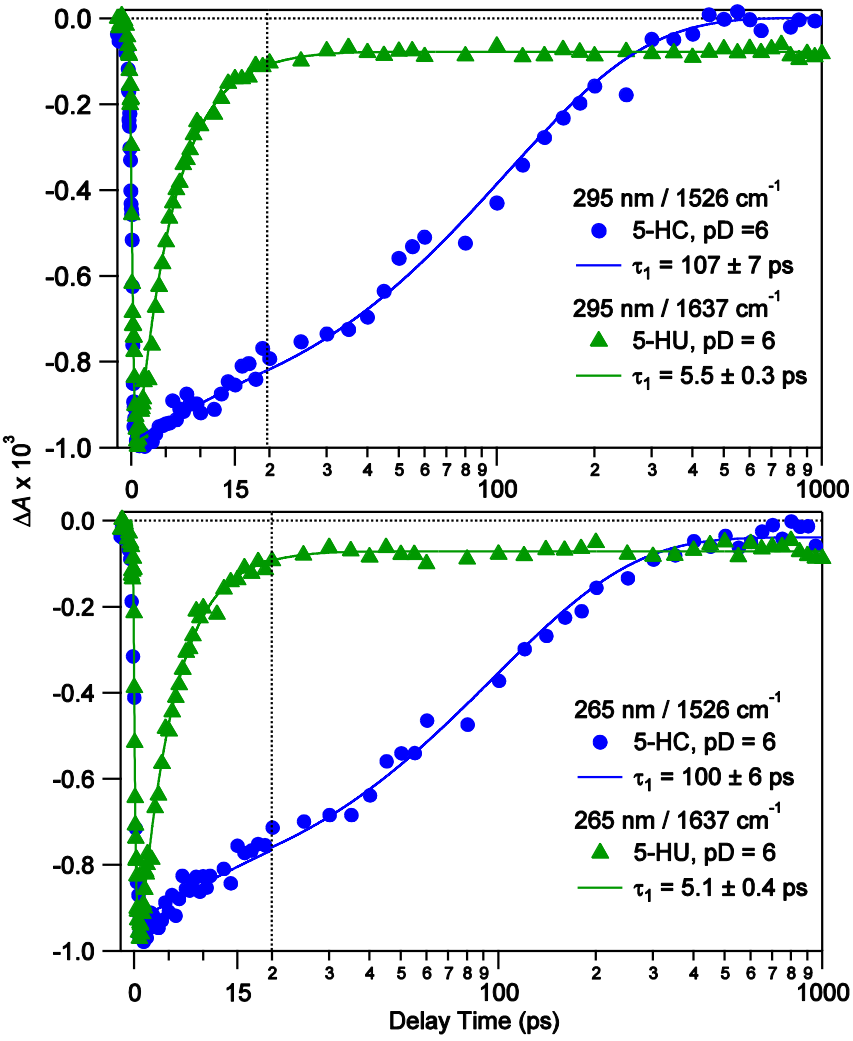


Figure 4.4. Normalized kinetic decay traces of 5-HC (closed blue circles) and 5-HU (closed green triangles) from TRIR GSB bands at 1526 and 1637 cm^{-1}, respectively, after 295 (a) and 265 nm (b) excitation. All kinetics were fit to monoexponential functions with negative offsets (solid traces) producing the time constants indicated.

At both pump wavelengths, the two sets of spectra for 5-HC are essentially identical. The spectra contain positive features due to ESA and three distinct negative bands. Figures 4.3(a,b) show the inverted FTIR spectrum of 5-HC at pD = 6 overlaid with the TRIR spectra. The negative TRIR signals at 1525, 1603 and 1669 cm^{-1} match those observed in the FTIR spectrum and thus represent GSB signals. Note that deprotonated 5-HC exhibits a distinguishing vibrational band at 1652 cm^{-1}, which is attributed to the C2 carbonyl of the imino tautomeric form that is dominant at high pH.[111] The absence of this band in the 5-HC FTIR spectrum shown in Figure 4.3(a) is further validation that the amino form of 5-HC is dominant at pD = 6.

ESA is minimal in the spectral probing region shown for 5-HU, although the positive band at 1720 cm^{-1} has a greater amplitude after 295 nm excitation. The inverted FTIR spectrum of 5-HU at pD = 6 shown in Figures 4.3(c,d) exhibits a strong vibrational band at 1639 cm^{-1} with two shoulders on the higher frequency edge. Again, the negative features in the TRIR appear at the same frequencies as the ground-state IR transitions and are due to GSB.

Single wavelength kinetics taken from the strongest GSB signals for 5-HC at 1526 cm^{-1} (closed blue circles) and for 5-HU at 1637 cm^{-1} (closed green triangles) at both pump wavelengths are normalized in Figure 4.4. The 5-HC traces were fit with monoexponential functions producing time constants of τ = 107 ± 7 ps (295 nm pump) and τ = 100 ± 6 ps (265 nm pump) with weak negative offsets. The kinetics of 5-HU also decay monoexponentially to negative offsets, and were fit using time components of τ = 5.5 ± 0.3 ps (295 nm pump) and τ = 5.1 ± 0.4 ps (265 nm pump). These lifetimes are consistent with

those obtained for 5-HC and 5-HU from the 266 nm pump / 570 nm probe TA kinetics (Figure 4.2(a)) and from global fits of the broadband spectra. The ESA bands in the TRIR spectra of 5-HC and 5-HU at both pump wavelengths decay in step with the GSB bands. Global fitting produced lifetimes of τ = 104 ± 2 ps for 5-HC and τ = 4.9 ± 0.1 ps for 5-HU.

4.3.2 Dinucleotides Containing Adenine

4.3.2.1 Temperature-Dependent CD and UV Absorption Spectra. Figures 4.5 and 4.6 display the results of temperature-dependent CD and UV absorption spectra measurements of d(5-HCA) and d(5-HUA) in pD = 6 D_2O phosphate buffer solution. The spectra were collected from 10 – 80°C at 10°C intervals.

The CD spectra of d(5-HCA) shown in Figure 4.5(a) are positive from 320 – 250 nm and do not vary greatly with temperature, although the signal amplitudes at 280 and 260 nm decrease and the negative signal amplitude at 270 nm increases slightly at higher temperatures. After a small dip below zero around 245 nm, the spectra exhibit a positive Cotton effect centered at 220 nm, followed by a negative Cotton effect at 208 nm about three times greater in amplitude than the former band. The amplitudes of this positive exciton-coupled CD (ECCD) couplet decrease (i.e., trend toward zero) as the temperature increases. Figure 4.5(b) illustrates how the amplitudes of the positive couplet at the maximum signals change with temperature. The UV absorption of d(5-HCA) increases slightly with temperature, as shown in Figures 4.5(c) and (d).

Temperature-dependent CD and UV absorption spectra for d(5-HUA) in pD = 6 D_2O phosphate buffer solution are shown in Figure 4.6. From 320 – 280 nm positive CD

signals (Figure 4.6(a)) peak at 280 nm and the amplitudes decrease slightly with temperature. A negative Cotton effect is observed at 255 nm followed by a bimodal positive Cotton effect between 240 – 210 nm. The signals of this negative couplet decrease with increasing temperature, as shown in Figure 4.6(b). Figures 4.6(c) and (d) show that the UV absorption spectra of d(5-HUA) do not appear to change as much with temperature as compared to the temperature-dependent UV absorption of d(5-HCA).

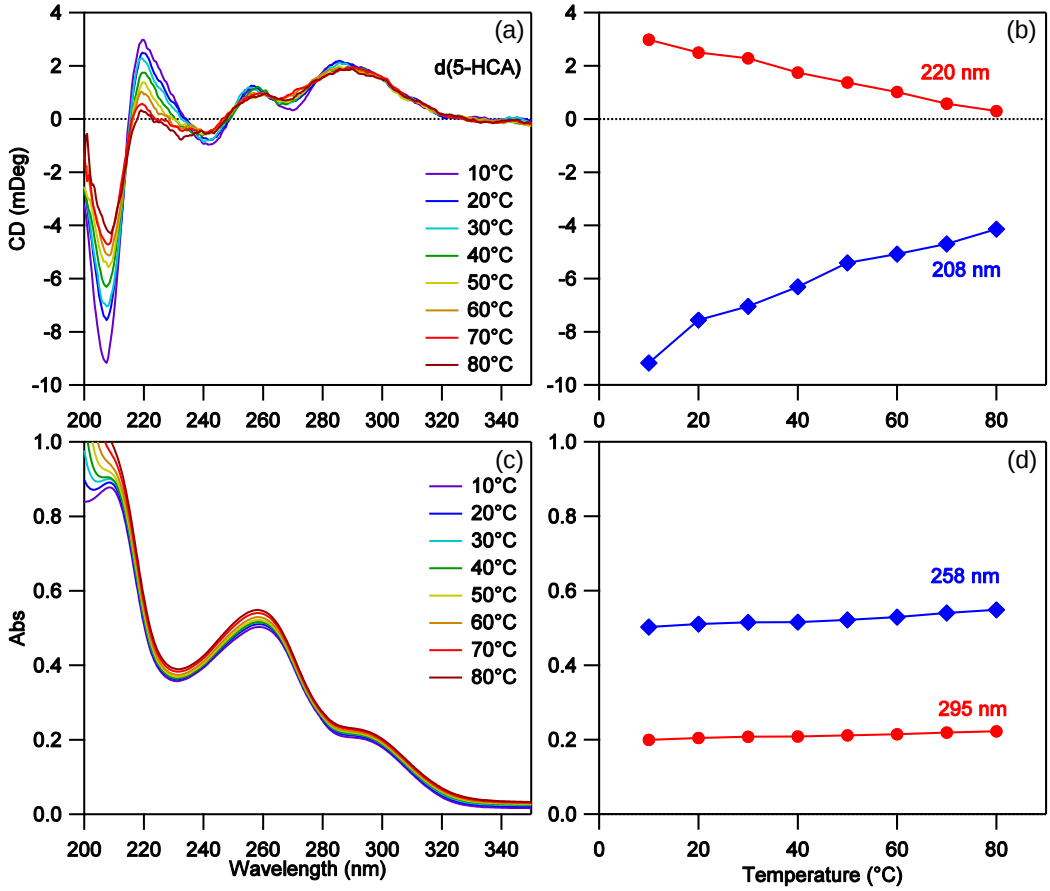


Figure 4.5. Temperature-dependent CD spectra (a), CD peak signals vs. temperature (b), UV absorption spectra (c) and UV peak signals vs. temperature (d) of d(5-HCA) in pD = 6 D_2O phosphate buffer solution collected from 10°C to 80°C at 10°C increments.

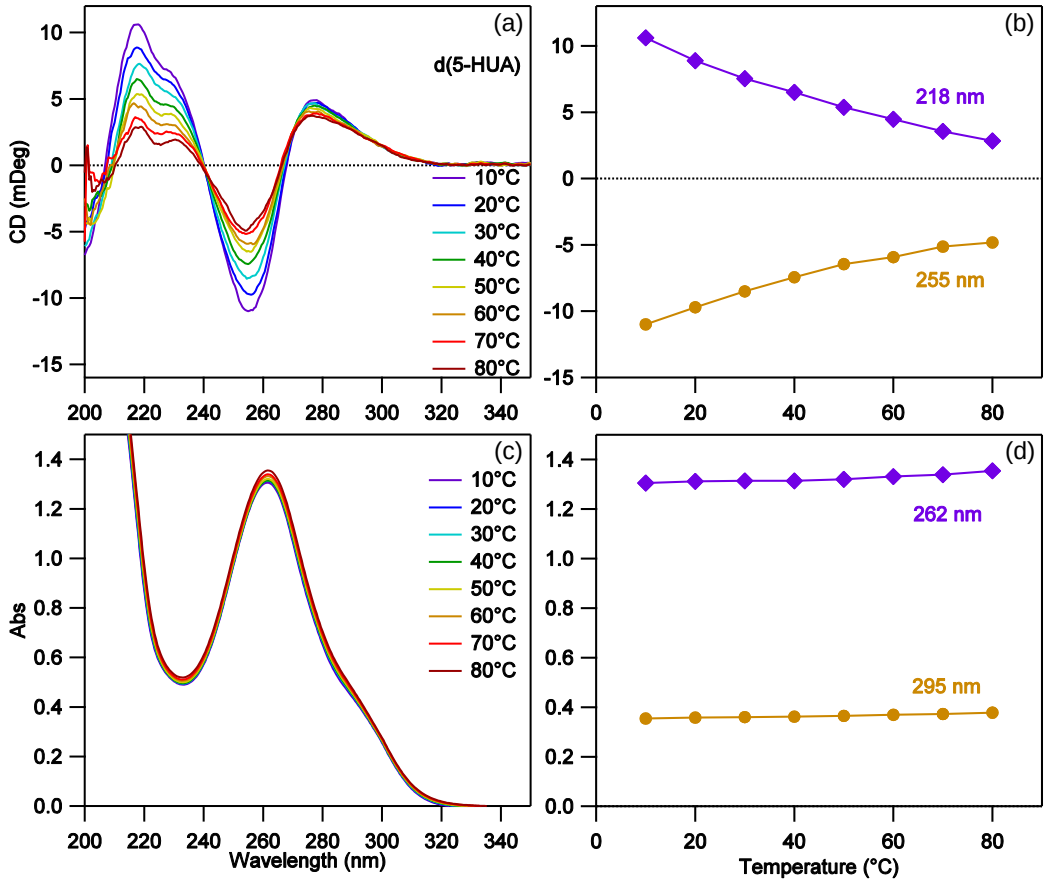


Figure 4.6. Temperature-dependent CD spectra (a), CD peak signals vs. temperature (b), UV absorption spectra (c) and UV peak signals vs. temperature (d) of d(5-HUA) in pD = 6 D_2O phosphate buffer solution collected from 10°C to 80°C at 10°C increments.

4.3.2.2 UV pump / Mid-IR Probe TRIR. The TRIR spectra of d(5-HCA) (a,b) and d(5-HUA) (c,d) collected after 295 (a,c) and 265 nm (b,d) excitation are displayed in Figure 4.7. As in the monomer TRIR spectra, all signals were collected from 1 ps (first purple trace) to 1 ns (last red trace) and recover to a featureless negative offset due to D_2O heating. The positive TRIR signals arise from ESA and the ground state absorption bands in the overlaid inverted FTIR show the negative TRIR signals that are due to GSB. Note that the FTIR spectra are cut off at 1500 cm^{-1} in the d(5-HCA) spectra and at 1610 cm^{-1} in the d(5-

HUA) spectra due to overlapping impurity absorption bands. During the synthesis of these compounds, the Burrows research group used ammonium acetate in one of the final drying

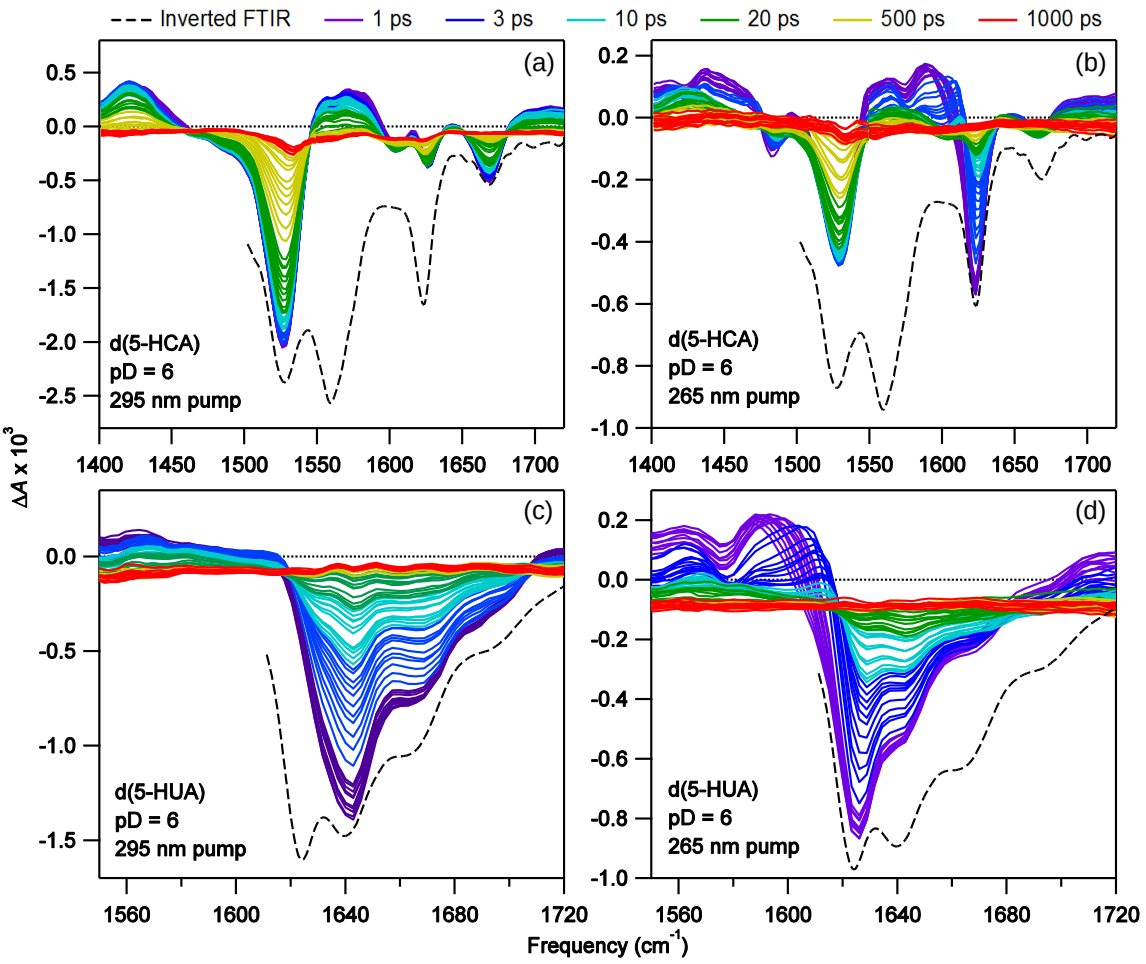


Figure 4.7. TRIR spectra of d(5-HCA) (a,b) and d(5-HUA) (c,d) after 295 (a,c) and 265 nm (b,d) excitation collected from 1 ps (first purple trace) to 1 ns (last red trace). Dotted horizontal lines at $\Delta A = 0$ indicate the ground-state baseline. The inverted FTIR spectra are shown as the black dashed traces.

steps, which exhibits vibrational bands at 1420 and 1560 cm^{-1}. Although the compounds were sent back to have this impurity removed, the purified dinucleotide samples still contained trace amounts of the impurity upon return, as their vibrational signatures showed.

The FTIR spectra of d(5-HCA) in Figures 4.7(a) and (b) show the impurity band at 1560 cm^{-1}. Regardless, the ammonium acetate does not absorb at either pump wavelength and is not expected to contribute to the dinucleotide excited-state dynamics.

The d(5-HCA) 295 nm pump TRIR spectra (Figure 4.7(a)) have ESA features at 1420, 1570 and 1710 cm^{-1}. The band at 1580 cm^{-1} has an additional shoulder on its higher frequency edge centered at 1557 cm^{-1}. GSB bands appearing at 1525, 1603 and 1669 cm^{-1} are also present in the monomer TRIR and FTIR spectra and thus correspond to the 5-HC chromophore. The GSB band at 1626 cm^{-1} is due to the in-plane stretching mode of A.

The TRIR spectra of d(5-HUA) after 295 nm excitation (Figure 4.7(c)) exhibit an ESA band at 1565 cm^{-1} and GSB bands where the 5-HU ground state absorbs at 1639 cm^{-1} and its two lower-frequency shoulders. An additional negative feature appears at 1629 cm^{-1}. Although this band is difficult to discern because it overlaps closely with the 1639 cm^{-1} vibrational band of 5-HU, it is possibly due to the same A vibrational band at 1626 cm^{-1} observed in d(5-HCA). The 3 cm^{-1} shift may be due to the pulling down effect of the strong 1639 cm^{-1} 5-HU vibrational band.

In contrast with the 5-hydroxypyrimidine monomers, the TRIR spectra of the dinucleotides are noticeably different after 265 vs. 295 nm excitation. With 265 nm excitation, the intensity of the A GSB signals increase and short-lived, shifting ESA signals appear. These differences can be attributed to the greater absorption of A than the 5-hydroxypyrimidines with 265 nm excitation. As shown in the UV absorption spectra in Figure 4.1(a) and (b), the extinction coefficient of A at 265 nm is more than twice as large as that of 5-HC and 5-HU in both dinucleotides.

In d(5-HCA) (Figure 4.7(b)), the A bleach band at 1626 cm^{-1} is significantly stronger and the weaker vibrational band of A at 1500 cm^{-1} becomes more defined after 265 nm excitation.[29] Similarly, in the d(5-HUA) spectra (Figure 4.7(d)) the A bleach band is stronger than the 5-HU in-plane ring stretching mode. Consequently, the spectra collectively red-shift toward and reach maximum negative amplitude at the A 1626 cm^{-1} band. This is in stark contrast to the maximum negative amplitude of the TRIR spectra peaking at the 5-HU ring stretching mode near 1640 cm^{-1} after 295 nm excitation and suggests that the weak GSB signal at 1629 cm^{-1} is indeed an A bleach band (Figure 4.7(c)). Differences in decay timescales are also evident, as the A GSB bands recover to ground-state much more quickly than the bands associated with the 5-hydroxypyrimidines. Single-frequency kinetic fitting of the A 1626 cm^{-1} GSB band produced a fast time component of about 4 ps in both dinucleotides, which is consistent with the ultrafast decay of A measured previously.[86] In both sets of 265 nm pump TRIR spectra, the ESA features that shift and decay faster than ESA signals in Figure 4.7(a,c) are due to VC dynamics of A.[32, 116] When monitoring ultrafast internal conversion dynamics using TRIR, the excess electronic energy deposited into the excited vibrational modes of the ground state is observed as hot ground-state absorption, which manifests in the characteristic "rise-blue-shift-decay" patterns shown in the 265 nm pump TRIR (Figure 4.7 (b,d)).[75]

Figure 4.8 shows the kinetic traces of d(5-HCA) and d(5-HUA) normalized with the kinetic traces of 5-HC and 5-HU, respectively, taken from the maximum of the most prominent GSB TRIR features. At 1526 cm^{-1}, the d(5-HCA) kinetic trace was fit with a monoexponential function and a negative offset of 10% signal amplitude. The dinucleotide

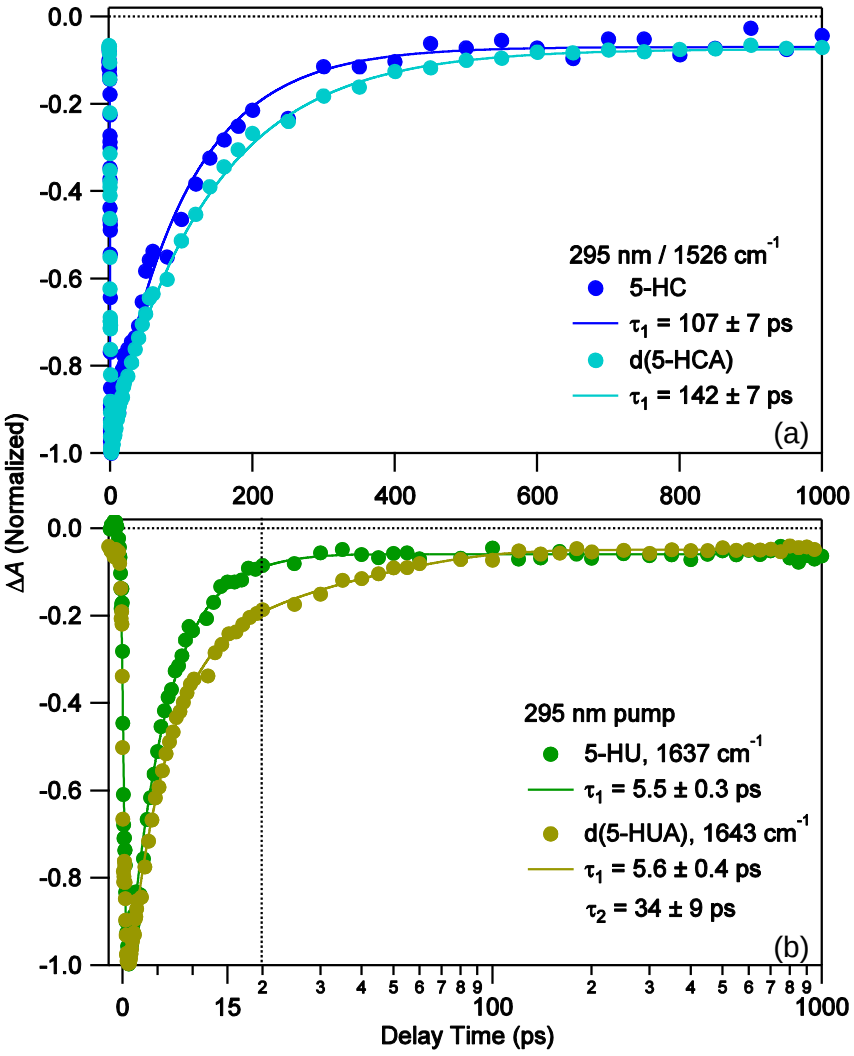


Figure 4.8. Kinetic traces of d(5-HCA) (a) and d(5-HUA) (b) from the TRIR GSB signals at 1526 and 1637 cm^{-1}, respectively, normalized with the kinetics from the monomer TRIR signals. Exponential fits (solid traces) produced the indicated time components.

kinetics decay with a lifetime of τ = 142 ± 7 ps, which is slightly longer than the lifetime of the 5-HC monomer. The normalized kinetics in Figure 4.8(a) illustrate the slightly longer lifetime of the dinucleotide. Using a biexponential function to fit the dinucleotide kinetics did not significantly improve the fit. Global fitting produced a lifetime of τ = 142 ± 7 ps. In Figure 4.8(b), the d(5-HUA) kinetics trace from the 1637 cm^{-1} GSB band decays

biexponentially and was also fit using a negative offset (4% amplitude). The biexponential fit produced a fast time component of $\tau = 5.6 \pm 0.4$ ps with about 80% signal amplitude and a longer time component of $\tau = 34 \pm 9$ ps. The first lifetime is the same as the 5-HU monomer lifetime, and the normalized kinetic traces in Figure 4.8(b) show the longer-lived lifetime in comparison with the faster decay of the monomer. Consistent lifetimes ($\tau = 5.1 \pm 0.1$ ps and $\tau = 28 \pm 1$ ps) were obtained from global fitting.

4.4 Discussion

4.4.1 Monomer Photophysics

Table 4.1 lists experimental data of 5-HU and 5-HC at pD = 6 compared with corresponding C and U in nucleoside form. The UV absorption spectra of 5-HC in Figure 4.1(a) and of 5-HU in Figure 4.1(b) show that the first absorption band is significantly red-shifted compared to the canonical bases. C and U have absorption maxima at 272 and 262 nm,[117-118] whereas 5-HC and 5-HU have absorption maxima at 289 and 280 nm, respectively (Table 4.1). Red-shifted ground-state absorption upon substitution at the C5 position is commonplace for pyrimidines and their derivatives. The lowest-energy absorption band of 5-methylcytosine, for instance, peaks at approximately 280 nm.[33] 5-Fluorocytosine (5-FC) and 5-fluorouracil (5-FU) also have red-shifted lowest-energy absorption bands.[119-120]

Also listed in Table 4.1 are the Stokes shifts for 5-HC and 5-HU, which are nearly 2000 cm^{-1} greater than those of C and U. Similar changes in the Stokes shift upon modification were observed in 5-FC and 5-FU and the effect was attributed to differences

in their excited-state geometries compared to C and U.[119-120] Pyrimidine C5 modification can also result in lengthened fluorescence lifetimes, consistent with the greater Stokes shifts.[119-120] Compared to the characteristically low emissions of canonical C and U (only 1.2×10^{-4} and 0.3×10^{-4}, respectively),[79, 118] our results show that both 5-hydroxypyrimidines have greater emission quantum yields, with 5-HC being significantly more emissive (Table 4.1).

Ground-state vibrational spectra of 5-HC and 5-HU (inverted FTIR spectra in Figure 4.3) have not been reported previously. In 5-HC, the vibrational band at 1669 cm^{-1} can be assigned to the carbonyl stretch because it is closest in frequency to the C2=O stretching mode of cytosine at 1654 cm^{-1}.[121] The higher frequency of the C2=O in 5-HC may arise from a decrease in the double bond length upon addition of the electronegative hydroxyl substituent. The two low-frequency bands at 1525 and 1603 cm^{-1} lie in the ring stretching region. 5-HU has a strong vibrational band at 1639 cm^{-1}, which is likely due to in-plane ring stretches. The C5=C6 ring stretch of uracil located at 1675 cm^{-1} shifts to 1710 cm^{-1} with C5-fluorination, and C5 substitutions with decreasingly electronegative halogens increasingly red-shifts the frequencies of this mode.[122] Iodine, the most electronegative uracil C5 substitution studied by the authors of ref 116, causes the mode to shift down to 1650 cm^{-1}. A hydroxyl group is less electronegative than any iodine and may cause this vibration to decrease to the even lower frequency of 1639 cm^{-1}. Based on FTIR vibrational mode assignments of uracil, the two shoulders appearing at the higher frequency edge of the 1639 cm^{-1} band at 1665 and 1690 cm^{-1} can be assigned to the C4=O8 and C2=O7

carbonyl stretching modes, respectively.[123] The lower energy vibration is assigned to the former mode, which is always at lower frequencies than the latter mode.

Table 4.2. Single-frequency and global fit parameters for 5-HC, 5-HU, d(5-HCA) and d(5-HUA) experimental TRIR spectra.

	fit	$A_1{}^a$	τ_1 (ps)	$A_2{}^a$	τ_2 (ps)	offset
5-HC	GSB[b]	0.99 ± 0.01	107 ± 7	−	−	0.01 ± 0.01
	Global	−	104 ± 2	−	−	−
d(5-HCA)	GSB[b]	0.90 ± 0.04	142 ± 7	−	−	0.10 ± 0.04
	Global	−	129 ± 1	−	−	−
5-HU	GSB[c]	0.93 ± 0.03	5.5 ± 0.3	−	−	0.07 ± 0.01
	Global	−	4.9 ± 0.1	−	−	−
d(5-HUA)	GSB[c]	0.8 ± 0.2	5.6 ± 0.4	0.2 ± 0.2	34 ± 9	0.04 ± 0.02
	Global	−	5.1 ± 0.1	−	28 ± 1	−

[a]Signals were fit using $A_1\, e^{-t/\tau_1} + A_2\, e^{-t/\tau_2} + A_3$, with normalized amplitudes ($\sum_i A_i = 1$) and offsets (A_3). Uncertainties reported as 2σ. [b]Parameters from 1526 cm^{-1} fits. [c]Parameters from 1637 cm^{-1} fits.

Table 4.2 lists the excited-state lifetimes of 5-HC and 5-HU from TRIR single-frequency GSB kinetics and global fits. After excitation to the optically bright, lowest-energy $^1\pi\pi^*$ state by 295 nm, 5-HC and 5-HU decay on a time scale of 107 ± 7 ps and 5.5 ± 0.3 ps, respectively. The lifetimes obtained from TA after 266 nm excitation, shown in Table 4.1, are identical within the uncertainty for both 5-hydroxypyrimidines, indicating that the two methods are probing the same state. In considering the origin of these excited states, we considered several possibilities. Due to the high-energy pump wavelengths used, we considered that the longer 5-HC lifetime could reflect photoionization timescales. Both hydrated electrons and radical ions of the DNA bases could be observed with the visible probe wavelength used in our TA measurements. However, care was taken to subtract the solvated electron signals and the reproducible 5-HC lifetime is not likely due to ionization

because more readily ionized purine bases do not exhibit slow decays at this wavelength.[21, 124] The lifetimes are also not likely due to decay channels through an nπ* state, which lasts tens of picoseconds in the pyrimidines.[125] Finally, we rule out triplet state decay because pyrimidine triplet state lifetimes span hundreds of nanoseconds,[126] which are incompatible with the picosecond lifetimes we observe for 5-HC and 5-HU.

Strong emission from 5-HC and much weaker emission from 5-HU indicated by their fluorescence quantum yields of 70×10^{-4} and 4.6×10^{-4}, respectively, suggest that the lifetimes may correspond to ππ* states. A Strickler-Berg analysis was performed to calculate the fluorescence lifetimes of 5-HC and 5-HU.[118] By integrating the longest wavelength absorption bands, the radiative lifetimes were calculated using the Strickler-Berg equation.[127] The fluorescence lifetimes were calculated by multiplying the radiative lifetimes by the fluorescence quantum yields, and the ratio of 5-HC to 5-HU fluorescence lifetimes is about 22. This result is in excellent agreement with the experimental lifetimes, which produce a corresponding ratio of 25, and leads us to assign the observed lifetimes to bright ππ* states.

Whereas C has a ππ* excited-state lifetime of 0.7 ps in H_2O,[125] the lifetime of 5-HC is about 150 times longer-lived in D_2O. U, which has one of the shortest observed excited-state lifetimes in H_2O, deactivates in about 0.2 ps.[118] In contrast, the 5-HU excited-state lifetime is lengthened to about 5 ps in D_2O. Several experimental and theoretical studies have also shown that C5 substitutions to canonical C and U result in lengthened ππ* excited-state lifetimes. Malone et al. observed an increase in the singlet excited-state lifetime of cytidine by a factor of 7 with C5 methylation ($\tau = 7.2 \pm 0.2$ ps) and by a factor

of almost 90 with C5 fluorination (τ = 88 ± 5 ps).[128] The ππ* lifetime of 5-HC is slightly longer-lived than that of 5-FC, which is consistent with the greater fluorescence quantum yield of 5-HC compared to that of 5-FU, which is $\phi_{fl} = 50 \times 10^{-4}$.[119] Nachtigallová and co-workers measured a lifetime of almost 2 ns for 5-HU in the gas phase and discovered sizeable barriers on their calculated minimum energy paths to the S_0/S_1 conical intersection (CI) after 290 nm excitation.[129] These authors attribute the long-lived lifetime to the longer excitation wavelength used, which excites 5-HU further below the barrier to the CI.[129] Our measurements reveal that the lifetime of 5-HU in aqueous solution is significantly shorter than the 2 ns, but more long-lived than other C5 modified U nucleobases, such as 5-chloro- and 5-fluorouracil, the latter having the longer lifetime of only about 1.7 ps.[120] In aqueous solution, 5-HC and 5-HU have the longest-lived ππ* excited states compared to other C5 modified C and U bases studied to date. C5 substitutions to C generally have more exaggerated effects on the excited-state lifetime than C5 substitutions to U,[120, 128] and this observation is consistent in our measurements of 5-HC and 5-HU.

The lengthened excited-state lifetimes may be understood when considering the molecular deformation that enables pyrimidines to efficiently access CIs to S_0, that is, torsion of the C5-C6 bond and pyramidalization of C5.[120-121, 130-131] Canonical C and U have hydrogens on the ethylenic carbons, which can access the aforementioned geometrical changes more rapidly than larger functional groups, such as a hydroxyl group. By this rationalization, a prevailing notion in the literature is that C5 and/or C6 substitutions strongly hinder the motion responsible for ultrafast internal conversion thereby slowing the deactivation rate.[120, 129-130, 132] Additionally, evidence suggests that C5 modifications to

pyrimidines have a more dramatic effect on their excited-state properties than other ring modifications.[120, 130, 132] For instance, fluorescence upconversion lifetime measurements of U and ten of its derivatives revealed that only C5 substituted forms exhibited new longer-lived lifetime components and biexponential fluorescence decays compared to C6 modifications.[120] Resonance Raman spectra of 5,6-dideuterouracil indicates that the in-plane bending mode is more sensitive to C5 than C6 substituents.[132] Thus, we propose that the lengthened excited-state lifetimes of 5-HC and 5-HU compared to C and U are due to the hindered motion of a main molecular coordinate responsible for deactivation in the pyrimidines, i.e., pyramidalization of C5. Geometry optimizations on the minimum energy paths leading to the CIs in 5-HC and 5-HU are currently underway to provide more mechanistic insights into excited-state deactivation in these systems.

Note that 5-HC and 5-HU decay monoexponentially in aqueous solution, whereas C and U were previously found to decay through two distinct channels.[125] Hare et al. attributed their observed long-lived lifetime components (10 – 150 ps) to deactivation via an intermediate dark $n\pi^*$ state,[125] which has been predicted for both C and U experimentally and theoretically.[118, 128, 131, 133] Modifications at C5 may reduce the coupling between the $\pi\pi^*$ and $n\pi^*$ states.[119, 134] Blancafort et al. explained that even slight shifts in the relative energies of the $\pi\pi^*$ and $n\pi^*$ states could produce barriers that hinder access to their CI and limit deactivation through the $n\pi^*$ state.[119] In our calculations, the lowest energy $n\pi^*$ states for 5-HC and 5-HU lie higher in energy than the optically accessed $S_1(\pi\pi^*)$ states and are shifted from the $n\pi^*$ states calculated for C and U.

TA and TRIR signals of both 5-HC and 5-HU decay to long-lived positive and negative offsets. As mentioned previously, the negative offsets in the TRIR are due to solvent heating resulting from vibrational cooling of the relaxing chromophores. The offsets in the TA data, however, may be evidence for intersystem crossing to triplet states in 5-HC and 5-HU. Triplet state lifetimes are much longer-lived[126] than our experimental timescales (4 ns total delay time) and their signals would manifest as long-lived offset signals much like the offsets observed in Figure 4.2(a). Similar offset signals were assigned to triplet states in the canonical pyrimidines.[125] The triplet states of C and U have non-negligible absorption near 300 nm,[135] and U has a triplet quantum yield of 0.015 in water after 265 nm excitation.[126] These observations lead us to tentatively assign the long-lived offsets to 5-HC and 5-HU triplet states.

4.4.2 Dinucleotide Photophysics

ECCD signals can be diagnostic of base-stacking within a strand.[49] The temperature-dependent CD spectra of both d(5-HCA) and d(5-HUA) show ECCD signals, which arise from the electronic coupling between π-stacked nucleobases in chiral helical strands.[136] The ECCD signals in d(5-HCA) and d(5-HUA) (Figures 4.5 and 4.6) indicate that both dinucleotides are base-stacked to a certain extent, as the complete lack of stacking would result in no ECCD signal. In d(5-HCA), the negative exciton couplet appears around 240 nm. The non-conservative (i.e., lacking the exciton couplet signals) CD spectra at higher wavelengths is likely due to decreased coupling between the 5-HC and A chromophores. As shown in the UV absorption spectra of the individual bases in Figure 4.1(a), the overlap in absorption is greatest below 240 nm. Absorption overlap between 5-

HU and A, shown in Figure 4.1(b), begins increasing near 270 nm, precisely where the positive exciton couplet in the d(5-HUA) CD spectra begins. Increasing the temperature disrupts the base-stacking interaction, and the amplitudes of the positive and negative signals decrease, as observed in Figures 4.5 and 4.6. The UV absorption spectra do not change drastically with temperature and do not show clear melting points indicating that the dinucleotides do not aggregate and or base-pair together.

Table 4.2 compares the lifetimes obtained from single-frequency kinetics and global fit parameters obtained from fitting the TRIR data of the 5-HC and 5-HU monomers and their dinucleotides. The lifetime of d(5-HCA) is slightly longer than that of the nucleoside (142 ± 7 ps compared to 107 ± 7 ps). In the 5-HU compounds, both the nucleoside and dinucleotide exhibit a common lifetime of about 5 ps (5.5 ± 0.3 ps and 5.6 ± 0.4 ps, respectively). The d(5-HUA) dinucleotide decay also involves a second long-lived component with a lifetime of about 35 ps. Our measurements indicate that the excited-state of the d(5-HCA) dinucleotide is longer-lived than either of its monomer components and that the d(5-HUA) dinucleotide exhibits an additional long-lived decay channel not present in the monomer.

Additional long-lived decay components present in strands of DNA compared to the single bases in solution have previously been enigmatic in the field of DNA photophysics research.[22] Our group hypothesized that excitation of single-stranded DNA generates excitons that decay on an ultrafast timescale to long-lived excimer/exciplex, or charge-separated, states between two π-stacked nucleobases.[26, 64] Very recently, we identified charge-separated species in a dinucleotide,[29] as discussed in Chapter 3 of this

dissertation, and similar observations by other groups have solidified the assignment of long-lived excited states in single-stranded DNA to CT states.[32-33] Studies that use an organic co-solvent or other means for disrupting ππ-stacking, or base-stacking, have revealed that this noncovalent interaction is essential for populating CT states.[26, 49] Based on their ECCD signals, d(5-HCA) and d(5-HUA) base stack in solution, which suggests that their longer-lived excited states may arise from population of CT states.

4.4.2.1 Evidence for Photoinduced Electron Transfer. The dinucleotide TRIR spectra in Figure 4.7 show more prominent A features after 265 than 295 nm excitation because A does not absorb significantly above 285 nm. Yet, the A bleach signals in the 265 nm pump TRIR dinucleotide spectra confirm that the GSB bands at 1626 cm^{-1} in the 295 nm pump TRIR spectra are due to the A chromophore. The observation of A bleach signals after selective excitation of the 5-hydroxypyrimidines with 295 nm photons strongly suggests CT state population via photoinduced ET.

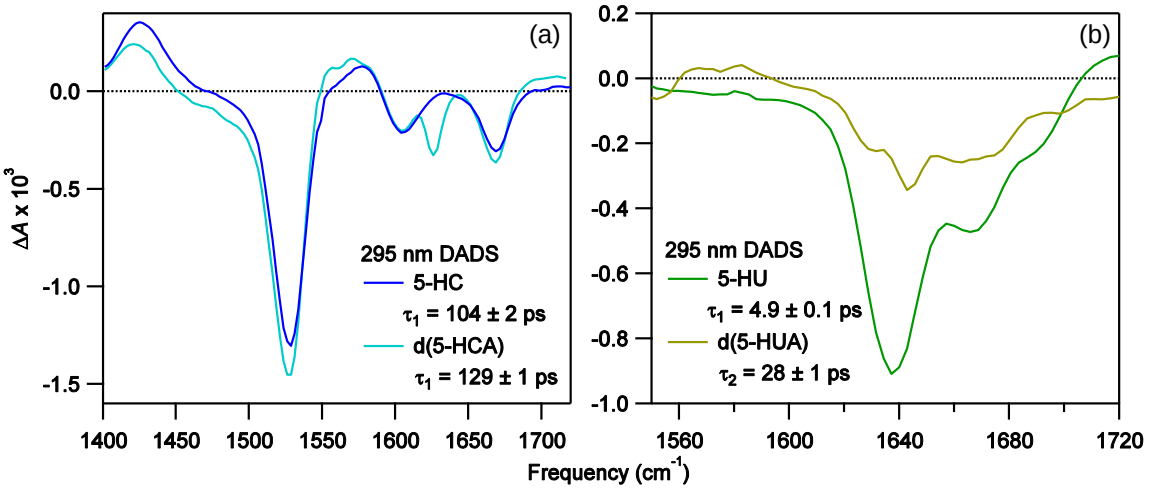


Figure 4.9. Decay-associated difference spectra (DADS) of d(5-HCA) compared to 5-HC (a) and d(5-HUA) compared to 5-HU (b) at the delay times indicated by the lifetimes.

In addition to the A GSB bands, the 295 nm pump TRIR spectra of the dinucleotides in Figures 4.7(a,c) also display additional positive features that are not present in the TRIR spectra of the 5-HC and 5-HU monomers (Figures 4.3(a,c)). ESA bands appear at 1560 and 1710 cm^{-1} in d(5-HCA) and at 1560 cm^{-1} in d(5-HUA). These ESA bands are very subtle in the broadband TRIR spectra, and can be seen more clearly in

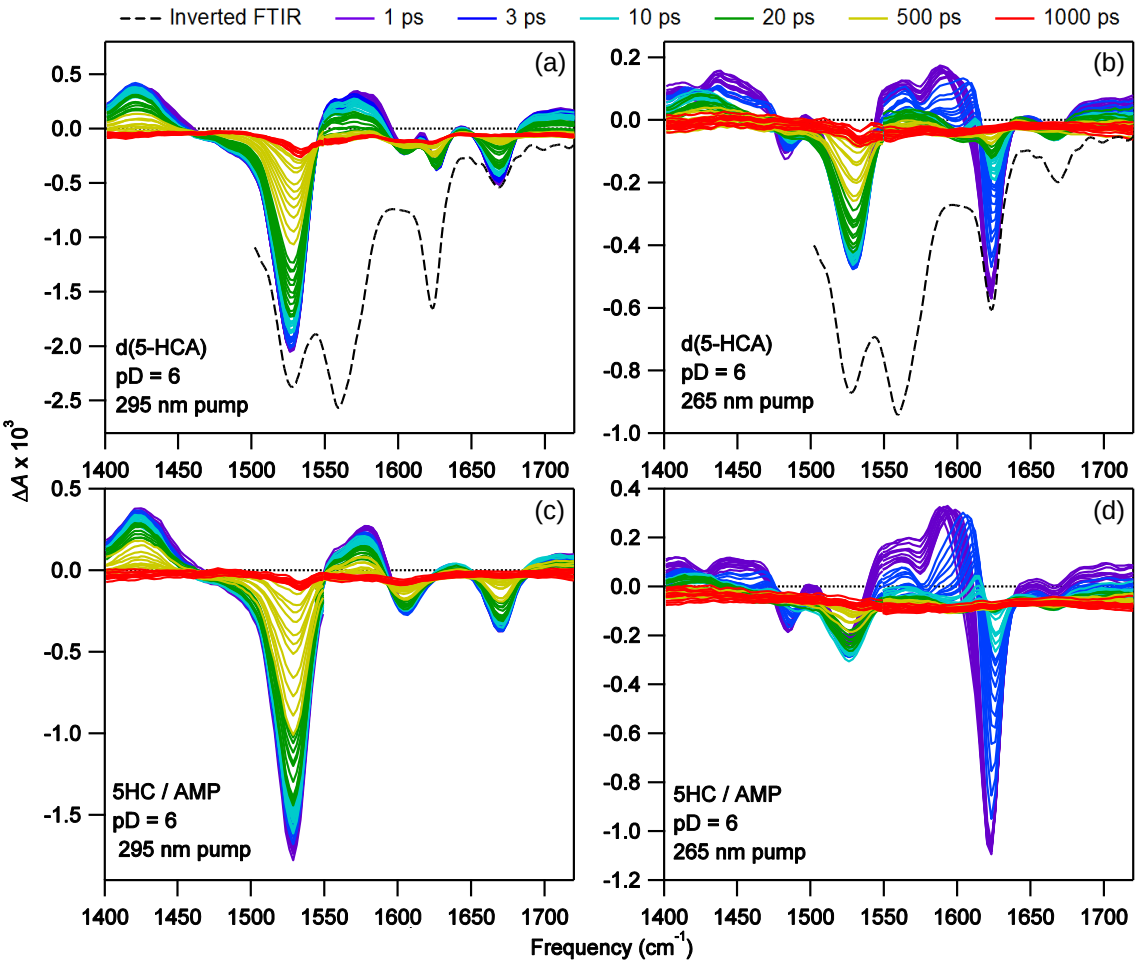


Figure 4.10. TRIR spectra of d(5-HCA) (a,b) compared with TRIR spectra of a solution containing equimolar amounts of its monomer components (c,d) in pD = 6 D_2O phosphate buffer solution after 295 (a,c) and 265 nm (b,d) excitation.

the decay-associated difference spectra (DADS) obtained from global fitting. Figure 4.9 shows the DADS of d(5-HCA) compared to 5-HC (Figure 4.9(a)) and of d(5-HUA) compared to 5-HU (Figure 4.9(b)). The dinucleotide DADS were obtained at the longer delay times corresponding to their lengthened excited-state lifetimes at 130 ps for d(5-HCA) and at 30 ps for d(5-HUA) where the additional GSB and ESA spectral features are clearly observed.

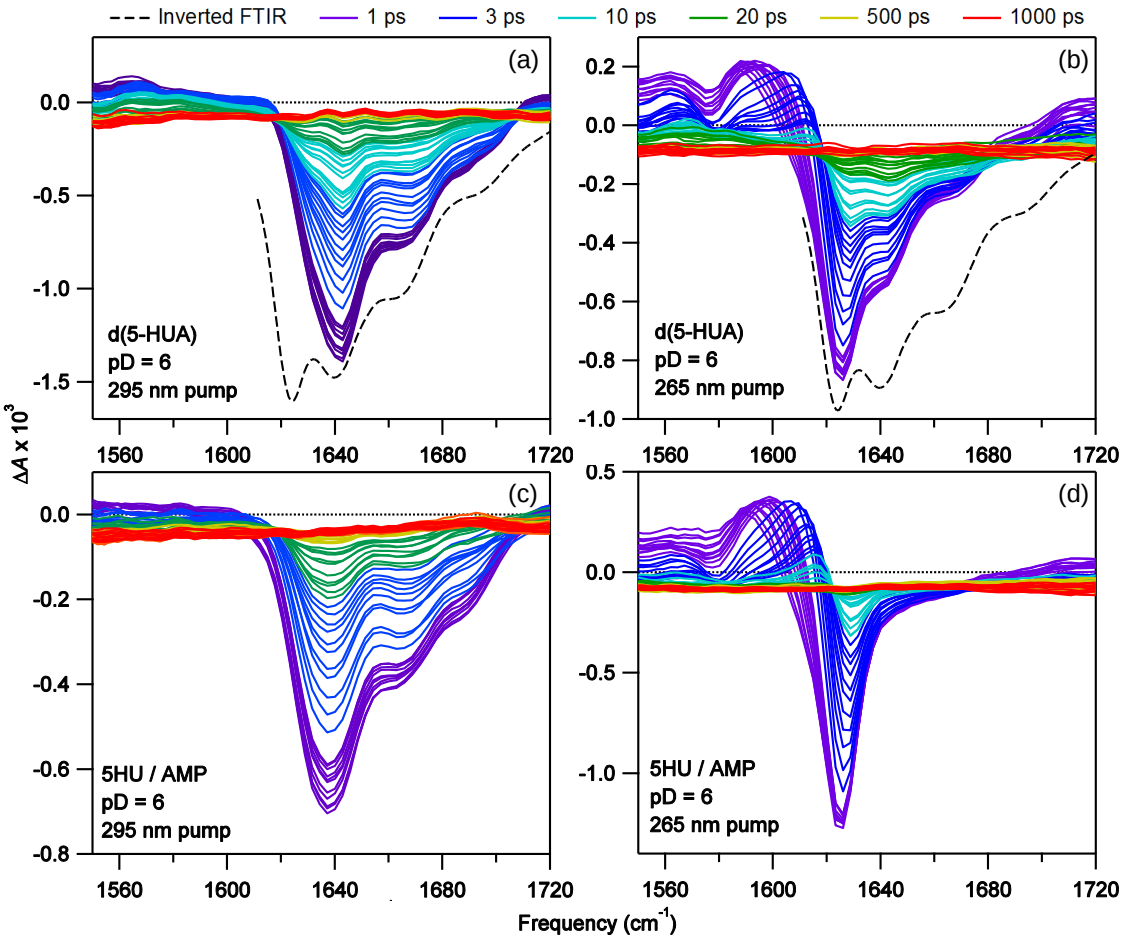


Figure 4.11. TRIR spectra of d(5-HUA) (a,b) compared with TRIR spectra of a solution containing equimolar amounts of its monomer components (c,d) in pD = 6 D_2O phosphate buffer solution after 295 (a,c) and 265 nm (b,d) excitation.

These additional features are also not present in the TRIR spectra of solutions containing equimolar amounts of the 5-hydroxypyrimidines and AMP (Figures 4.10 and 4.11). The bases in the equimolar mixtures are not stacked as in the covalently linked dinucleotides. Accordingly, the 295 nm pump TRIR spectra of the equimolar mixtures (Figures 4.10(c) and 4.11(c)) are identical to the spectra of the 5-HC and 5-HU monomers, which absorb the 295 nm photons. After 265 nm excitation, the A chromophore is also excited and the equimolar mixture TRIR spectra are very similar to the 265 nm pump TRIR spectra of the dinucleotides (compare Figures 4.10(b,d) and 4.11(b,d)). The absence of the A bleach band in the TRIR spectra of either equimolar mixture solution confirms that 295 nm excites only the 5-hydroxypyrimidines.

Positive features in TRIR spectra correspond to excited-state absorption and/or absorption of transient intermediate species. Radical ions formed via photoinduced ET are examples of such transient species that can be detected using TRIR spectroscopy.[29, 32-33] Based on their relative standard reduction potentials, E^0 = 0.99 V, 0.97 V, 1.96 V vs SHE for 5-HC, 5-HU and A, respectively, the 5-hydroxypyrimidines are better electron donors than A. Thus, photoinduced ET in these dinucleotides would generate radical ion contact pairs consisting of a 5-HC/5-HU radical cation and an adenine radical anion.

To investigate the possibility that the positive bands in the dinucleotide TRIR spectra arise from absorption of the 5-HC/5-HU radical cations, we performed two-photon ionization experiments on solutions of 5-HC and 5-HU using higher 295 nm pump energies. The results, shown in Figure 4.12, illustrate positive bands that represent IR signatures of the 5-HC$^{\bullet+}$ and 5-HU$^{\bullet+}$ species. Interestingly, the two-photon ionization

spectra of 5-HC and 5-HU have positive signals at the same frequencies as the new positive bands present in the dinucleotide TRIR spectra. Specifically, 5-HC$^{\bullet+}$ has signature bands at 1560 and 1710 cm^{-1} and 5-HU$^{\bullet+}$ has a signature band at 1560 cm^{-1}. The presence of these marker bands in the TRIR of the dinucleotides but not the monomers, where the pump energies used were too low to result in two-photon ionization of the bases, is strong evidence for photoinduced ET.

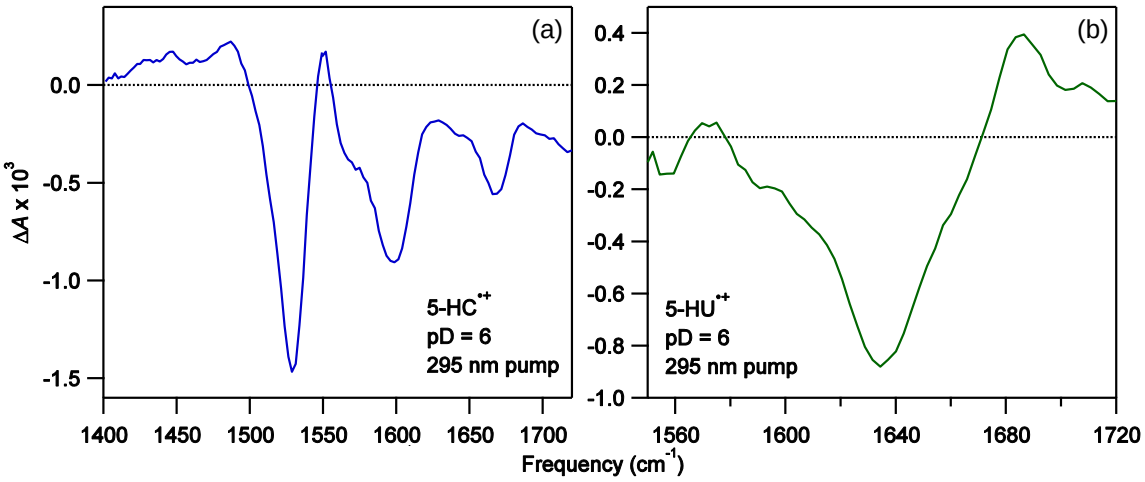


Figure 4.12. Transient spectra of the 5-HC (a) and 5-HU (b) radical cations generated by two-photon absorption of 295 nm.

Based on these observations, we propose that the 5-hydroxypyrimidine-containing dinucleotides undergo photoinduced ET in a dynamical model analogous to that proposed for the 8-oxo-dGuo-containing dinucleotide (see Chapter 3).[29] Upon excitation by a 295 nm photon, the 5-HC, or 5-HU, excited state transfers an electron to A when the two bases are stacked, producing a CT state consisting of a 5-HC/5-HU radical cation and an adenine radical anion contact pair. The resulting charge-separated species are held within van der Waals contact with one another, and the charges recombine due to the Coulombic

electrostatic interaction. This model requires two ET processes, namely forward ET from the 5-hydroxypyrimidine to the A and back ET. The two-photon ionization spectra suggest that we are observing ESA of 5-HC and 5-HU radical cation vibrational marker bands in the TRIR spectra. Based on the observation of these radical ion species, we assign the lengthened excited-state lifetimes of the dinucleotides to the timescale of back ET. Population of the CT state via forward ET is proposed to be faster than the resolution of our instrument (<0.5 ps) because the radical ion bands appear in the dinucleotide TRIR spectra at the earliest delay times.

4.4.2.2 Driving Force Calculations and Marcus Theory. Based on our proposed model, we assign the ~140 ps lifetime of d(5-HCA) and the ~30 ps lifetime of d(5-HUA) to the rate of back ET, whereas forward ET occurs on an ultrafast timescale in both cases. Asymmetry in the rates of forward and back ET, as proposed here, have been reported previously.[29, 82] Depending on the thermodynamic driving forces for ET, the stacked donor-acceptor chromophore complex forms a radical ion contact pair. Observing the signatures of the radical ion contact pair in the transient spectrum is possible when the rate for back ET is slower than the rate for forward ET, and is slowed enough that it can be observed within the time resolution of ultrafast measurements.

To determine whether the asymmetry in our lifetime assignments are physically reasonable, we calculated $\Delta G°$ for forward (FET) and back ET (BET) using eqns. (3.2) and (3.3), respectively. Assuming that 5-HC and 5-HU are the electron donors, $\Delta G°_{FET}$ is calculated to be –0.76 eV in d(5-HCA) and –0.78 eV in d(5-HUA) with 295 nm (4.20 eV) excitation. The Gibbs energy for the back ET process is $\Delta G°_{BET}$ for CR is –3.44 eV in d(5-

HCA) and –3.42 eV in d(5-HUA). In both dinucleotides, these thermodynamic driving force calculations show that the back ET process is more exergonic than the forward ET process. This suggests that back ET is the more thermodynamically favorable process, and the rate would occur on a faster timescale. However, the asymmetry between back and forward ET that we are proposing for these dinucleotides, i.e., ultrafast forward ET and the slower back ET, can be rationalized by a more accurate model which includes an estimate for the corresponding activation energies. Using semi-classical non-adiabatic ET theory,[82] a new parameter, called the reorganization energy, is introduced to account for how the solvent dipole reorients around the CT excited-state molecule. Because the driving force for forward ET is nearly equal to the reorganization energy in these donor-acceptor systems (~1 eV), the forward ET process occurs on an ultrafast timescale. The more thermodynamically favorable back ET process takes place on slower timescales because this process falls in the Marcus inverted region, where the rates for ET occur on slower timescales despite increasing reaction exergonicity.[137]

4.5 Conclusion

In this work, the excited-state dynamics of two oxidatively damaged bases, 5-hydroxycytosine and 5-hydroxyuracil, as monomer nucleosides and as dinucleotides with adenine, were investigated for the first time. Using steady-state and ultrafast spectroscopic techniques and excited-state calculations, we determined that the monomers exhibit lengthened $\pi\pi^*$ excited-state lifetimes and greater fluorescence quantum yields compared to their unmodified canonical forms, with the lifetime of 5-hydroxycytidine being 150

times greater than cytidine. After selective excitation of the red-shifted absorption bands of the 5-hydroxypyrimidines at 295 nm, the time-resolved IR spectra of the dinucleotides contain spectral evidence for photoinduced ET to adenine in both cases. The forward and back ET processes occur on ultrafast and ps timescales, respectively, despite thermodynamic driving force calculations predicting that back ET is the more exergonic process. Apart from adding to the field of DNA excited-state dynamics and fundamental photochemistry, this work provides insight into the potential role of oxidatively damaged nucleobases as participants in photoinduced redox processes on the early Earth before the appearance of more complex redox enzymes.

4.6 References

96. Wagner, J. R.; Hu, C. C.; Ames, B. N., Endogenous Oxidative Damage of Deoxycytidine in DNA. *Proc. Natl. Acad. Sci. USA* **1992**, *89*, 3380-3384.

97. Yanagawa, H.; Ogawa, Y.; Ueno, M.; Sasaki, K.; Sato, T., A Novel Minimum Ribozyme with Oxidoreductive Activity. *Biochemistry* **1990**, *29*, 10585-10589.

98. Yanagawa, H.; Ogawa, Y.; Ueno, M., Redox Ribonucleosides: Isolation and Characterization of 5-Hydroxyuridine, 8-Hydroxyguanosine, and 8-Hydroxyadenosine from Torula Yeast RNA. *J. Biol. Chem.* **1992**, *267*, 13320-13326.

99. Thiviyanathan, V.; Somasunderam, A.; Volk, D. E.; Gorenstein, D. G., 5-Hydroxyuracil Can Form Stable Base Pairs with All Four Bases in a DNA Duplex. *Chem. Commun.* **2005**, *3*, 400-402.

100. Thiviyanathan, V.; Somasunderam, A.; Volk, D. E.; Hazra, T. K.; Mitra, S.; Gorenstein, D. G., Base-Pairing Properties of the Oxidized Cytosine Derivative, 5-Hydroxy Uracil. *Biochem. Biophys. Res. Commun.* **2008**, *366*, 752-757.

101. Kuepfer, P. A.; Leumann, C. J., Synthesis, Base Pairing Properties and Trans-Lesion Synthesis by Reverse Transcriptases of Oligoribonucleotides Containing the Oxidatively Damaged Base 5-Hydroxycytidine. *Nucleic Acids Res.* **2011**, *39*, 9422-9432.

102. Cockell, C. S.; Horneck, G., The History of the UV Radiation Climate of the Earth-Theoretical and Space-Based Observations. *Photochem. Photobiol.* **2001**, *73*, 447-451.

103. Liang, M.-C.; Hartman, H.; Kopp, R. E.; Kirschvink, J. L.; Yung, Y. L., Production of Hydrogen Peroxide in the Atmosphere of a Snowball Earth and the Origin of Oxygenic Photosynthesis. *Proc. Natl. Acad. Sci. USA* **2006**, *103*, 18896-18899.

104. Gilbert, W., Origin of Life: The RNA World. *Nature* **1986**, *319*, 618-618.

105. Cech, T. R.; Bass, B. L., Biological Catalysis by RNA. *Annu. Rev. Biochem* **1986**, *55*, 599-629.

106. Johnston, W. K.; Unrau, P. J.; Lawrence, M. S.; Glasner, M. E.; Bartel, D. P., RNA-Catalyzed RNA Polymerization: Accurate and General RNA-Templated Primer Extension. *Science* **2001**, *292*, 1319-1325.

107. Reader, J. S.; Joyce, G. F., A Ribozyme Composed of Only Two Different Nucleotides. *Nature* **2002**, *420*, 841-844.

108. La Francois, C. J.; Jang, Y. H.; Cagin, T.; Goddard, W. A.; Sowers, L. C., Conformation and Proton Configuration of Pyrimidine Deoxynucleoside Oxidation Damage Products in Water. *Chem. Res. Toxicol.* **2000**, *13*, 462-470.

109. Steenken, S., Electron-Transfer-Induced Acidity/Basicity and Reactivity Changes of Purine and Pyrimidine Bases: Consequences of Redox Processes for DNA Base Pairs. *Free Rad. Res. Commun.* **1992**, *16*, 349-379.

110. LaFrancois, C. J.; Fujimoto, J.; Sowers, L. C., Synthesis and Characterization of Isotopically Enriched Pyrimidine Deoxynucleoside Oxidation Damage Products. *Chem. Res. Toxicol.* **1998**, *11*, 75-83.

111. Suen, W.; Spiro, T. G.; Sowers, L. C.; Fresco, J. R., Identification by UV Resonance Raman Spectroscopy of an Imino Tautomer of 5-Hydroxy-2'-deoxycytidine, a Powerful Base Analog Transition Mutagen with a Much Higher Unfavored Tautomer Frequency Than That of the Natural Residue 2'-Deoxycytidine. *Proc. Natl. Acad. Sci. USA* **1999**, *96*, 4500-4505.

112. Rueda, M.; Luque, F. J.; López, J. M.; Orozco, M., Amino-Imino Tautomerism in Derivatives of Cytosine: Effect on Hydrogen-Bonding and Stacking Properties. *J. Phys. Chem. A* **2001**, *105*, 6575-6580.

113. Lukmanov, T.; Ivanov, S. P.; Khamitov, E. M.; Khursan, S. L., Relative Stability of Keto-Enol Tautomers in 5,6-Substituted Uracils: Ab Initio, DFT and PCM Study. *Computational and Theoretical Chemistry* **2013**, *1023*, 38-45.

114. Lu, Z.; Beckstead, A. A.; Kohler, B.; Matsika, S., Excited State Relaxation of Neutral and Basic 8-Oxoguanine (vol 119, pg 8293, 2015). *J. Phys. Chem. B* **2016**, *120*, 597-597.

115. Schreier, W. J.; Schrader, T. E.; Koller, F. O.; Gilch, P.; Crespo-Hernández, C. E.; Swaminathan, V. N.; Carell, T.; Zinth, W.; Kohler, B., Thymine Dimerization in DNA is an Ultrafast Photoreaction. *Science* **2007**, *315*, 625-629.

116. Kuimova, M. K.; Cowan, A. J.; Matousek, P.; Parker, A. W.; Sun, X. Z.; Towrie, M.; George, M. W., Monitoring the Direct and Indirect Damage of DNA Bases and Polynucleotides by Using Time-Resolved Infrared Spectroscopy. *Proc. Natl. Acad. Sci. USA* **2006**, *103*, 2150-2153.

117. Banyasz, A.; Douki, T.; Improta, R.; Gustavsson, T.; Onidas, D.; Vaya, I.; Perron, M.; Markovitsi, D., Electronic Excited States Responsible for Dimer Formation upon UV Absorption Directly by Thymine Strands: Joint Experimental and Theoretical Study. *J. Am. Chem. Soc.* **2012**, *134*, 14834-14845.

118. Cohen, B.; Crespo-Hernández, C. E.; Kohler, B., Strickler-Berg Analysis of Excited Singlet State Dynamics in DNA and RNA Nucleosides. *Faraday Discuss.* **2004**, *127*, 137-147.

119. Blancafort, L.; Cohen, B.; Hare, P. M.; Kohler, B.; Robb, M. A., Singlet Excited-State Dynamics of 5-Fluorocytosine and Cytosine: An Experimental and Computational Study. *J. Phys. Chem. A* **2005**, *109*, 4431-4436.

120. Gustavsson, T.; Bányász, Á.; Lazzarotto, E.; Markovitsi, D.; Scalmani, G.; Frisch, M. J.; Barone, V.; Improta, R., Singlet Excited-State Behavior of Uracil and Thymine in Aqueous Solution: A Combined Experimental and Computational Study of 11 Uracil Derivatives. *J. Am. Chem. Soc.* **2006**, *128*, 607-619.

121. Keane, P. M.; Wojdyla, M.; Doorley, G. W.; Watson, G. W.; Clark, I. P.; Greetham, G. M.; Parker, A. W.; Towrie, M.; Kelly, J. M.; Quinn, S. J., A Comparative Picosecond Transient Infrared Study of 1-Methylcytosine and 5 '-dCMP That Sheds Further Light on the Excited States of Cytosine Derivatives. *J. Am. Chem. Soc.* **2011**, *133*, 4212-4215.

122. Singh, J. S., FT-IR and Raman Spectra, Ab Initio and Density Functional Computations of the Vibrational Spectra, Molecular Geometries and Atomic Charges of Uracil and 5-Halogenated Uracils (5-X-uracils; X = F, Cl, Br, I). *Spectrochimica Acta Part a-Molecular and Biomolecular Spectroscopy* **2014**, *117*, 502-518.

123. Singh, J. S., FT-IR and Raman Spectra, Ab Initio and Density Functional Computations of the Vibrational Spectra, Molecular Geometries and Atomic Charges of Uracil and 5-Methyluracil (Thymine). *Spectrochimica Acta Part a-Molecular and Biomolecular Spectroscopy* **2015**, *137*, 625-640.

124. Steenken, S., Purine Bases, Nucleosides, and Nucleotides: Aqueous Solution Redox Chemistry and Transformation Reactions of Their Radical Cations and e- and OH Adducts. *Chem. Rev.* **1989**, *89*, 503-520.

125. Hare, P. M.; Crespo-Hernández, C. E.; Kohler, B., Internal Conversion to the Electronic Ground State Occurs via Two Distinct Pathways for Pyrimidine Bases in Aqueous Solution. *Proc. Natl. Acad. Sci. USA* **2007**, *104*, 435-440.

126. Salet, C.; Bensasson, R.; Becker, R. S., Triplet Excited States of Pyrimidine Nucleosides and Nucleotides. *Photochem. Photobiol.* **1979**, *30*, 325-329.

127. Strickler, S. J.; Berg, R. A., Relationship Between Absorption Intensity and Fluorescence Lifetime of Molecules. *J. Chem. Phys.* **1962**, *37*, 814-822.

128. Malone, R. J.; Miller, A. M.; Kohler, B., Singlet Excited-state Lifetimes of Cytosine Derivatives Measured by Femtosecond Transient Absorption. *Photochem. Photobiol.* **2003**, *77*, 158-164.

129. Nachtigallova, D.; Lischka, H.; Szymczak, J. J.; Barbatti, M.; Hobza, P.; Gengeliczki, Z.; Pino, G.; Callahan, M. P.; de Vries, M. S., The Effect of C5 Substitution on the Photochemistry of Uracil. *Phys. Chem. Chem. Phys.* **2010**, *12*, 4924-4933.

130. Zgierski, M. Z.; Fujiwara, T.; Kofron, W. G.; Lim, E. C., Highly Effective Quenching of the Ultrafast Radiationless Decay of Photoexcited Pyrimidine Bases by Covalent Modification: Photophysics of 5,6-Trimethylenecytosine and 5,6-Trimethyleneuracil. *Phys. Chem. Chem. Phys.* **2007**, *9*, 3206-3209.

131. Matsika, S., Radiationless Decay of Excited States of Uracil through Conical Intersections. *J. Phys. Chem. A.* **2004**, *108*, 7584-7590.

132. Teimoory, F.; Loppnow, G. R., Resonance Raman Intensities Demonstrate that C5 Substituents Affect the Initial Excited-State Structural Dynamics of Uracil More than C6 Substituents. *ChemPhysChem* **2016**, *17*, 1349-1355.

133. Blancafort, L.; Migani, A., Water Effect on the Excited-State Decay Paths of Singlet Excited Cytosine. *J. Photochem. Photobiol., A* **2007**, *190*, 283-289.

134. Canuel, C.; Mons, M.; Piuzzi, F.; Tardivel, B.; Dimicoli, I.; Elhanine, M., Excited States Dynamics of DNA and RNA Bases: Characterization of a Stepwise Deactivation Pathway in the Gas Phase. *J. Chem. Phys.* **2005**, *122*, article no. 074316.

135. Gut, I. G.; Wood, P. D.; Redmond, R. W., Interaction of Triplet Photosensitizers with Nucleotides and DNA in Aqueous Solution at Room Temperature. *J. Am. Chem. Soc.* **1996**, *118*, 2366-2373.

136. Nielsen, L. M.; Hoffmann, S. V.; Nielsen, S. B., Electronic Coupling Between Photo-Excited Stacked Bases in DNA and RNA Strands with Emphasis on the Bright States Initially Populated. *Photochem. Photobiol. Sci.* **2013**, *12*, 1273-1285.

137. Closs, G. L.; Miller, J. R., Intramolecular Long-Distance Electron Transfer in Organic Molecules. *Science* **1988**, *240*, 400-447.

CHAPTER FIVE

EXCITED-STATE DEACTIVATION OF VIOLACEIN ISOLATED FROM ANTARCTIC BACTERIA

5.1 Introduction

Ultraviolet radiation from the sun is harmful to living organisms because the highly energetic photons can damage biomolecules such as DNA. Organisms that spend significant amounts of their lifetimes in the sun must adapt strategies to avoid photodamages that may lead to mutations or cell death. Some phototrophic micro-organisms produce UV-screening molecules as a defense mechanism against solar irradiation.[138] For example, high solar irradiances induce the production of UV-absorbing compounds, such as scytonemin in cyanobacteria[139-140] and mycosporine-like amino acids in coral algae and phytoplankton.[141-142] In addition, it has been shown that organisms equipped with carotenoid pigments are more resistant to photodamage.[143]

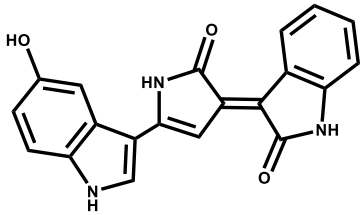
Bacterial colonies in Antarctica particularly benefit from this passive photoprotection strategy due to the presence of both continuous sunlight through the Austral summer and the additional UVC incident on this polar region.[144-145] Supraglacial streams are short-lived and seasonally subject to continuous solar irradiation. Studying bacterial populations in the harsh environmental conditions of supraglacial streams provides insight into the requirements necessary for survival at life's limits.[146] *Janthinobacterium* sp. CG23_2, an aerobic psychrotolerant rod-shaped organism isolated from the Cotton Glacier supraglacial stream in the Antarctic Dry Valleys (77° 07S, 161°

50E), produces the bisindole, purple pigment violacein.[41] Although violacein is produced in several bacterial species,[44] its unusual dimeric structure consisting of two indole rings is not common among other natural pigments.[147]

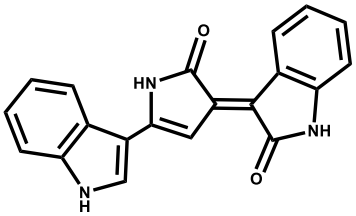
Amid many beneficial properties, such as antiobacterial and antitumoral properties,[42] it has also been suggested that violacein protects bacteria from harmful solar radiation.[43-45] One reason for this hypothesis is based on the antioxidative properties of violacein, as the pigment may alleviate cellular oxidative stress by scavenging reactive oxygen species generated by excess UV irradiation.[148-149] There is also evidence that violacein protects against solar radiation by absorbing the harmful photons.[43-44, 150] Violacein absorbs strongly across the UV ($\varepsilon = 1.6 \times 10^3\ M^{-1}\ cm^{-1}$ at $\lambda = 310$ nm) and visible ($\varepsilon = 3.4 \times 10^3\ M^{-1}\ cm^{-1}$ at $\lambda = 570$ nm) spectral regions due to its highly conjugated molecular structure (see Figure 5.1), which consists of 5-hydroxyindole (5-HI), 2-pyrollidone (2-PYR) and oxindole (OX). The latter two moieties are connected by a double bond contributing to the pigment's overall conjugation.

In the bacterial isolates collected by the Foreman group from Cotton Glacier, violacein production was increased in response to UV irradiation, suggesting the pigment provides photoprotection for the organisms much like sunscreen. Molecules are classified as sunscreens if they absorb sunlight strongly (i.e., have high molar extinction coefficients at UV and visible wavelengths) and are photostable, which means that the molecule is able to efficiently dissipate the energy of absorbed photons without undergoing photoreactions.[46] Molecular photostability is characterized by an ultrashort (hundreds of femtoseconds to tens of picoseconds) excited-state lifetime and complete recovery of the

ground-state population.[4] This occurs when the molecule undergoes UIC to the ground state, a hallmark of molecular photostability.[151] To date, a spectroscopic study of the photophysics of violacein has not been reported.



Violacein



Deoxyviolacein

Figure 5.1. Structures of the pigment molecules violacein and deoxyviolacein. The former structure consists of (from left to right) 5-hydroxyindole, 2-pyrollidone and oxindole heterocycles. The latter structure contains an indole in place of the 5-hydroxyindole.

The results of a combined fluorescence and femtosecond TA spectroscopic study of violacein isolated from *Janthinobacterium* sp. CG23_2 are presented in this chapter for the first time. The pigment has an excited-state lifetime of about 3 ps in methanol, consistent with its low fluorescence quantum yield. We observed that both the excited-state lifetime and fluorescence quantum yield increase with increasing solvent viscosity, indicating that the rate of deactivation is dependent on the solvent environment. I discuss the implications of these results for the deactivation mechanism of violacein by drawing parallels between our observations and those of similar spectroscopic studies of other

molecules that deactivate via large amplitude molecular motions. Finally, I consider the relevance of our findings to the proposed sunscreening role of violacein in bacteria by comparing its excited-state properties with those of several carotenoid pigments also isolated from the Antarctic supraglacial stream samples.

5.2 Experimental

5.2.1 Pigment Production and Composition

The supraglacial stream water samples from Cotton Glacier were collected by Prof. Christine Foreman and her research group from the Department of Biofilm Engineering at Montana State University.[41] In the Foreman lab, Dr. Heidi J. Smith grew the bacterial colonies and extracted the violacein pigment. *Janthinobacterium* sp. CG23_2 was grown to mid-exponential in the dark in a general-recovery low-nutrient media, R2A (Difco). Samples were concentrated via centrifugation (10,000 g for 15 min). The supernatant, insoluable in aqueous solution, was removed and replaced with an equal volume of methanol (99.8% Sigma) to extract violacein. Samples were incubated for 12 hrs at 4°C and centrifuged (10,000 g for 15 min) once again to separate the extracted pigment and cell debris. Although solvent extraction separated the pigment from most of the cell components, the sample purity was not satisfactory for spectroscopic measurements because the extract solutions still contained impurities (see Section 5.3.1 below). The crude pigment extract solutions were further processed using the SPE purification procedure described in Chapter 2.

Through the course of our collaboration, the Foreman group has provided us with five crude pigment extract solutions. Purification of pigment solutions extracted from *Janthinobacterium* sp. CG23_2 yielded very low violacein concentrations (see Section 5.3.1). To generate higher concentrations, the Foreman group extracted pigment from violacein hyper-producing *Janthinobacterium* sp. CG23_2 mutant colonies, which were genetically modified to generate greater quantities of violacein per growth period. Pigment extracts from the WT and mutant bacteria were evaluated and compared to ensure the violacein molecule had not been chemically altered.

Another purity consideration is that bacterial production of the violacein pigment generates a mixture of molecular forms: violacein and deoxyviolacein, which lacks the C5 hydroxyl group of the 5-HI, (Figure 5.1). The biochemical pathway for violacein production in bacteria also leads to the parallel synthesis of deoxyviolacein, and studies that isolate crude violacein extracts are generally referring to a mixture of violacein and deoxyviolacein.[42, 152-153] Although violacein is produced in excess, deoxyviolacein concentrations range from 10 – 30% of total pigment produced.[153-154] As a mixture of molecular forms could influence spectroscopic measurements, control experiments, presented in Section 5.3.1.1, were conducted to determine differences in photophysical properties between violacein and deoxyviolacein.

5.2.2 Spectroscopic Methods

UV absorption spectra were recorded before and after laser irradiation. Steady-state emission spectra were collected after 600 nm excitation using 3.0 nm bandpass slit widths, 2.5 nm sampling, and 20.0 s integration time. Sample concentrations were adjusted to an

optical density of 0.2 to avoid reabsorption of emitted light. TA instrumentation is described in detail in Chapter 2. In the experiments reported in this chapter, TA measurements were collected for all samples using 600 nm pump with 570 and 720 nm probe wavelengths. The 600 nm pump was attenuated to 0.9 μJ and focused to a spot size of about 670 μm (fwhm). TA kinetics of violacein in methanol was also collected using 265 nm pump and 570 nm probe wavelengths. The 265 nm pump energy was also attenuated to 0.9 μJ with a spot size of about 300 μm (fwhm). All violacein solutions were held within a steady-state 1 mm path length quartz cuvette for TA measurements.

5.3 Results

5.3.1 Purification Results

This section describes the results that led to the development of the SPE purification procedure outlined in Chapter 2 and the determination of the pigment extract molecular composition. In the following paragraphs, SPE purification refers to the procedure described in Chapter 2 unless otherwise indicated.

The base peak chromatogram of the crude pigment extract from WT *Janthinobacterium* sp. CG23_2, shown in Figure 5.2(a), contains several well-separated peaks eluting between 2.1 and 3.9 minutes. The selected peak eluted at 2.4 minutes (peak labeled 1) is assigned to $[M + H]^+$ = 344.1 g/mol, which, after subtracting the weight of the ESI-added proton, corresponds to the molecular weight of violacein (M = 343.1 g/mol). Based on the relative intensities of the violacein peak and the other peaks in the chromatogram, violacein appears to comprise a small percentage of the total solution.

HPLC provides only a rough estimate of the number of molecules present in a solution, however. The chromatogram peak intensities of different compounds cannot be quantitatively compared due to differences in column retention times. A more quantitative estimate can be gained from the mass spectrum shown in Figure 5.2(b). Upon comparing the intensity of the violacein peak at 344.1 m/z with the other m/z peak intensities, the results clearly indicate that the solution contains over 50% impurities, with most impurity compounds weighing between 120 and 250 g/mol. These initial analyses confirmed that the crude pigment extract solutions indeed contained a significant amount of impurities and required further purification before undergoing sensitive spectroscopic measurements.

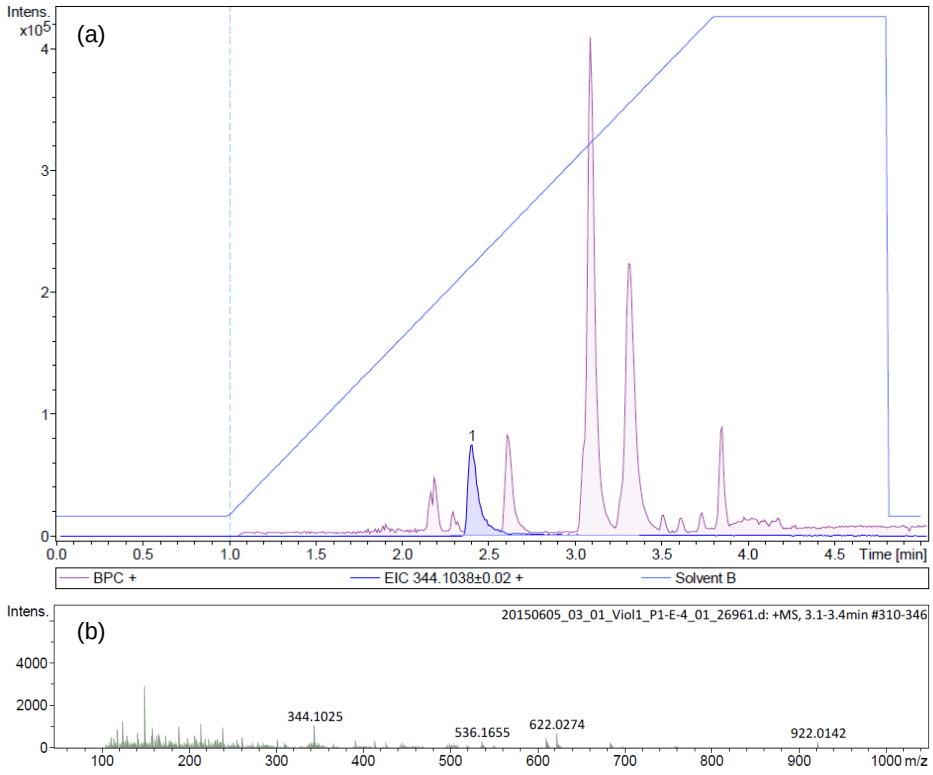


Figure 5.2. HPLC base peak chromatogram (BPC trace) of a diluted crude pigment extract as received from the Foreman group (a). Peak 1 (highlighted purple) corresponds to violacein. Mass spectrum of the same solution (b).

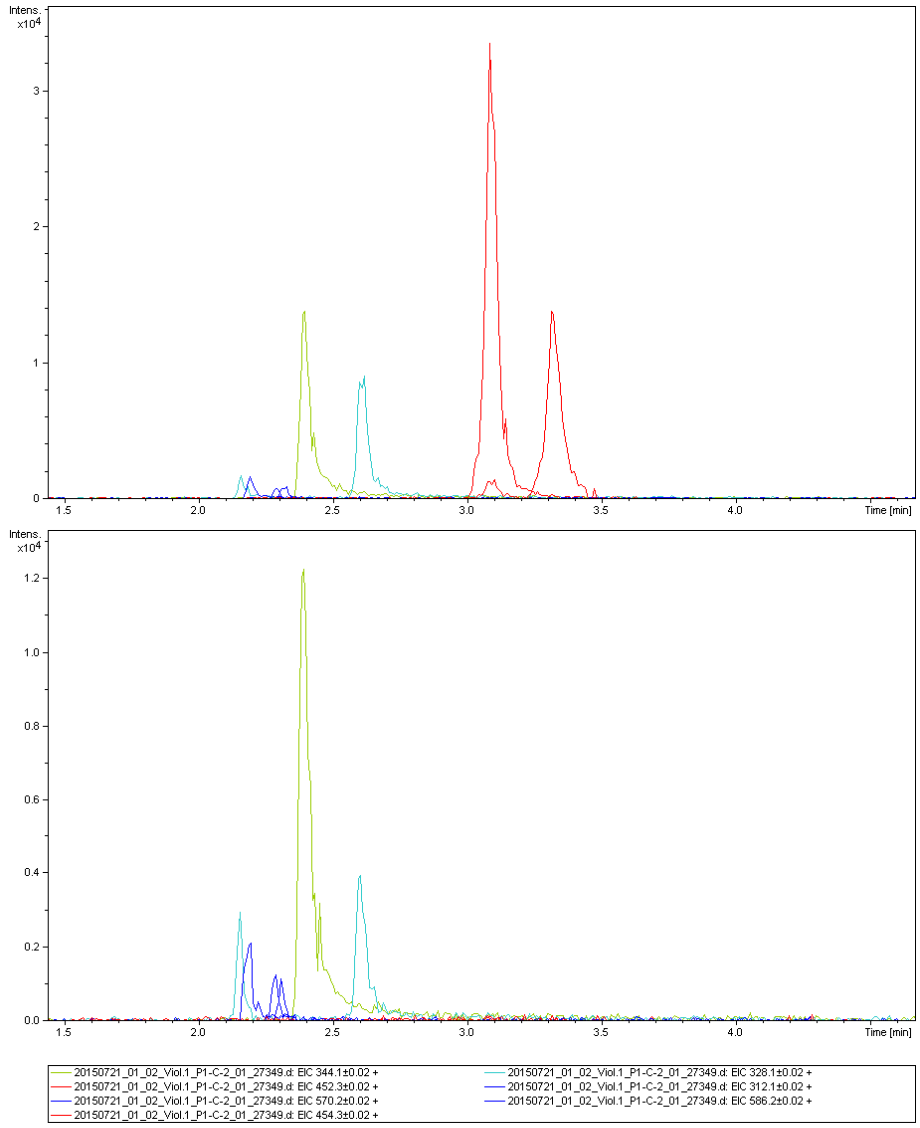


Figure 5.3. Upper panel: HPLC chromatogram of the crude pigment extract before SPE purification. The green peak corresponds to violacein, the light blue peak corresponds to deoxyviolacein and the red peaks are due to impurities. Lower panel: HPLC chromatogram after SPE purification illustrating the successful removal of impurities.

The upper panel in Figure 5.3 shows the chromatogram of the pigment extract before further purification with three distinct peak regions highlighted. The green and light blue peaks eluted at 2.4 and 2.6 minutes have $[M + H]^+$ values of 344.1 and 328.1 g/mol,

respectively, which correspond to the molecular weights of violacein and deoxyviolacein (M = 327.1 g/mol). The third peak region between 3.0 and 3.5 minutes, shown in red, is due to elution of impurities, as the molecular weights associated with these peaks do not correspond to either violacein or deoxyviolacein. This solution was loaded onto a SPE column and washed with 20% ACN to remove excess impurities. The pigment was eluted with 6 mL of 40% ACN, and the HPLC chromatogram of the collected solution is shown in the lower panel of Figure 5.3. Once again, molecular weight assignments confirmed the presence of violacein (green peak) and deoxyviolacein (light blue peak). However, the chromatogram no longer contained the impurity peaks that were present in the unpurified solution. This result demonstrated that SPE purification indeed removes impurities and the purified pigment can be conserved. In addition, the relative intensities of the green and light blue peaks indicate that the ratio of forms produced by the WT bacteria is comparable to the molar ratio of about 7:3 violacein to deoxyviolacein produced by other violacein-producing bacteria.[42, 153]

The pigment extract solutions from WT *Janthinobacterium* sp. CG23_2 were very dilute, and after purification, the procedure did not yield enough pure pigment for TA experiments. The Foreman group extracted pigment from the violacein hyper-producing mutant strain and MS measurements were performed to ensure the pigment molecules from both strains were identical. Figure 5.4 compares the fragmentation pattern of violacein purified from the hyper-producer (red peaks) and the WT CG23_2 (black peaks). MS fragmentation patterns provide a molecular fingerprint, and can be used to unambiguously identify molecules. The fragmentation peaks of violacein from both strains are present at

the same m/z and reach similar relative abundances. This is strong evidence that the pigment molecules produced by the different bacterial strains are identical and confirms that genetic modification did not affect violacein. Note that small differences in the position and magnitude of some low intensity peaks arise from instrumental noise and fall within the typical signal-to-noise ratio.

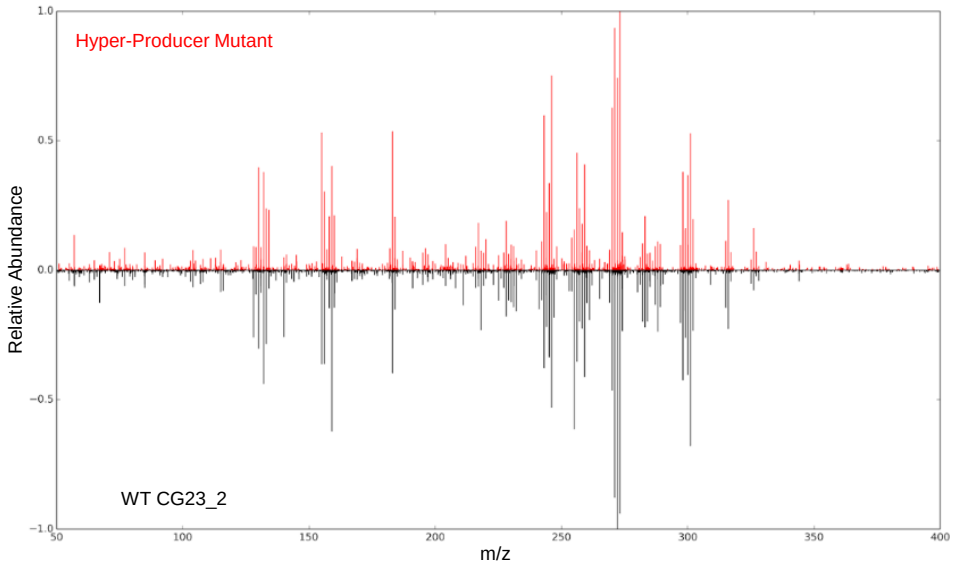


Figure 5.4. Mass spectrometry fragmentation patterns of violacein purified from the hyper-producing mutant compared to violacein purified from the wild-type CG23_2 strain. The identical pattern proves the pigment molecule is the same from both strains.

SPE purification of pigment extracts from the mutant strain yielded sufficient quantity of violacein for TA experiments. Although HPLC with ESI-MS detection confirmed the composition of the separations, steady-state UV-visible absorption, shown in Figure 5.5, provides further justification that SPE purification was effective. The spectrum of the crude pigment extract as received from the Foreman group (black trace labeled “extract”) shows an absorption band from 700 – 500 nm, and the absorption

increases significantly below ~450 nm. The absorption spectrum of pure violacein, previously published by Rettori and Durán,[155] exhibits well-separated absorption bands below 450 nm. In another study, the absorption spectrum of violacein purified from bacterial cultures using a single ethanol solvent extraction shows a similar increase in absorption below 450 nm.[44]

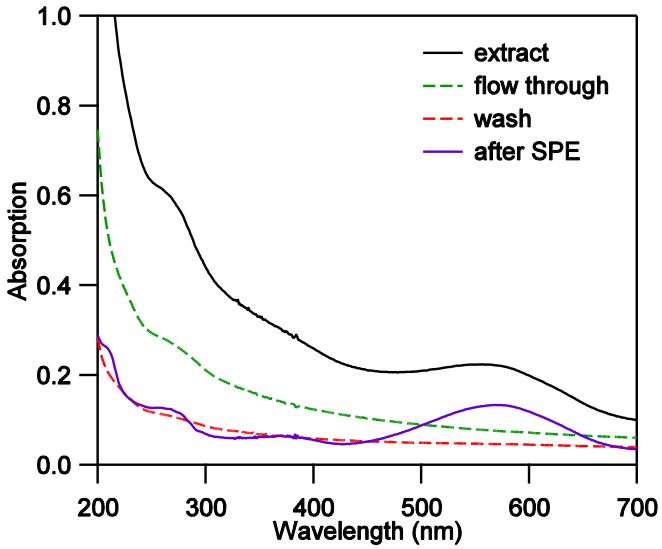


Figure 5.5. UV-visible absorption spectra of the crude pigment extract (black trace), the flow through (dashed green trace) and wash (dashed red trace) solutions collected during SPE, and the purified violacein after SPE.

This increase in absorption may be attributed to residual bacterial components, such as protein segments or DNA, which absorb in the UV region. Figure 5.5 also shows the absorption spectrum of the FT solution (dashed green trace) collected while loading pigment onto the SPE column, and the W solution (dashed red trace) collected after washing the pigment to remove impurities. Both FT and W solutions appear to lack violacein (no absorption band between 700 – 500 nm) and have increasing absorption

below 450 nm similar to the rise observed in the extract. These spectra indicate that the impurities causing the absorption below 450 nm either passed through the SPE column in the FT solution or were removed by washing the loaded pigment. The eluted violacein (purple trace labeled "after SPE") shows distinct absorption bands below 450 nm after SPE purification, and the spectrum is identical to that of highly pure violacein.[155]

The SPE purification method described in Chapter 2 includes two pigment elution steps. Highly purified violacein was eluted within the first 2 mL of eluent (E1) whereas the remainder of the pigment, which consisted of a mixture of 70% violacein and 30% deoxyviolacein, was eluted in the final step (E2). Pure violacein is isolated in the first couple mL, but deoxyviolacein elutes with violacein as more solution is used. This is because the two forms have very similar HPLC elution times (2.4 and 2.6 minutes as shown in Figure 5.3), making it difficult to elute one form without the other. Theoretically, the method could have been developed further to obtain solutions consisting of just violacein and just deoxyviolacein. However, as discussed in the next section, very little difference was observed in our excited-state measurements of the E1 and E2 solutions.

5.3.1.1 Violacein vs. Deoxyviolacein Control Measurements. Whereas violacein has been shown to offer many physiological benefits to bacteria, the biological role of deoxyviolacein, which is always synthesized in parallel, remains uncertain.[43] Several research groups have devised genetic or analytical methods for isolating deoxyviolacein,[42-43, 153] and one group has suggested that deoxyviolacein is more resistant to both UV and visible photodegradation than violacein.[43] To determine the difference in violacein and deoxyviolacein photophysics, initial spectroscopic measurements were performed on

solutions of the E1 and E2 SPE separations. If the photophysics differ greatly, TA measurements on a solution consisting of solely violacein (E1) versus a solution of about 70% violacein and 30% deoxyviolacein (E2) would reveal different deactivation lifetimes. To test this hypothesis, we carried out excited-state lifetime measurements on E1 and E2.

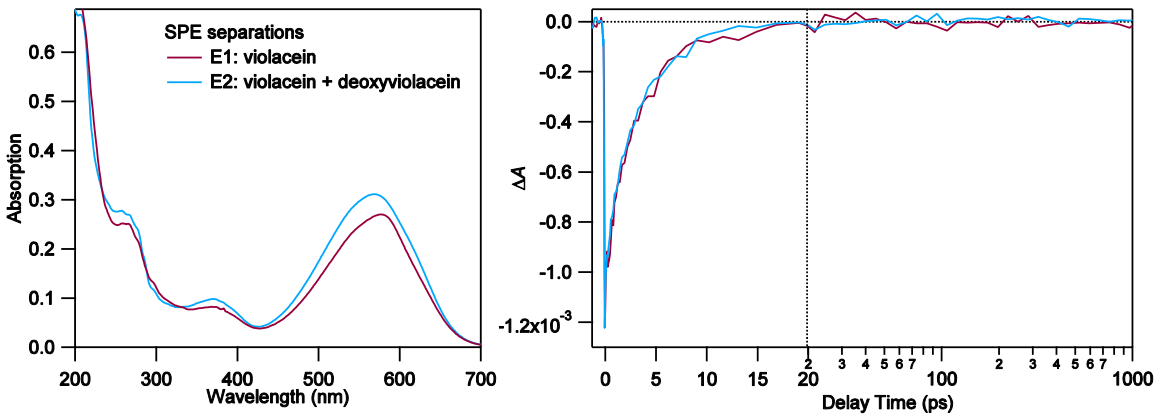


Figure 5.6. Left: UV-visible absorption spectra of the E1 and E2 SPE separations. Right: 600 nm pump / 720 nm probe TA kinetics of the same solutions.

After SPE, the E1 and E2 separations were in 35% and 50% ACN solutions, respectively. These solvents were removed via overnight dry N_2 air purging and the pigment samples were dissolved in 1.8 mL of pure methanol. UV-visible absorption spectra and 600 nm pump / 720 nm probe fs-TA measurements were measured on the solutions held in a 1 mm path length quartz cuvette. Figure 5.6 displays the E1 (maroon trace) and E2 (blue trace) absorption spectra in the left panel and the fs-TA kinetics in the right panel. Subtle differences are observed in the absorption spectra of E1 and E2. In particular, the first absorption band of the violacein solution is red-shifted by 9 nm compared to that of the mixture. Similar red-shifting of this visible band between the two forms has been observed previously, with magnitudes between 4 and 12 nm.[43, 153, 156] This slight red shift

is not large enough to suggest major changes in the excited states corresponding to this visible transition. The TA spectra shown in the right panel of Figure 5.6 corroborate this finding, as the scaled kinetics show no observable difference within the instrument signal-to-noise ratio.

Due to these control experiments, continued method development for purification of the two forms was deemed unnecessary. Hence, all other spectroscopy measurements were carried out on solutions of the 70% violacein, 30% deoxyviolacein mixture dissolved in pure solvents. Solution concentrations were calculated using the average molecular weight, i.e., 0.7(343.3 g/mol) + 0.3(327.3 g/mol) = 338.5 g/mol. Throughout the rest of this chapter, I will use violacein when referring to the mixture of forms.

5.3.2 Emission and Ultrafast Spectroscopy in Methanol

The UV-visible absorption spectrum of violacein in methanol (Figure 5.7(a)) is consistent with the spectrum of purified violacein pigment extract,[155] and exhibits a large absorption band at 569 nm (λ_{max}^{abs}). Based on semi-empirical calculations of violacein, Dias et al. assigned this band to a $\pi\pi^*$ transition localized on the central 2-PYR ring, and the second band centered at 370 nm to charge transfer from the 5-HI to the central 2-PYR.[157] The extinction coefficient (ε) based on our measurement is 3.4×10^3 M^{-1} cm^{-1} at 570 nm, comparable to the value 3.7×10^3 M^{-1} cm^{-1} at 570 nm measured by Wang et al.[158] Mende et al. reported an ε value of 1.9×10^4 M^{-1} cm^{-1} at 575 nm, but it is possible their measurement reflects significant error due to partial pigment purification.[152] In both studies, the researchers measured extinction coefficients of violacein from bacterial extracts, but the method of purification used by Mendes et al. consisted of a single solvent

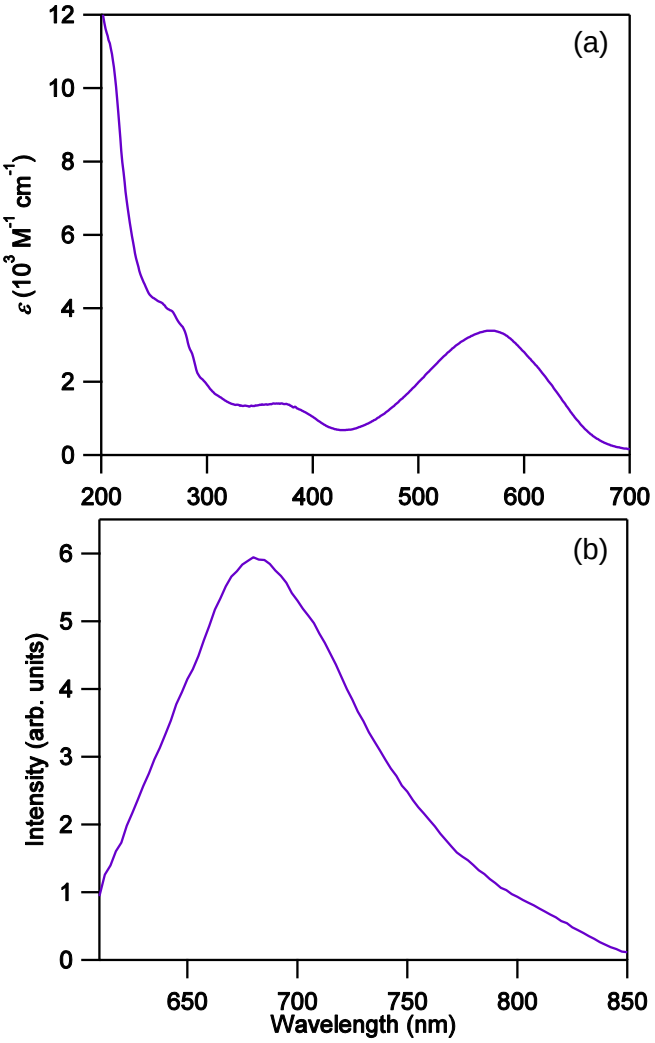


Figure 5.7. UV-visible absorption spectrum of violacein in methanol (a). Steady-state emission spectrum of violacein in methanol collected after 600 nm excitation, with 3.0 nm bandpass slit widths and 20.0 s integration (b). The spectrum was corrected for lamp intensity and solvent background emission.

extraction step whereas Wang et al. repeated solvent extraction several times to ensure pigment purity. As discussed in Section 5.3.1, a single solvent extraction step is insufficient for purifying the pigment from cell components, and results in greater absorbance than pure solutions (see Figure 5.5).

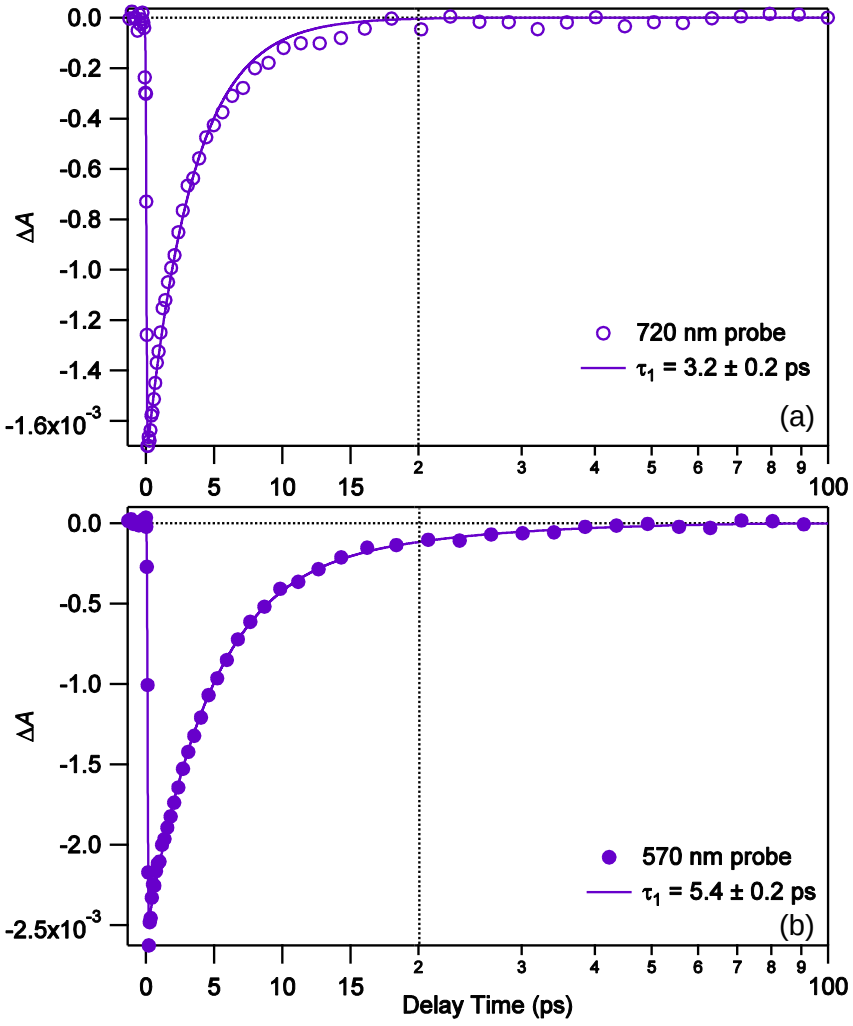


Figure 5.8. Single wavelength TA kinetics of violacein in methanol collected with 600 nm pump and 720 (a) and 570 nm (b) probe wavelengths. Both traces were fit to single exponentials with the time constants provided in the figures. Note the vertical dashed lines in both spectra represent the break between linear and logarithmic scales on the x-axis.

Figure 5.7(b) displays the emission spectrum of violacein in methanol after 600 nm excitation. Using the laser dye LDS 751 in methanol as a standard,[159] the fluorescence quantum yield of violacein was determined to be 1.37×10^{-4}. Both the emission spectrum and the fluorescence quantum yield of violacein are presented here for the first time.

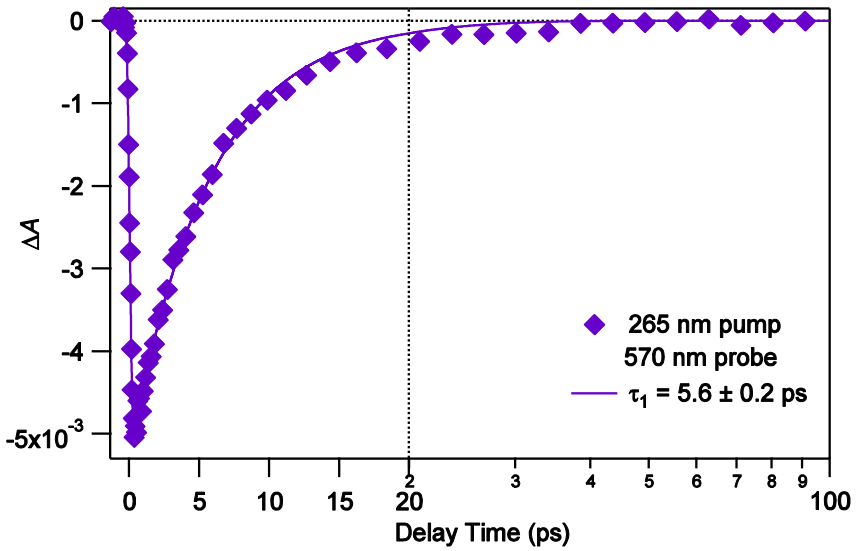


Figure 5.9. 265 nm pump / 570 nm probe TA kinetics of violacein in methanol.

TA measurements of violacein in methanol were collected with 600 nm pump and 720 (Figure 5.8(a)) and 570 nm (Figure 5.8(b)) probe beams. At both probe wavelengths, the negative ΔA signals recover monoexponentially and completely return to baseline with time constants of τ = 3.2 ± 0.2 ps and τ = 5.4 ± 0.2 ps for 720 and 570 nm probing, respectively. Identical TA kinetics are observed for the methanol solution using 265 nm pump / 570 nm probe wavelengths. The 265 nm pump pulses are intense enough to ionize the methanol solvent via two-photon excitation and generate solvated electrons, which absorb strongly at 570 nm.[57] Figure 5.9 shows the violacein kinetics after subtraction of the solvated electron signal according to the procedure described in Chapter 2.

Violacein UV-visible absorption spectra were collected before and after 600 and 265 nm laser exposure to determine whether photodegradation or photoproduct formation had occurred (Figure 5.10). In the 600 nm excitation experiments, the absorption spectrum did not change after about 2 hours of laser exposure (Figure 5.10(a)). With 265 nm

excitation, the absorption decreased slightly (less than 20%) after irradiation, indicating that a typical amount of photodegradation had occurred, as is common for 265 nm pump TA experiments (Figure 5.10(b)). There was no evidence for the formation of photoproducts after either visible or UV excitation. Additionally, the TA kinetics from 600

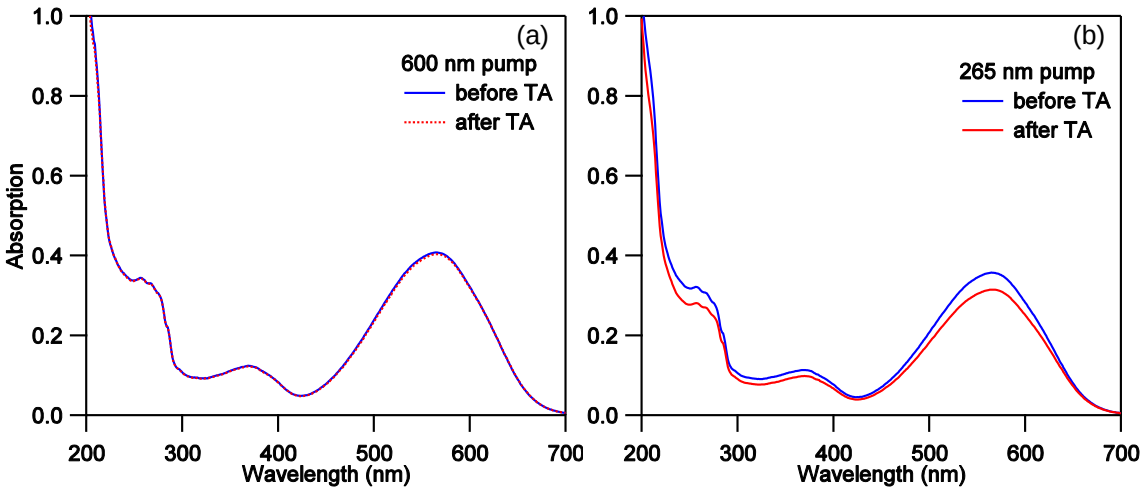


Figure 5.10. UV-visible absorption spectra of violacein in methanol recorded before (blue traces) and after (red traces) TA with 600 (a) and 265 nm (b) laser irradiance.

nm pump / 570 nm probe measurements are identical for solutions held in either a steady-state quartz cuvette or the flow cell (results not shown here). Due to the lack of photodegradation after 600 nm laser exposure, subsequent 600 nm pump TA experiments were conducted on violacein samples held in the steady-state cell. This eliminated the need to use the flow cell for measurements using the viscous solvents, which do not flow well, and required less pigment sample for each solution.

5.3.3 Emission and Ultrafast Spectroscopy in Viscous Solvents

Violacein was dissolved in several other solvents of varying viscosities, including acetone, ethylene glycol and glycerol. Ethylene glycol and glycerol have similar dielectric constants but drastically different viscosities (see Table 5.1).[160] Compared to methanol (0.54 mPa·s), the viscosities of ethylene glycol and glycerol are 16.1 and 934 mPa·s, respectively.[160] Acetone (0.31 mPa·s) was used as a control because it has a similar viscosity as methanol.[160] All solvents also have similar refractive indices.[160-162] All of the following spectroscopic measurements of violacein in these solvents were carried out at room temperature (20 ± 2°C).

Table 5.1. Physical properties of the different solvents used for violacein spectroscopy measurements.

	Viscosity (η, mPa·s)[a]	Dielectric (ε)[a]	Refractive Index (n)
Acetone	0.31	21.0	1.36[a]
Methanol	0.54	33.0	1.33[a]
Ethylene Glycol	16.1	41.4	1.43[b]
Glycerol	934	46.5	1.47[c]

[a]Measured at 25°C from ref 160. [b]Measured at 25°C from ref 161. [c]Measured at 20°C from ref 162.

UV-visible absorption and steady-state emission spectra of violacein in these solvents are presented in Figure 5.11. The absorption spectra of violacein in the different solvents are compared in Figure 5.11(a). Note that the spectra have been scaled for comparison of the visible band. As shown in Figure 5.11(b), violacein is much more emissive in the more viscous ethylene glycol and glycerol solutions compared to the low-viscosity acetone and methanol solutions. The fluorescence quantum yield of violacein in

ethylene glycol and glycerol increased by approximately 10 and 30 times compared to methanol, respectively.

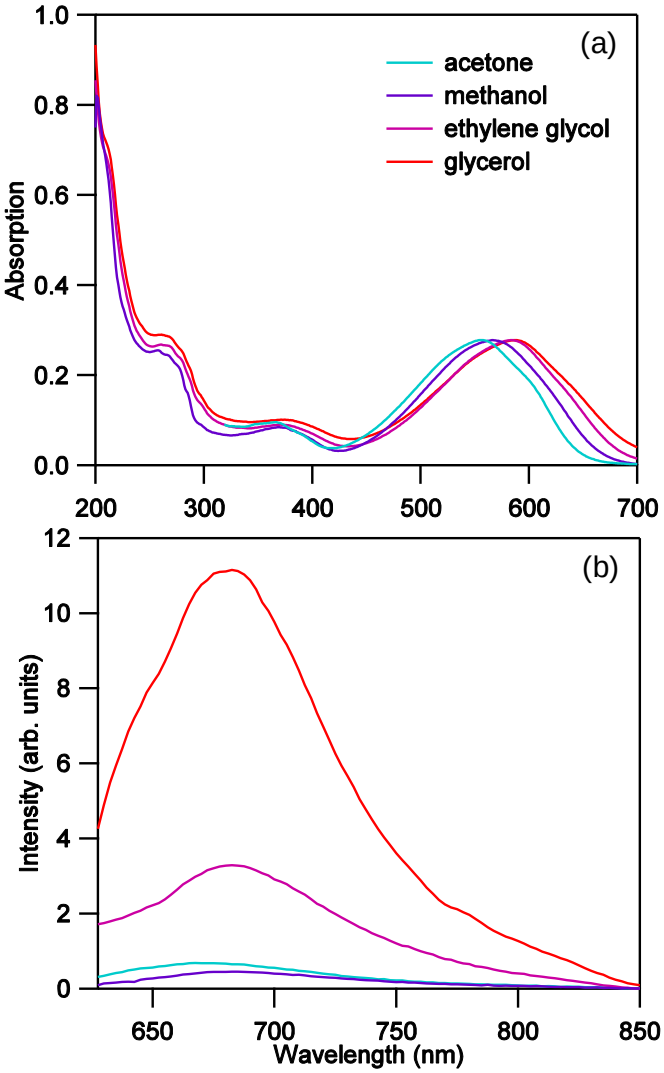


Figure 5.11. UV-visible absorption (a) and steady-state emission (b) spectra of violacein in the solvents indicated.

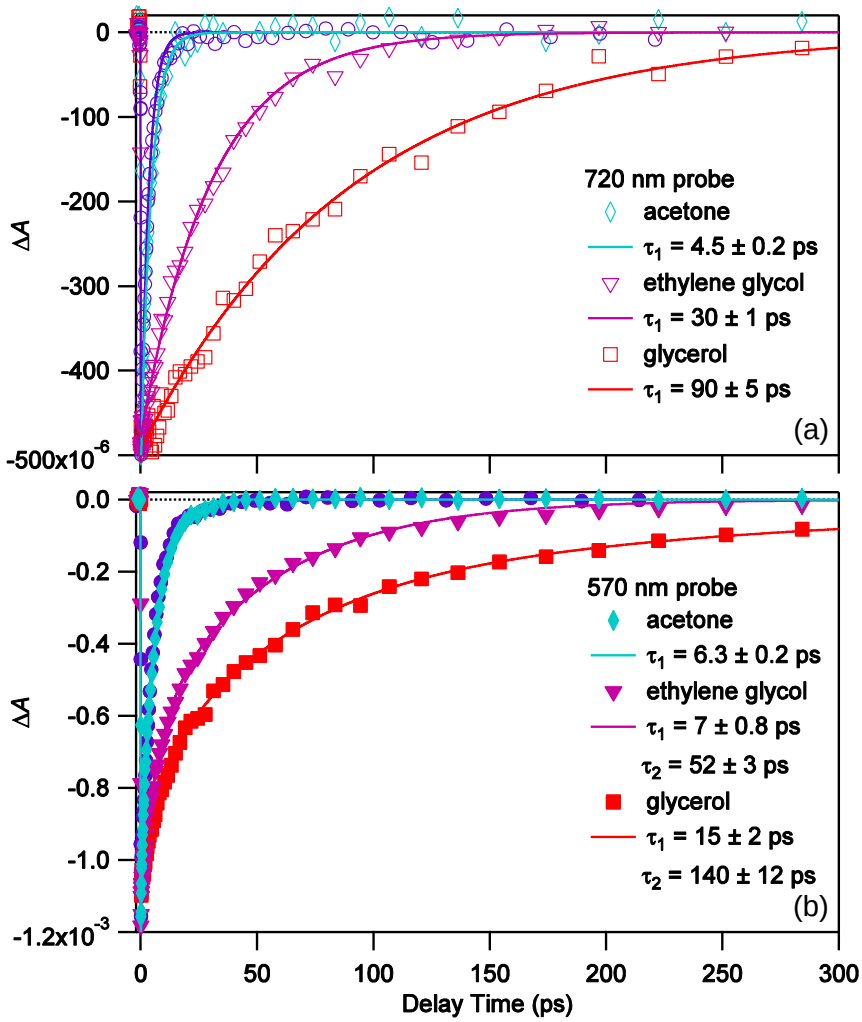


Figure 5.12. 600 nm pump TA kinetics of violacein in the solvents indicated collected with 720 (a) and 570 nm (b) probe beams. The kinetics of violacein in acetone were fit with a monoexponential function at both probe wavelengths. The kinetics in ethylene glycol and glycerol were fit with monoexponential functions at 720 nm and biexponential functions at 570 nm. Note that the methanol kinetics are included in both panels for comparison.

The kinetics of violacein in the different solvents observed at 720 nm (Figure 5.12(a)) reveal that the signals decay much more slowly in the viscous solutions than in the low-viscosity solutions. The 600 nm pump / 720 nm probe TA kinetics were fit using single exponential functions, which produced lifetimes of τ = 30 ± 1 ps for violacein in ethylene glycol and τ = 90 ± 5 ps for violacein in glycerol. By contrast, the violacein 720 nm kinetics

decay on a similar several-picosecond timescale in acetone as in methanol (τ = 3.2 ± 0.2 ps), with a proportionally low fluorescence quantum yield. Kinetics obtained with 570 nm

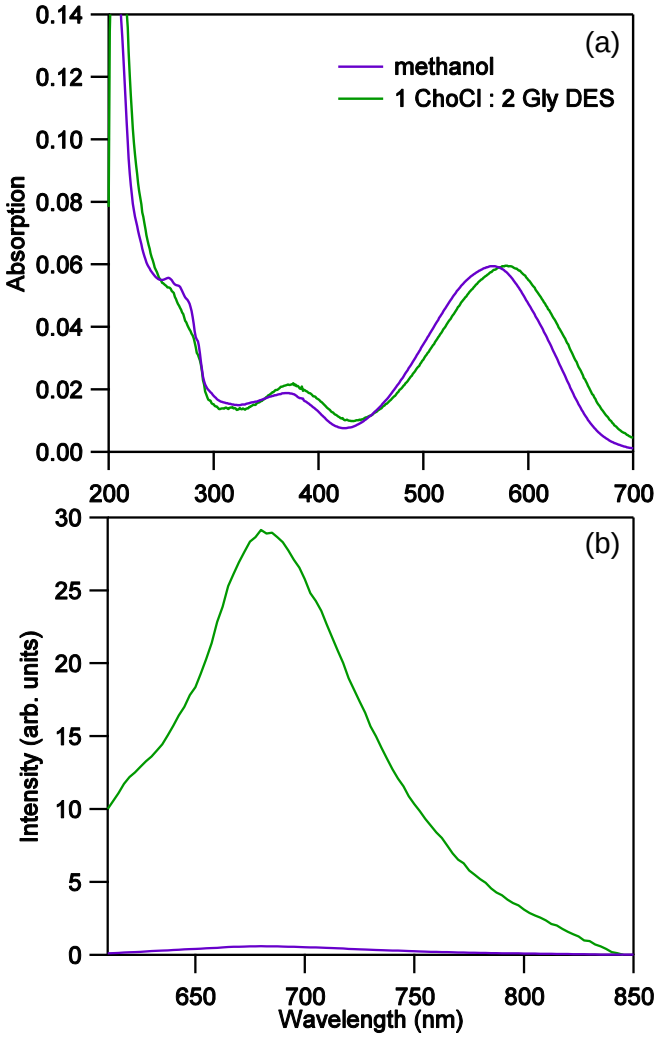


Figure 5.13. UV-visible absorption (a) and steady-state emission (b) spectra of violacein in GlyDES compared to methanol.

probing, shown in Figure 5.12(b), show that violacein deactivates on two distinct timescales in ethylene glycol and glycerol. Biexponential fitting produced lifetimes of τ = 7 ± 0.8 ps and τ = 52 ± 3 ps for violacein in ethylene glycol and τ = 15 ± 2 ps and τ = 140

± 12 ps for violacein in glycerol. In acetone, the 570 nm probe signal decays monoexponentially, as in the 570 nm probe kinetics observed in methanol, with a lifetime of τ = 6.3 ± 0.2 ps.

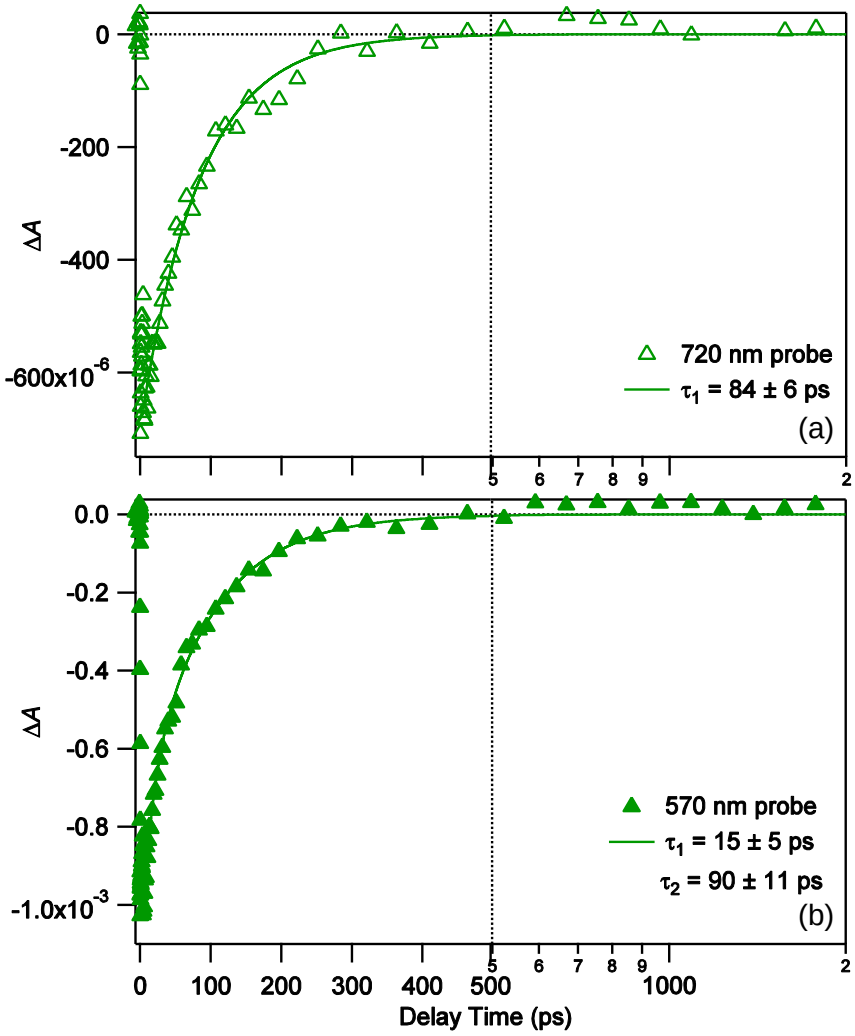


Figure 5.14. 720 (a) and 570 nm (b) probe TA kinetics of violacein in GlyDES collected after 600 nm excitation.

Our observations presented in Figures 5.11 and 5.12 suggest a solvent viscosity dependence on the deactivation lifetimes observed for violacein. To further test this

viscosity dependence, violacein was also dissolved in a DES consisting of choline chloride and glycerol in 1:2 molar ratio (designated as GlyDES). See Chapter 2 for the DES preparation procedure. It has been reported that this DES has a viscosity of 376 mPa·s at 33% ChoCl by mass.[53] Our DES, as prepared using the 1 ChoCl : 2 Gly molar ratio, contains 43% ChoCl by mass, indicating that the viscosity of our solution may actually be lower based on the available data.[53]

Figure 5.13 shows the UV-visible absorption and emission spectra of violacein in the GlyDES and in methanol for comparison. Our measured fluorescence quantum yield for violacein in this solution is 30×10^{-4}. TA kinetics, shown in Figure 5.14, were collected at both 570 nm and 720 nm probe wavelengths. Signals collected with 720 nm probing decay monoexponentially with a lifetime of $\tau = 84 \pm 6$ ps. Similar to our observations in the viscous ethylene glycol and glycerol solutions, the kinetics obtained using 570 nm probing decay biexponentially, producing one shorter time constant of $\tau = 15 \pm 5$ ps and one longer time constant of $\tau = 90 \pm 11$ ps.

5.3.4 Time-Resolved Emission in an Optical Glass at 77 K

Time-resolved emission measurements of violacein in an ethanol / methanol rigid optical glass formed at 77 K were collected using the TCSPC technique, as described in Chapter 2. Emission decays were collected after 310 nm excitation between 630 and 770 nm at 20 nm increments. Figure 5.15(a) shows the emission decay at 690 nm and illustrates the stark difference in decay lifetimes of violacein between room and cryogenic temperatures. The emission collected at room temperature (red trace) looks like the IRF (gray trace), which is about 50 ps, and contains a baseline due to background scattering. In

contrast, the emission collected at 77 K clearly decays more slowly and was fit using two exponentials, as described in Chapter 2.

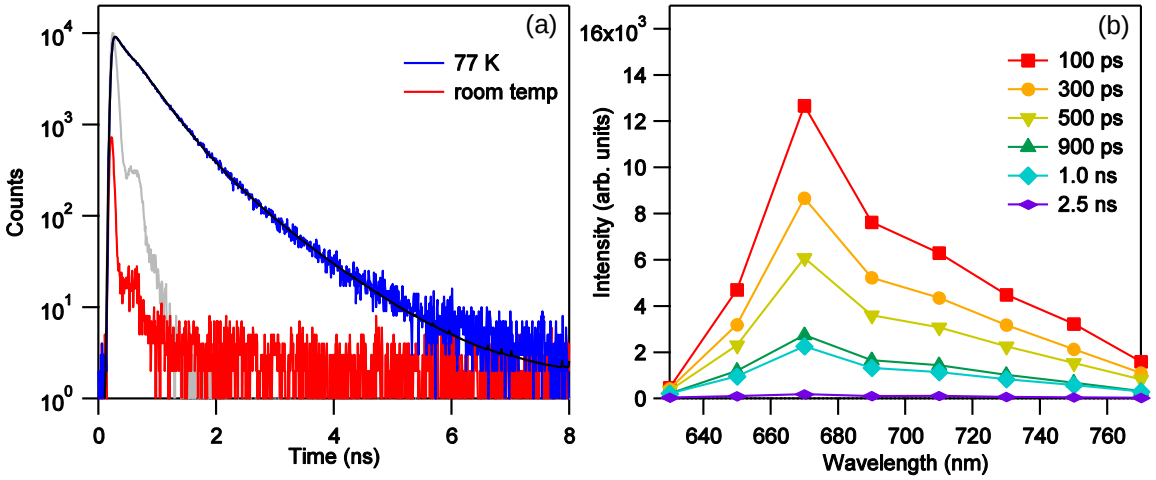


Figure 5.15. Time-resolved emission decay of violacein in a 5:1 volume ratio ethanol / methanol solution measured at 77 K (blue trace) and room temperature (red trace) collected at 690 nm (a). The 77 K decay was fit to two exponentials (black trace). The instrument response (IRF, gray trace) has FWHM of 50 ps. Time-resolved emission spectra of violacein in the same solution collected at the indicated wavelengths (b).

Lifetimes and their percent amplitudes are tabulated in Table 5.2. At 77 K, violacein emission in the alcoholic solution occurs on two timescales, approximately 400 ps and 1 ns. Note that the factor N_0/N is the percent of contributions from unresolvable emission components (those faster than the IRF) and background scattering. Time-resolved emission spectra (TRES) from these TCSPC measurements are plotted in Figure 5.15(b). At 77 K, violacein maximum emission occurs at 670 nm, which is consistent with the room temperature emission of violacein in methanol (see Figure 5.7(b)). The TRES also show that at each decay time the wavelength of maximum emission does not shift, and at each wavelength the emission decays completely by 2.5 ns.

Table 5.2. Fit parameters of 310 nm excitation TCSPC decays at the indicated emission wavelengths (λ_{em}) of violacein in the 5:1 volume ratio ethanol / methanol mixture at 77 K.

λ_{em} (nm)	$\%A_1$[a]	τ_1 (ns)[b]	$\%A_2$[a]	τ_2 (ns)[b]	N_o/N (%)[c]
630	59.6	0.64	40.4	1.30	7.28
650	84.7	0.45	15.3	1.00	8.63
670	87.4	0.42	12.6	0.87	8.42
690	87.0	0.41	13.0	0.94	8.78
710	90.1	0.43	9.86	1.06	8.62
730	93.3	0.43	6.69	1.17	8.65
750	93.9	0.43	6.14	1.26	8.93
770	93.1	0.43	6.95	1.32	9.38

[a]Percent amplitude (A) of the indicated [b]decay lifetime components (τ) as given by eqn. 2.4. [c]Factor accounting for background scattering and decay components not detected in TCSPC.

The time-integrated emission spectra of violacein at 77 K shown in Figure 5.16(a) depict the contribution of all emitting states to the total sample emission (labeled "sum", blue triangles). In this data, the total number of photons contributed come from the two emissive states multiplied by a TCSPC wavelength correction factor, quantified by $A_1\tau_1$ for the 400 ps decay component (green circles) and $A_2\tau_2$ for the 1 ns decay component (magenta squares). Contributions from any unresolvable fast decay components and background scattering are quantified by the factor $0.008B_o$ (pink inverted triangles), which is the same quantity as N_0, described in Table 5.2.[62] The steady-state emission spectrum of violacein was measured at 77 K by colleague Prof. Kimberly de La Harpe at the United States Air Force Academy in Colorado Springs. Shown in Figure 5.16(b), the violacein emission spectrum has the same maximum (about 670 nm) at cryogenic temperatures as the room temperature spectrum (Figure 5.7(b)) but exhibits a weak shoulder that peaks near 720 nm. This shoulder is also observed in the emission spectrum reconstructed from the TCSPC data ("sum" trace shown in Figure 5.16(a)), confirming that the total sample

emission obtained from TCSPC measurements is equivalent with the steady-state emission spectrum.

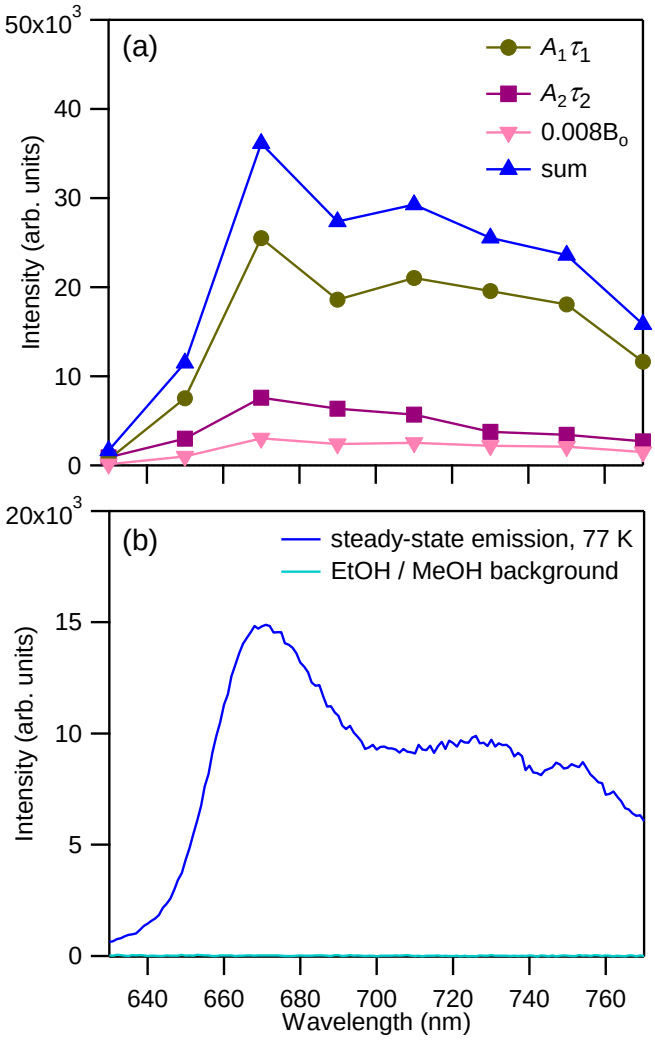


Figure 5.16. Time-integrated (a) and steady-state (a) emission spectra of violacein in the ethanol / methanol mixture collected at 77 K. The time-integrated emission spectra were corrected as described in the text.

5.4 Discussion

Table 5.3 lists the spectral characteristics of the steady-state UV-visible absorption and emission spectra of violacein in the different solvents studied in this chapter. As shown in Figures 5.11(a) and 5.13(a), minor differences are observed in violacein absorption below 400 nm. The visible transition between about 450 – 700 nm, which peaks at 569 nm in methanol, appears to shift in the other solvents. The wavelengths of maximum absorption, listed in Table 5.3, show that this visible band red-shifts with increasing solvent polarity and viscosity (acetone < methanol < ethylene glycol < 1 ChoCl : 2 Gly DES < glycerol). The greatest red-shift observed, from acetone to glycerol, is as much as 31 nm. Despite this substantial shifting in the visible absorption band, the emission spectra show negligible solvatochromism in the polar solvents after 600 nm excitation, as indicated by the wavelengths of maximum emission listed in Table 5.3. A solvatochromic shift of about

Table 5.3. Wavelengths of maximum absorption (λ_{max}^{abs}) and emission (λ_{max}^{fl}) and fluorescence quantum yields (ϕ_{fl}) of violacein in the solvents listed. All parameters were obtained experimentally in this study.

	λ_{max}^{abs} (nm)	λ_{max}^{fl} (nm)	$\phi_{fl} \times 10^4$
Acetone	556	668	2.0
Methanol	569	680	1.2
Ethylene Glycol	584	683	10.8
DES	580	683	30.0
Glycerol	587	683	33.0

12 nm occurs on going from the non-polar acetone solvent to the polar solvents, but little to no shifting of the emission band is observed as the solvent polarity increases. Solvent viscosity, however, strongly affects the fluorescence quantum yield of violacein. Our

calculated fluorescence quantum yields indicate that violacein emissions increase drastically as solvent viscosity increases (see Figure 5.11(b) and Table 5.3). Generally, fluorescence quantum yields and excited-state lifetimes are strongly correlated, although this is not always the case.[4] In the next section, we explore the connections between the fluorescence quantum yield and excited-state lifetime of violacein in these different solvents, and evaluate the implications of our observations for the mechanism of excited-state deactivation.

5.4.1 Violacein Excited-State Deactivation and Dynamics

The lifetimes and fitting parameters obtained from TA measurements using 600 nm pump and 720 and 570 nm probe wavelengths for all solutions are compared in Table 5.4. As violacein emission spans from about 600 – 850 nm, the 720 nm probe wavelength is expected to monitor stimulated emission, which is consistent with the negative ΔA signals observed in our 720 nm probe experiments. Stimulated emission produces more photons, resulting in a more negative signal according to the TA theory discussed in Chapter 2. We performed a systematic check to validate the phase of our signals were correct (see Chapter 2). Thus, the stimulated emission decays observed with 720 nm probing provide measurements of excited-state lifetimes. The negative ΔA signals observed with the 570 nm probe provide measurements of ground-state repopulation, or ground-state bleaching (GSB).

From the stimulated emission kinetics measured at 720 nm, violacein has an excited-state lifetime of approximately 3 ps in methanol (Figure 5.8(a)). The monoexponential kinetics show that the excited-state population fully recovers to the

ground state, as indicated by the absence of long-lived offsets due to population of dark states or intersystem crossing to a long-lived triplet state. This also indicates that the excited state does not lead to permanent photoproduct formation channels, which was also verified by recording the UV-visible absorption spectrum after laser irradiation. The violacein absorption spectrum did not change after either 600 or 265 nm irradiation (Figure 5.10). The observation of monoexponential decays at both probe wavelengths (Figure 5.8) suggest that transient photoreaction channels are also not accessed. Thus, virtually all excited-state violacein molecules return to the ground state on a picosecond time scale.

Table 5.4. Stimulated emission (720 nm) and ground-state bleach (570 nm) kinetic fit parameters of violacein in the solvents listed.

	λ_{probe} (nm)	τ_1 (ps)	τ_2 (ps)
Acetone	720	4.5 ± 0.2	−
	570	6.3 ± 0.2	−
Methanol	720	3.2 ± 0.2	−
	570	5.4 ± 0.2	−
Ethylene Glycol	720	30 ± 1	−
	570	7 ± 0.8	52 ± 3
DES	720	84 ± 6	−
	570	15 ± 5	90 ± 11
Glycerol	720	90 ± 5	−
	570	15 ± 2	140 ± 12

A picosecond excited-state lifetime of violacein in methanol is further supported by the low fluorescence quantum yield measured in this solvent (Table 5.3). Both the low fluorescence quantum yield and picosecond excited-state lifetime indicate that violacein deactivates predominantly nonradiatively in methanol. As the solvent viscosity increases, the fluorescence quantum yield of violacein increases and consistently, the stimulated

emission lifetime also increases. The proportionality between the fluorescence quantum yield and stimulated emission lifetimes is strong evidence that the lifetimes correspond to the S_1 excited state. This agreement also further validates that the 720 nm wavelength probes stimulated emission, and we tentatively assign the 720 nm kinetics to the S_1 excited-state lifetime of violacein.

Note that the fluorescence quantum yield measured in GlyDES is identical to that in glycerol, despite the significant difference in solvent viscosity (Table 5.1). The viscosity measurement given in Table 5.1 corresponds to 33% ChoCl by mass, but our DES contains about 43% ChoCl by mass and was very viscous by qualitative comparison with glycerol. Due to the limited information available for these relatively novel DESs, it is possible that the reported viscosity is inconsistent with the actual viscosity of our DES used in these measurements. Thus, the discrepancy does not negate a solvent viscosity dependence on the fluorescence quantum yield (or the excited-state lifetimes), and we focus more on the observations made in the other, more well-defined solvents.

GSB measurements capture the thermal equilibration of the vibrationally hot ground state, as the excess vibrational energy is dissipated as heat via intermolecular energy transfer to the solvent molecules.[163] Single-wavelength measurements record the rate of the so-called vibrational cooling process in addition to the ground-state repopulation by deactivation of the excited-state. Thus, the observed GSB lifetimes are slightly longer-lived than lifetime measurements from directly probing the excited state. Our 570 nm GSB kinetics are slightly longer-lived than the excited-state lifetimes measured in the stimulated emission kinetics. Due to this we tentatively assign the violacein GSB lifetimes to

vibrational cooling, which occurs in about 5.4 and 6.3 ps in methanol and acetone, respectively. This timescale is consistent with previous measurements of vibrational cooling rates in methanol and acetone.[163-165]

Two distinct lifetimes were observed in the 570 nm GSB kinetics of violacein in the more viscous ethylene glycol and glycerol solvents. As listed in Table 5.4, ground-state recovery occurs on two timescales in these solvents, including one fast and one slow component. In ethylene glycol, the fast timescale is 7 ± 0.8 ps and the slower timescale is 52 ± 3 ps, and in glycerol, the fast and slow timescales are slightly longer-lived than the kinetics observed in ethylene glycol (15 ± 2 and 140 ± 12 ps). The longer-lived time components are both slightly longer than the stimulated emission lifetimes observed in these solvents. Based on our previous conjecture, these GSB lifetimes may also arise from the convolution of excited-state deactivation and vibrational cooling timescales. Vibrational relaxation of betaine-30 in ethylene glycol occurs in about 15 ps,[164] and vibrational relaxation likely occurs on even slower timescales in glycerol.[166] However, the stimulated emission lifetimes in these solvents are too long for us to be observing VC dynamics. TA measurements are only sensitive to VC dynamics when the rate of excited-state deactivation competes with the rate of VC.

Due to the inherent difficulty in interpreting single-wavelength kinetic measurements in complex molecules such as violacein, it is difficult to definitively determine the origin of the lifetimes observed in the ethylene glycol and glycerol 570 nm kinetics. These solvents are both more polar and more viscous than methanol and acetone. We may speculate that the shorter lifetime may be due to the population of an intermediate

CT state that is more stabilized in more polar solvents. However, the relative amplitudes of the short and long 570 nm decay components are not well defined by the fitting program, i.e., their uncertainties are too high to attribute the associated time components to distinct populations. Based on this observation, we are more inclined to the possibility that the 570 nm photon probes a region consisting of competing photophysical processes. For instance, we may be probing a region where the ground-state absorption overlaps with some excited-state absorption. Broadband UV-visible transient spectra of violacein are needed to provide more definitive assignments for the possible transitions observed in this complex chromophore.

Compared to methanol, violacein excited-state deactivation lengthens by factors of approximately 9 in ethylene glycol, 30 in GlyDES and glycerol, and 125 at 77 K glass. The cause of this lifetime lengthening effect in the viscous solvents is not likely due to dynamic solvent effects brought on by changes in diffusive molecular motion, as diffusional processes typically exhibit non-exponential behavior.[167] In all solvent environments investigated here, violacein exhibits either single or double exponential decays, which are not indicative of diffusive processes. The lengthened excited-state lifetimes are not likely due to different timescales of solvent reorganization, which frequently exhibits dynamic red-shifting of emission.[168] Both the steady-state emission spectra of violacein in the different solvents at room temperature (Figure 5.11(b)) and the 77 K TRES measurements (Figure 5.15(b)) show that the maximum emission wavelength of violacein does not change over time.

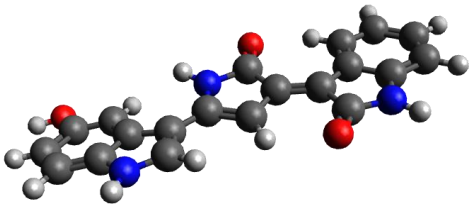
Our observations suggest that as the solvent environment becomes more constricting, either through increased solvent viscosity or at 77 K, the rate of violacein excited-state deactivation decreases. This solvent viscosity dependence on the fluorescence quantum yield and the excited-state lifetime of violacein suggests that a significant change in the molecular framework or a large amplitude molecular motion may be operative in deactivation. With the first solvent layer consisting of bulky, tightly bound solvent molecules, a large nuclear motion would occur more slowly in high solvent viscosity than in low solvent viscosity environments. Consequently, the rate of deactivation would be slowed significantly. Similar explanations have been invoked to explain the so-called viscous drag effect on excited-state deactivation of triphenylmethane dyes.[169] This could explain why the violacein excited-state lifetime increases in ethylene glycol, glycerol and the glycerol DES, which are all much more viscous than methanol, whereas the excited-state decays on a similar timescale in acetone, which has a viscosity similar in magnitude to methanol.

Decreasing the temperature to 77 K would also hinder a large amplitude molecular motion, as the rigid glass environment constrains the molecular degrees of freedom of the solute. The 77 K TCSPC results show increased emissions from violacein, and the decays slow to the several hundred picosecond and nanosecond timescale. Low-temperature studies have shown a similar effect on the rates of excited-state deactivation in the green fluorescent protein[170] and in modified stilbenes,[171] which deactivate via large amplitude molecular motions.

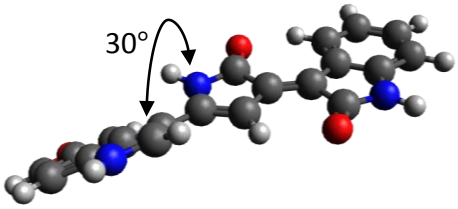
It was initially hypothesized that deactivation occurs via photoisomerization about the C=C double bond connecting the central 2-PYR and OX. Although *cis-trans* isomerization is generally associated with a large barrier on the electronic ground state potential energy surface, it can readily occur on π-π* electronic excited-state surfaces.[168] These ubiquitous unimolecular reactions, observed in the green fluorescent protein,[172] and retinal, the chromophore of rhodopsin,[173] can occur on ultrafast timescales. In high-viscosity solvents, this large-amplitude motion is hindered by the frictional forces of the viscous solvent environment, resulting in decreased rates of isomerization. The solvent viscosity dependent fluorescence quantum yield of violacein may be indicative of a photoisomerization mechanism, as similar experimental observations have been made in stilbenes[174] and cyanine dyes.[175] However, if *cis-trans* isomerization of the double bond were occurring, the TA signals should be consistent with the formation of two products, i.e., *cis* and *trans* isomers. This would be evidenced by an incomplete return of transient signal to baseline in the kinetic traces, but this was not observed.

Alternatively, violacein excited-state deactivation could involve a large-amplitude motion that enables access to a CI with the ground state. Evidence for this lies in the calculated molecular geometries of violacein in its ground and first excited state. Theoretical calculations were performed by Dr. Tom A.A. Oliver from the University of Bristol in Bristol, U.K. The optimized ground- and excited-state molecular geometries were calculated at the RICC2 level of theory using def-SVP and def2-TZVP basis sets for both violacein and deoxyviolacein in the gas phase. The results are shown in Figure 5.17. In the ground state, the non-planar geometry is more stable than the planar geometry by about

552 cm^{-1}, suggesting that the pigment is predominantly non-planar at room temperature. In the non-planar geometry, the OX is in plane with the central 2-PYR, whereas the 5-HI is out-of-plane with a dihedral angle (N-C-C-C, as shown) of 30°. A dihedral angle of about 20° between the 5-HI and the coplanar 2-PYR and OX was predicted previously for violacein using both semiempirical INDO/S[157] and DFT calculations.[176] The 10° difference may be due to the different levels of theory. In the excited state, the optimized geometry of violacein is much more planar, although not perfectly planar, with a dihedral angle near zero. Interestingly, the computational results were identical for both violacein and deoxyviolacein, which adds to the argument made in Section 5.3.1.1 that the electronic structure is not appreciably altered by the presence or absence of the C5-hydroxyl, and may explain the identical excited-state lifetimes observed in both forms.



(b) S_1 geometry



(a) S_0 geometry

Figure 5.17. RICC2 quantum calculations of the (a) ground state and (b) excited state optimized geometries of violacein in the gas phase.

These geometry calculations may provide an explanation for the solvent viscosity dependence of violacein excited-state deactivation. Upon absorption of a photon, the non-planar violacein molecule is instantaneously excited to the Frank-Condon region, where it initially maintains its non-planar geometry. The molecule subsequently moves to its more planar geometry through a single bond torsional motion between the 5-HI and the coplanar 2-PYR and OX moieties, which enables it to access the CI with the electronic ground state. After deactivation, the single bond torsion is reversed and the molecule once again occupies its minimum energy non-planar geometry. In the low viscosity environment of methanol and acetone, these molecular motions may occur with relative ease. However, these molecular motions may be slowed considerably in more viscous or rigid solvent environments considering the 5-HI group would have to rotate ~30° against frictional forces of the solvent when transitioning between conformations. A rotation of this magnitude would be slower in a more viscous solvent environment, which is consistent with the observations in viscous solvents and optical glasses at 77 K.

5.4.2 Photostability and Comparison with Other Natural Pigments

In methanol, violacein excited-state deactivation occurs on an ultrafast timescale, with an excited-state lifetime of 3 ps and an ultralow fluorescence quantum yield of 1.2×10^{-4}. This measured fluorescence quantum yield is comparable in magnitude to the low fluorescence quantum yields of the canonical nucleobases, which are known to be highly photostable.[79] Furthermore, TA signals show complete recovery to baseline, indicating that no excited-state violacein molecules returned to their ground state energies without

undergoing photoreactions or photoproduct formation. Taken together, the photophysics in methanol suggest that violacein can be characterized as a photostable molecule.

Of course, violacein excited-state behavior in vivo may be drastically different than in methanol. The measurements in viscous solvents illustrate how violacein deactivation sensitively depends on the surrounding environment. Being water insoluble, it is likely the pigment resides within the lipid bilayer of the CG23_2 bacterial cells. Konzen et al. showed that violacein can be incorporated into the lipid bilayer of *Chromobacterium violaceum* with high yields and that extraction of the pigment requires breaking of the cell walls.[148] The molecularly crowded cell membrane is likely to have a similar lifetime-lengthening effect on the chromophore excited-state dynamics as the high viscosity solvent and low temperature environments. With longer lifetimes, reactive excited states are more likely to undergo potentially harmful photoreactions. Despite this possibility, excited-state duration alone cannot adequately determine the sunscreening role of a molecule, especially one that resides within the molecularly complex environment of a bacterial cell.

Evaluating the photoprotective role of a bacterial secondary metabolite is not a trivial task. Not only should the molecule absorb solar radiation, its production must be induced upon irradiation, and it must provide effective screening and enhance the survivability of the organism under irradiation.[177] Violacein meets the first two criteria, but the second two are often complicated by several factors and are thus difficult to determine. Oftentimes the evidence in support of a molecule acting as a sunscreen is circumstantial. For instance, a major complication arises if the molecule in question also serves other vitally important physiological purposes.[138] Violacein may increase bacterial survivability

due to its antioxidative properties,[148] and this active property complicates the determination of its efficacy as a passive sunscreen molecule. The difficulty inherent in designating a molecule as a sunscreen is the reason that of the many natural pigments found in biological systems (e.g., mycosporine-like amino acids, flavonoids in plants, melanin in humans, etc.), scytonemin produced in the sheaths of cyanobacteria is one of the only confirmed screening compounds.[138]

Interestingly, the molecular structure of violacein can be compared to that of scytonemin to a certain extent, and compared to carotenoids, both pigments have extended absorption into longer visible wavelengths.[139] In fact, one clear difference between violacein and other carotenoid pigments is its increased long wavelength visible region absorption. Zeaxanthin, astaxanthin and staphyloxanthin were also isolated from bacteria in the Antarctic supraglacial stream water samples collected by the Foreman group. In solution, these compounds exhibit ultrafast excited-state deactivation, with lifetimes of 9 ps for zeaxanthin and 5 ps for astaxanthin.[178-179] This is consistent with the characteristically low emissions of carotenoids in general.[178] However, these carotenoids absorb strongest between 350 – 500 nm,[180-181] whereas violacein has a broad absorption band between 500 – 700 nm.

5.5 Conclusion

An ultrafast photophysical study of violacein in methanol, and several other solvent environments, was presented for the first time. Violacein, a pigment produced by *Janthinobacterium* sp. CG23_2 in Antarctica, has been proposed to protection the bacteria

from harmful solar rays.[44] This work provides an ultrafast spectroscopic determination of the intrinsic photoproperties of the pigment and a measurement of its fluorescence spectra in methanol, acetone, ethylene glycol, glycerol, a glycerol-based DES, and in an alcoholic glass at 77 K. Violacein has an ultrafast excited-state lifetime of about 3 ps in methanol, and the deactivation mechanism via single bond torsion between the 5-HI and coplanar 2-PYR and OX groups was supported by experiments in viscous solvents, cryogenic temperatures and quantum chemical calculations. Further work is warranted to determine the relevance of these results to the sunscreen capability of this pigment, and to further understand the role of violacein in providing photoprotection for bacteria under elevated solar irradiation.

5.6 References

138. Cockell, C. S.; Knowland, J., Ultraviolet Radiation Screening Compounds. *Biological Reviews of the Cambridge Philosophical Society* **1999**, *74*, 311-345.

139. Proteau, P. J.; Gerwick, W. H.; Garcia-Pichel, F.; Castenholz, R., The Structure of Scytonemin, an Ultraviolet Sunscreen Pigment from the Sheaths of Cyanobacteria. *Experientia* **1993**, *49*, 825-9.

140. Castenholz, R. W.; Garcia-Pichel, F., Cyanobacterial Responses to UV-Radiation. *Ecol. Cyanobacteria* **2000**, 591-611.

141. Karsten, U.; Sawall, T.; Hanelt, D.; Bischof, K.; Figueroa, F. L.; Flores-Moya, A.; Wiencke, C., An Inventory of UV-Absorbing Mycosporine-Like Amino Acids in Macroalgae from Polar to Warm-Temperate Regions. *Bot. Mar.* **1998**, *41*, 443-453.

142. Dunlap, W. C.; Shick, J. M.; Yamamoto, Y., Sunscreens, Oxidative Stress and Antioxidant Functions in Marine Organisms of the Great Barrier Reef. *Redox Rep.* **1999**, *4*, 301-306.

143. Dieser, M.; Greenwood, M.; Foreman, C. M., Carotenoid Pigmentation in Antarctic Heterotrophic Bacteria as a Strategy to Withstand Environmental Stresses. *Arctic Antarctic and Alpine Research* **2010**, *42*, 396-405.

144. Nienow, J. A.; McKay, C. P.; Friedmann, E. I., The Cryptoendolithic Microbial Environment in the Ross Desert of Antarctica: Light in the Photosynthetically Active Region. *Microbial Ecology* **1988**, *16*, 271-289.

145. Staehelin, J.; Harris, N. R. P.; Appenzeller, C.; Eberhard, J., Ozone Trends: A Review. *Reviews of Geophysics* **2001**, *39*, 231-290.

146. Foreman, C. M.; Cory, R. M.; Morris, C. E.; SanClements, M. D.; Smith, H. J.; Lisle, J. T.; Miller, P. L.; Chin, Y.-P.; McKnight, D. M., Microbial Growth Under Humic-Free Conditions in a Supraglacial Stream System on the Cotton Glacier, Antarctica. *Environmental Research Letters* **2013**, *8*, article no. 35022..

147. Margalith, P. Z., *Pigment Microbiology*. Chapman and Hall: London, 1992.

148. Konzen, M.; De Marco, D.; Cordova, C. A. S.; Vieira, T. O.; Antonio, R. V.; Creczynski-Pasa, T. B., Antioxidant Properties of Violacein: Possible Relation on its Biological Function. *Biorg. Med. Chem.* **2006**, *14*, 8307-8313.

149. Cao, W.; Chen, W.; Sun, S.; Guo, P.; Song, J.; Tian, C., Investigating the Antioxidant Mechanism of Violacein by Density Functional Theory Method. *Journal of Molecular Structure-Theochem* **2007**, *817*, 1-4.

150. Antonio, R. V.; Creczynski-Pasa, T. B., Genetic Analysis of Violacein Biosynthesis by Chromobacterium Violaceum. *Genetics and Molecular Research : GMR* **2004**, *3*, 85-91.

151. Otterstedt, J.-E. A., Photostability and Molecular Structure. *J. Chem. Phys.* **1973**, *58*, 5716-5725.

152. Mendes, A. S.; de Carvalho, J. E.; Duarte, M. C. T.; Duran, N.; Bruns, R. E., Factorial Design and Response Surface Optimization of Crude Violacein for Chromobacterium Violaceumi Production. *Biotechnol. Lett* **2001**, *23*, 1963-1969.

153. Rodrigues, A. L.; Goecke, Y.; Bolten, C.; Brock, N. L.; Dickschat, J. S.; Wittmann, C., Microbial Production of the Drugs Violacein and Deoxyviolacein: Analytical Development and Strain Comparison. *Biotechnol. Lett* **2012**, *34*, 717-720.

154. Wang, H.; Wang, F.; Zhu, X.; Yan, Y.; Yu, X.; Jiang, P.; Xing, X.-H., Biosynthesis and Characterization of Violacein, Deoxyviolaceiri and Oxyviolacein in Heterologous Host, and Their Antimicrobial Activities. *Biochem. Eng. J.* **2012**, *67*, 148-155.

155. Rettori, D.; Duran, N., Production, Extraction and Purification of Violacein: an Antibiotic Pigment Produced by Chromobacterium Violaceum. *World Journal of Microbiology & Biotechnology* **1998**, *14*, 685-688.

156. Sanchez, C.; Brana, A. F.; Mendez, C.; Salas, J. A., Reevaluation of the Violacein Biosynthetic Pathway and its Relationship to Indolocarbazole Biosynthesis. *ChemBioChem* **2006**, *7*, 1231-1240.

157. Dias, L. C.; Neto, J. D. D.; Rettori, D.; Duran, N., Semiempirical INDO/S Study on the Absorption Spectrum of Violacein. *Journal of Molecular Structure-Theochem* **2002**, *580*, 85-90.

158. Wang, H.; Jiang, P.; Lu, Y.; Ruan, Z.; Jiang, R.; Xing, X.-H.; Lou, K.; Wei, D., Optimization of Culture Conditions for Violacein Production by a New Strain of Duganella sp B2. *Biochem. Eng. J.* **2009**, *44*, 119-124.

159. Hebert, P.; Baldacchino, G.; Gustavsson, T.; Mialocq, J. C., Photochemistry of an Unsymmetrical Polymethine-Cyanine Dye: Solute Solvent Interactions and Relaxation Dynamics of LDS-751. *J. Photochem. Photobiol., A* **1994**, *84*, 45-55.

160. Lide, D. R., *Handbook of Chemistry and Physics*. 84th ed.; CRC Press: Boca Raton, **2004**.

161. Fogg, E. T.; Hixson, A. N.; Thompson, A. R., Densities and Refractive Indexes for Ethylene Glycol-Water Solutions. *Anal. Chem.* **1955**, *27*, 1609-1611.

162. Hoyt, L. F., New Table of the Refractive Index of Pure Glycerol at 20 degrees C. *Ind. Eng. Chem.* **1934**, *26*, 329-332.

163. Middleton, C. T.; Cohen, B.; Kohler, B., Solvent and Solvent Isotope Effects on the Vibrational Cooling Dynamics of a DNA Base Derivative. *J. Phys. Chem. A* **2007**, *111*, 10460-10467.

164. Terazima, M., Vibrational Relaxation from Electronically Photoexcited States in Solution Studied by the Acoustic Peak Delay Method: Hydrogen Bonding Effect to Betaine-30. *Chem. Phys. Lett.* **1999**, *305*, 189-196.

165. Miyata, R.; Kimura, Y.; Terazima, M., Intermolecular Energy Transfer from the Photo-Excited Molecule to Solvent: Malachite Green. *Chem. Phys. Lett.* **2002**, *365*, 406-412.

166. Stratt, R. M.; Maroncelli, M., Nonreactive Dynamics in Solution: The Emerging Molecular View of Solvation Dynamics and Vibrational Relaxation. *J. Phys. Chem.* **1996**, *100*, 12981-12996.

167. Horng, M. L.; Gardecki, J. A.; Papazyan, A.; Maroncelli, M., Subpicosecond Measurements of Polar Solvation Dynamics: Coumarin 153 Revisited. *J. Phys. Chem.* **1995**, *99*, 17311-17337.

168. Rosspeintner, A.; Lang, B.; Vauthey, E., Ultrafast Photochemistry in Liquids. In *Annual Review of Physical Chemistry, Vol 64*, Johnson, M. A.; Martinez, T. J., Eds. 2013; Vol. 64, pp 247-271.

169. Duxbury, D. F., The Photochemistry and Photophysics of Triphenylmethane Dyes in Solid and Liquid-Media. *Chem. Rev.* **1993**, *93*, 381-433.

170. Litvinenko, K. L.; Webber, N. M.; Meech, S. R., Internal Conversion in the Chromophore of the Green Fluorescent Protein: Temperature Dependence and Isoviscosity Analysis. *J. Phys. Chem. A* **2003**, *107*, 2616-2623.

171. Imamoto, Y.; Kuroda, T.; Kataoka, M.; Shevyakov, S.; Krishnamoorthy, G.; Liu, R. S. H., Photoisomerization by Hula Twist: 2,2 '-Dimethylstilbene and a Ring-Fused Analogue. *Angew. Chem. Int. Ed.* **2003**, *42*, 3630-3633.

172. Vengris, M.; van Stokkum, I. H. M.; He, X.; Bell, A. F.; Tonge, P. J.; van Grondelle, R.; Larsen, D. S., Ultrafast Excited and Ground-State Dynamics of the Green Fluorescent Protein Chromophore in Solution. *J. Phys. Chem. A* **2004**, *108*, 4587-4598.

173. Liu, R. S. H.; Asato, A. E., Photochemistry of Polyenes.22. The Primary Process of Vision and the Structure of Bathorhodopsin: A Mechanism for Photoisomerization of Polyenes. *Proc. Natl. Acad. Sci. USA* **1985**, *82*, 259-263.

174. Sharafy, S.; Muszkat, K. A., Viscosity Dependence of Fluorescence Quantum Yields. *J. Am. Chem. Soc.* **1971**, *93*, 4119-4125.

175. Murphy, S.; Sauerwein, B.; Drickamer, H. G.; Schuster, G. B., Spectroscopy of Cyanine Dyes in Fluid Solution at Atmospheric and High Pressure: The Effect of Viscosity on Nonradiative Processes. *J. Phys. Chem.* **1994**, *98*, 13476-480.

176. Jehlicka, J.; Edwards, H. G. M.; Nemec, I.; Oren, A., Raman Spectroscopic Study of the Chromobacterium Violaceum Pigment Violacein Using Multiwavelength Excitation and DFT Calculations. *Spectrochimica Acta Part a-Molecular and Biomolecular Spectroscopy* **2015**, *151*, 459-467.

177. Garcia-Pichel, F.; Wingard, C. E.; Castenholz, R. W., Evidence Regarding the UV Sunscreen Role of A Mycosporine-Like Compound in the Cyanobacterium Gleoecapsa sp. *Applied and Environmental Microbiology* **1993**, *59*, 170-176.

178. Staleva, H.; Zeeshan, M.; Chabera, P.; Partali, V.; Sliwka, H.-R.; Polivka, T., Ultrafast Dynamics of Long Homologues of Carotenoid Zeaxanthin. *J. Phys. Chem. A* **2015**, *119*, 11304-11312.

179. Ilagan, R. P.; Christensen, R. L.; Chapp, T. W.; Gibson, G. N.; Pascher, T.; Polivka, T.; Frank, H. A., Femtosecond Time-Resolved Absorption Spectroscopy of Astaxanthin in Solution and in Alpha-Crustacyanin. *J. Phys. Chem. A* **2005**, *109*, 3120-3127.

180. Asker, D.; Awad, T. S.; Beppu, T.; Ueda, K., Isolation, Characterization, and Diversity of Novel Radiotolerant Carotenoid-Producing Bacteria. *Methods in molecular biology (Clifton, N.J.)* **2012**, *892*, 21-60.

CHAPTER SIX

CONCLUSION AND OUTLOOK

6.1 Summary

Femtosecond pump-probe TA and TRIR spectroscopy, the two main techniques used in this thesis, are powerful tools for studying the fleeting processes that govern excited-state deactivation in biological molecules. In this dissertation, we have presented research on the excited-state dynamics of base-stacked DNA and spectroscopic investigations of excited-state processes in oxidatively damaged DNA and the pigment violacein. Below we summarize the main findings of the research presented in each chapter, and conclude by providing suggestions for future experimental work.

Over the last 20 years, excited-state deactivation in monomer bases has been well characterized. Only recently were the deactivation pathways operative in DNA strands more definitively assigned, in part due to the contributions discussed in this dissertation. In Chapter 3, we discussed our recent observation of the vibrational signatures of radical ion species generated via photoinduced ET from the oxidative product 8-oxo-7,8-dihydro-2'-deoxyguanosine (O) to a base-stacked adenine (A) in the dinucleotide d(OA).[29] Agreement between the theoretically calculated difference spectrum and the TRIR experimental decay-associated difference spectrum at 60 ps, in addition to observing A vibrational modes after selective excitation of O with 295 nm, enabled us to unambiguously assign the long-lived transient signal to a CT excited state consisting of an O radical cation

and an A radical anion. The CT state deactivates on a timescale consistent with the rate of BET, which occurs in tens of picoseconds in d(OA).[29]

The amplitude of the long-lived transient signal in d(OA) is 4-fold greater after 265 nm than 295 nm excitation, showing that the CT state is accessed with relatively high quantum yield using the shorter wavelength. This observation suggests that similar CT states could be accessed in natural DNA and potentially with high yield considering the canonical bases have greater extinction coefficients at 265 nm than the oxidatively damaged bases. Our results, and the recent observations made by other groups,[32, 82] provide experimental evidence supporting that CT excited states give rise to the long-lived transient signals observed in DNA strands. Since these spectroscopic observations of photoinduced ET in DNA strands, CT species in double-stranded DNA have also been observed.[33, 35-36, 38]

The photophysics of two oxidatively damaged pyrimidine nucleosides and their dinucleotides with adenine were studied using steady-state and ultrafast spectroscopic techniques. The results of these investigations were presented in Chapter 4. The excited-state lifetimes of 5-hydroxycytosine and 5-hydroxyuridine in aqueous solution were measured for the first time. Our results are consistent with previous experimental observations showing that C5 modification to the canonical bases results in lengthened singlet lifetimes.[120, 128-129] In the case of 5-HC, the lifetime of cytosine was increased 150-fold, which is greatest among the other C5-modified cytosines studied to date. The measured excited-states of 5-HC and 5-HU reflect the lifetimes of the emitting states observed in their steady-state emission spectra. This was validated by a Strickler-Berg

analysis, which showed that the fluorescence lifetimes of 5-HC and 5-HU, calculated using their fluorescence quantum yields, are consistent with the lifetimes observed in TA measurements.

Time-resolved IR spectra of the two 5-hydroxypyrimidine dinucleotides containing A showed spectral evidence for photoinduced ET, including the appearance of A bleach bands and absorption bands corresponding to radical ion species, after selective excitation of the oxidatively damaged bases. The lifetimes of the dinucleotide excited states were assigned to back ET, whereas the forward ET process occurs on a timescale that is faster than our instrument resolution (<0.5 ps). The asymmetry observed in the timescales for forward and back ET is consistent with rates that occur in the Marcus inverted region, and is justified by our estimated driving forces for forward and back ET. In these dinucleotides, the CT state is populated on an ultrafast timescale because the driving force for forward ET is nearly equal in energy with the reorganization energy.[82] These results provide further evidence of CT state population in DNA strands when the nucleobases are stacked, in addition to corroborating the ET mechanism proposed for the photoinduced repair of photoproducts by oxidatively damaged bases.[30, 40]

Using time-resolved methods, we conducted the first ultrafast spectroscopic investigation of violacein, a bisindolic pigment produced by Antarctic bacteria isolated from samples collected by the Christine Foreman group from MSU's Department of Biofilm Engineering. Measurements of violacein's excited-state lifetime in methanol showed that the pigment deactivates on a picosecond timescale. We observed that the lifetime lengthens and the fluorescence quantum yield increases when the pigment is in

solvents with increasing viscosity. The picosecond lifetime of violacein in methanol shows a distinctive solvent viscosity dependence, indicating that excited-state deactivation in violacein is highly sensitive to the solvent environment. In Chapter 5, we discussed these observations in the contexts of deactivation mechanisms that show similar solvent-viscosity dependences and the proposed photoprotective role of violacein in bacteria.

6.2 Future Directions

The studies presented in this thesis show the powerful potential of ultrafast spectroscopic techniques to unravel the complex photophysics of biological molecules, such as DNA and violacein. This dissertation adds to the field of DNA excited-state dynamics research by presenting definitive spectroscopic evidence for assigning enigmatic long-lived excited states in DNA to CT states. In addition, this work shows that photoinduced ET occurs from three oxidatively damaged bases positioned next to canonical nucleobases, an observation that supports their proposed roles as prebiotic redox cofactors. Finally, this thesis contributes the first steady-state and ultrafast spectroscopic measurements of the UV- and visible-induced excited states of the 5-hydroxypyrimidine nucleosides, 5-HC and 5-HU, and of the pigment violacein. Through the course of this doctoral work, the excited-state dynamics of DNA, in both canonical and oxidatively damaged forms, and violacein were thoroughly investigated, but many unanswered questions remain. In these concluding paragraphs, we give suggestions for future experiments that may increase understanding of the excited-state dynamics in the systems we have discussed.

The studies discussed within this thesis helped define a more specific understanding of the excited-state deactivation pathways available in natural DNA. A remaining question in DNA excited-state dynamics research involves determining how charge separation occurs and the extent of charge delocalization in DNA. There is high interest in understanding charge migration dynamics in DNA strands and higher-order systems[182-183] for the development of novel DNA photovoltaic devices.[184-185] Bucher et al. provided spectroscopic evidence for charge delocalization in single strands after selective excitation of 5-methylcytosine.[33] Charge separated states spanning across up to four uracil spacer molecules were observed using TRIR spectroscopy.[33] However, it is unclear that the uracil spacing bases are effective charge conductors, considering they do not base stack very well. In addition, length-dependent studies suggest that single DNA strands actually contain significant structural heterogeneity,[62, 84] and that the average base stacking length in strands is 2 bases.[186]

Continued investigation of DNA charge separation is warranted to clarify the extent of charge delocalization in single and double strands. A suggested experiment is to measure TRIR spectra of the excited-state dynamics leading to charge separation between donor and acceptor bases in a series of DNA single and double strands containing an increasing number of A spacing bases, which has a higher stacking probability than the pyrimidines. As shown in this thesis, TRIR spectroscopy monitors narrow vibrational transitions and can thus identify transient species more definitively than electronic spectroscopic methods. By monitoring the pump fluence, the number of excited states generated can be roughly estimated. This quantity can be compared with the amplitudes of the vibrational marker

bands of the transient species to determine how many excitations lead to charge separation. Then the spatial extent of the charge delocalization can be determined by the number of spacer bases required to eliminate the deactivation channel that leads to charge separation.

Oxidatively damaged DNA bases can lead to strand scission, base-pair mismatches, and eventually miscoding errors that can be highly mutagenic.[39, 100-101] However, the studies presented in this thesis have shown that the oxidative products also undergo photoinduced ET with stacked DNA bases, supporting the mechanism proposed for their ability to repair other photodamages such as CPDs in DNA. An interesting research direction for studying the excited-state dynamics of DNA containing oxidative products would be to investigate whether the harmful effects of oxidative damages in DNA are balanced by the beneficial effects of photoinduced CPD repair mediated by the oxidative products. TRIR spectroscopy could be used to study the excited-state dynamics of DNA strands incorporating oxidative products and CPDs. If there are non-overlapping vibrational features specific to the oxidatively damaged bases and the CPDs, the amplitude of the photoproduct bands could be related to the concentration of CPDs, and if photoinduced CPD repair occurs, the timescales of the different species' bands can be used to determine the relative rates of degradation and repair.

Preliminary spectroscopic measurements of the excited-state properties of violacein were presented in this thesis, but the fundamental deactivation mechanism and the potential bacterial sunscreen role of violacein need to be more thoroughly studied. Single-wavelength TA experiments, such as those presented in Chapter 5, may not provide adequate information for fully elucidating the mechanism of molecular excited-state

deactivation. Broadband UV-visible TA would provide a more complete survey of the excited-state properties necessary for determining the mechanism of deactivation. Broadband measurements in low viscosity solutions can be compared with those in the more viscous solutions to determine how the mechanism of deactivation is affected by the solvent environment.

More spectroscopic measurements are needed to confidently determine the efficiency of violacein excited-state deactivation and whether its excited-state properties support the claim that violacein provides photoprotection for the bacteria that produce it. Our excited-state observations of violacein deactivation in viscous solvents show that the excess electronic energy is deactivated on lengthened timescales. Longer excited-state lifetimes mean the molecule is in its reactive excited state for a longer amount of time, which may increase the potential for photoproduct formation.[4] The longer lifetimes of violacein in the viscous media may indicate decreased photostability and negate its ability to act as a sunscreen. Steady-state photodegradation experiments could be used to quantify the rate of violacein photodegradation in the different solvents.

The excited-state properties of violacein could also be investigated in environments similar to its natural bacterial environment. The pigment likely resides in either the bacterial membrane or cell wall, as indicated by the work of Konzen et al.[148] In a bacterial cell membrane the molecular motions of violacein would be constrained by the lipid environment. The pigment would be even more constrained in the cell wall. The excited-state properties of violacein in a bacterial cell can be modeled by incorporating the pigment into model lipid membrane vesicle systems. Spectroscopic measurements of violacein as it

has naturally incorporated within model vesicle systems can be used to evaluate the efficiency of violacein excited-state deactivation in a molecularly-crowded lipid environment. The additional insight gained would be helpful for evaluating the ability of violacein to provide photoprotection for Antarctic bacteria.

6.3 References

181. Clauditz, A.; Resch, A.; Wieland, K.-P.; Peschel, A.; Goetz, F., Staphyloxanthin Plays a Role in the Fitness of Staphylococcus Aureus and its Ability to Cope with Oxidative Stress. *Infection and Immunity* **2006**, *74*, 4950-4953.

182. Genereux, J. C.; Barton, J. K., Mechanisms for DNA Charge Transport. *Chem. Rev.* **2010**, *110*, 1642-1662.

183. Kawai, K.; Majima, T., Hole Transfer Kinetics of DNA. *Acc. Chem. Res.* **2013**, *46*, 2616-2625.

184. Steckl, A. J., DNA - A New Material for Photonics? *Nature Photonics* **2007**, *1*, 3-5.

185. Pinheiro, A. V.; Han, D.; Shih, W. M.; Yan, H., Challenges and Opportunities for Structural DNA Nanotechnology. *Nature Nanotechnology* **2011**, *6*, 763-772.

186. Lee, C.-H.; Ezra, F. S.; Kondo, N. S.; Sarma, R. H.; Danyluk, S. S., Conformational Properties of Dinucleoside Monophosphates in Solution: Dipurines and Dipyrimidines. *Biochemistry* **1976**, *15*, 3627-39.

REFERENCES

1. Chen, J.; Zhang, Y.; Kohler, B., Excited States in DNA Strands Investigated by Ultrafast Laser Spectroscopy. In *Photoinduced Phenomena in Nucleic Acids II: DNA Fragments and Phenomenological Aspects*; Barbatti, M.; Borin, A. C., Ullrich, S., Eds.; Springer International Publishing Switzerland: New York, **2015**, *356*, pp. 39-87.

2. Berera, R.; van Grondelle, R.; Kennis, J. T. M., Ultrafast Transient Absorption Spectroscopy: Principles and Application to Photosynthetic Systems. *Photosynth. Res.* **2009**, *101*, 105-118.

3. Kohler, B., Excited States of Single-Stranded DNA Revealed by Femtosecond Transient Absorption Spectroscopy. In *Ultrafast Dynamics at the Nanoscale: Biomolecules and Supramolecular Assemblies*; Burghardt, I., Haacke, S., Eds. Pan Stanford Publishing Pte. Ltd.: Singapore, **2017**, pp. 1-31.

4. Beckstead, A. A.; Zhang, Y. Y.; de Vries, M. S.; Kohler, B., Life in the Light: Nucleic Acid Photoproperties as a Legacy of Chemical Evolution. *Phys. Chem. Chem. Phys.* **2016**, *18*, 24228-24238.

5. Dodd, M. S.; Papineau, D.; Grenne, T.; Slack, J. F.; Rittner, M.; Pirajno, F.; O'Neil, J.; Little, C. T. S., Evidence for Early Life in Earth's Oldest Hydrothermal Vent Precipitates. *Nature* **2017**, *543*, 60-64.

6. Canuto, V. M.; Levine, J. S.; Augustsson, T. R.; Imhoff, C. L., Oxygen and Ozone in the Early Earth's Atmosphere. *Precambrian Res.* **1983**, *20*, 109-120.

7. Bekker, A.; Holland, H. D.; Wang, P. L.; Rumble, D.; Stein, H. J.; Hannah, J. L.; Coetzee, L. L.; Beukes, N. J., Dating the Rise of Atmospheric Oxygen. *Nature* **2004**, *427*, 117-120.

8. Cockell, C. S.; Raven, J. A., Ozone and Life on the Archaean Earth. *Philos. Trans. R. Soc. London, Ser. A* **2007**, *365*, 1889-1901.

9. Serrano-Andrés, L.; Merchán, M., Are the Five Natural DNA/RNA Base Monomers a Good Choice from Natural Selection? A Photochemical Perspective. *J. Photochem. Photobiol., C* **2009**, *10*, 21-32.

10. American Society for Testing and Materials Standardized Solar Irradiance Spectra. http://rredc.nrel.gov/solar/spectra (Accessed July 2006).

11. Barbatti, M.; Borin, A. C.; Ullrich, S., Photoinduced Processes in Nucleic Acids. In *Photoinduced Phenomena in Nucleic Acids I: Nucleobases in the Gas Phase and in Solvents*, Barbatti, M., Borin, A. C., Ullrich, S., Eds.; Springer International Publishing Switzerland: New York, **2015**, *355*, pp. 1-32.

12. de Gruijl, F. R., Skin Cancer and Solar UV Radiation. *Eur. J. Cancer* **1999**, *35*, 2003-9.

13. U.S. Department of Health and Human Services. The Surgeon General's Call to Action to Action to Prevent Skin Cancer. Washington, DC: U.S. Department of Health and Human Services, Office of the Surgeon General; 2014.

14. Schreier, W. J.; Gilch, P.; Zinth, W., Early Events of DNA Photodamage. *Annu. Rev. Phys. Chem.* **2015**, *66*, 497-519.

15. Pfeifer, G. P.; You, Y.-H.; Besaratinia, A., Mutations Induced by Ultraviolet Light. *Mutation Research* **2005**, *571*, 19-31.

16. Cadet, J.; Vigny, P., The Photochemistry of Nucleic Acids. In *Bioorganic Photochemistry*, Morrison, H., Ed.; Wiley: New York, **1990**, *1*, pp. 1-272.

17. Lemaire, D. G. E.; Ruzsicska, B. P., Quantum Yields and Secondary Photoreactions of the Photoproducts of dTpdT, dTpdC and dTpdU. *Photochem. Photobiol.* **1993**, *57*, 755-69.

18. Görner, H., Photochemistry of DNA and Related Biomolecules - Quantum Yields and Consequences of Photoionization. *J. Photochem. Photobiol., B* **1994**, *26*, 117-139.

19. Pecourt, J.-M. L.; Peon, J.; Kohler, B., Ultrafast Internal Conversion of Electronically Excited RNA and DNA Nucleosides in Water. *J. Am. Chem. Soc.* **2000**, *122*, 9348-9349.

20. Pecourt, J.-M. L.; Peon, J.; Kohler, B., DNA Excited-State Dynamics: Ultrafast Internal Conversion and Vibrational Cooling in a Series of Nucleosides. *J. Am. Chem. Soc.* **2001**, *123*, 10370-10378..

21. Middleton, C. T.; de La Harpe, K.; Su, C.; Law, Y. K.; Crespo-Hernández, C. E.; Kohler, B., DNA Excited-State Dynamics: From Single Bases to the Double Helix. *Annu. Rev. Phys. Chem.* **2009**, *60*, 217-239.

22. Kohler, B., Nonradiative Decay Mechanisms in DNA Model Systems. *J. Phys. Chem. Lett.* **2010**, *1*, 2047-2053.

23. Markovitsi, D.; Talbot, F.; Gustavsson, T.; Onidas, D.; Lazzarotto, E.; Marguet, S., Molecular Spectroscopy: Complexity of Excited-State Dynamics in DNA. *Nature* **2006**, *441*, E7.

24. Crespo-Hernández, C. E.; Cohen, B.; Kohler, B., Molecular Spectroscopy: Complexity of Excited-State Dynamics in DNA (Reply). *Nature* **2006**, *441*, E8.

25. Crespo-Hernández, C. E.; Cohen, B.; Kohler, B., Base Stacking Controls Excited-State Dynamics in A·T DNA. *Nature* **2005**, *436*, 1141-1144.

26. Su, C.; Middleton, C. T.; Kohler, B., Base-Stacking Disorder and Excited-State Dynamics in Single-Stranded Adenine Homo-oligonucleotides. *J. Phys. Chem. B* **2012**, *116*, 10266-10274.

27. Buchvarov, I.; Wang, Q.; Raytchev, M.; Trifonov, A.; Fiebig, T., Electronic Energy Delocalization and Dissipation in Single- and Double-Stranded DNA. *Proc. Natl. Acad. Sci. USA* **2007**, *104*, 4794-4797.

28. Emanuele, E.; Markovitsi, D.; Millie, P.; Zakrzewska, K., UV Spectra and Excitation Delocalization in DNA: Influence of the Spectral Width. *ChemPhysChem* **2005**, *6*, 1387-1393.

29. Zhang, Y.; Dood, J.; Beckstead, A. A.; Li, X.-B.; Nguyen, K. V.; Burrows, C. J.; Improta, R.; Kohler, B., Efficient UV-Induced Charge Separation and Recombination in an 8-Oxoguanine-Containing Dinucleotide. *Proc. Natl. Acad. Sci. USA* **2014**, *111*, 11612-11617.

30. Nguyen, K. V.; Burrows, C. J., A Prebiotic Role for 8-Oxoguanosine as a Flavin Mimic in Pyrimidine Dimer Photorepair. *J. Am. Chem. Soc.* **2011**, *133*, 14586-14589.

31. Nguyen, K. V.; Burrows, C. J., Whence Flavins? Redox-Active Ribonucleotides Link Metabolism and Genome Repair to the RNA World. *Acc. Chem. Res.* **2012**, *45*, 2151-2159..

32. Doorley, G. W.; Wojdyla, M.; Watson, G. W.; Towrie, M.; Parker, A. W.; Kelly, J. M.; Quinn, S. J., Tracking DNA Excited States by Picosecond-Time-Resolved Infrared Spectroscopy: Signature Band for a Charge-Transfer Excited State in Stacked Adenine-Thymine Systems. *J. Phys. Chem. Lett.* **2013**, *4*, 2739-2744.

33. Bucher, D. B.; Pilles, B. M.; Carell, T.; Zinth, W., Charge Separation and Charge Delocalization Identified in Long-Living States of Photoexcited DNA. *Proc. Natl. Acad. Sci. USA* **2014**, *111*, 4369-4374.

34. Pilles, B. M.; Bucher, D. B.; Liu, L.; Gilch, P.; Zinth, W.; Schreier, W. J., Identification of Charge Separated States in Thymine Single Strands. *Chem. Commun.* **2014**, *50*, 15623-15626.

35. Zhang, Y.; de La Harpe, K.; Beckstead, A. A.; Improta, R.; Kohler, B., UV-Induced Proton Transfer between DNA Strands. *J. Am. Chem. Soc.* **2015**, *137*, 7059-7062.

36. Zhang, Y.; de La Harpe, K.; Beckstead, A. A.; Martinez-Fernandez, L.; Improta, R.; Kohler, B., Excited-State Dynamics of DNA Duplexes with Different H-Bonding Motifs. *J. Phys. Chem. Lett.* **2016**, *7*, 950-954.

37. Bucher, D. B.; Schlueter, A.; Carell, T.; Zinth, W., Watson-Crick Base Pairing Controls Excited-State Decay in Natural DNA. *Angew. Chem. Int. Ed.* **2014**, *53*, 11366-11369.

38. Zhang, Y.; Li, X.-B.; Fleming, A. M.; Dood, J.; Beckstead, A. A.; Orendt, A. M.; Burrows, C. J.; Kohler, B., UV-Induced Proton-Coupled Electron Transfer in Cyclic DNA Miniduplexes. *J. Am. Chem. Soc.* **2016**, *138*, 7395-7401.

39. Burrows, C. J.; Muller, J. G., Oxidative Nucleobase Modifications Leading to Strand Scission. *Chem. Rev.* **1998**, *98*, 1109-1151.

40. Nguyen, K. V.; Burrows, C. J., Photorepair of Cyclobutane Pyrimidine Dimers by 8-Oxopurine Nucleosides. *J. Phys. Org. Chem.* **2012**, *25*, 574-577.

41. Smith, H. J.; Foreman, C. M.; Akiyama, T.; Franklin, M. J.; Devitt, N. P.; Ramaraj, T., Genome Sequence of Janthinobacterium sp. CG23_2, a Violacein-Producing Isolate from an Antarctic Supraglacial Stream. *Genome Announcements* **2016**, *4*, 1-2.

42. Choi, S. Y.; Yoon, K. H.; Lee, J. I.; Mitchell, R. J., Violacein: Properties and Production of a Versatile Bacterial Pigment. *Biomed Research International* **2015**, article no. 465056.

43. Jiang, P.-X.; Wang, H.-S.; Xiao, S.; Fang, M.-Y.; Zhang, R.-P.; He, S.-Y.; Lou, K.; Xing, X.-H., Pathway Redesign for Deoxyviolacein Biosynthesis in Citrobacter Freundii and Characterization of This Pigment. *Appl. Microbiol. Biotechnol.* **2012**, *94*, 1521-1532.

44. Mojib, N.; Farhoomand, A.; Andersen, D. T.; Bej, A. K., UV and Cold Tolerance of a Pigment-Producing Antarctic Janthinobacterium sp Ant5-2. *Extremophiles* **2013**, *17*, 367-378.

45. Suryawanshi, R. K.; Patil, C. D.; Borase, H. P.; Narkhede, C. P.; Stevenson, A.; Hallsworth, J. E.; Patil, S. V., Towards an Understanding of Bacterial Metabolites Prodigiosin and Violacein and Their Potential for Use in Commercial Sunscreens. *International Journal of Cosmetic Science* **2015**, *37*, 98-107.

46. Pickett, J. E.; Moore, J. E., Photodegradation of UV Screeners. *Polym. Degrad. Stab.* **1993**, *42*, 231-244.

47. Maine, P.; Strickland, D.; Bado, P.; Pessot, M.; Mourou, G., Generation of Ultrahigh Peak Power Pulses by Chirped Pulse Amplification. *IEEE Journal of Quantum Electronics* **1988**, *24*, 398.

48. Zhang, Y.; Chen, J.; Kohler, B., Hydrogen Bond Donors Accelerate Vibrational Cooling of Photoexcited Purine Derivatives in Heavy Water. *J. Phys. Chem. A* **2013**, *117*, 6771-6780.

49. Chen, J.; Kohler, B., Base Stacking in Adenosine Dimers Revealed by Femtosecond Transient Absorption Spectroscopy. *J. Am. Chem. Soc.* **2014**, *136*, 6362-6372.

50. Winefordner, J. D.; Stjohn, P. A., Solvents for Phosphorimetry. *Anal. Chem.* **1963**, *35*, 2211-2212.

51. Scott, D. R.; Allison, J. B., Solvent Glasses for Low Temperature Spectroscopic Studies. *J. Phys. Chem.* **1962**, *66*, 561-562.

52. Laatsch, H.; Thomson, R. H.; Cox, P. J., Spectroscopic Properties of Violacein and Related Compounds: Crystal Structure of Tetramethylviolacein. *J. Chem. Soc. Perkin Trans. II* **1984**, *8*, 1331-1339.

53. Abbott, A. P.; Harris, R. C.; Ryder, K. S., Application of Hole Theory to Define Ionic Liquids by Their Transport Properties. *J. Phys. Chem. B* **2007**, *111*, 4910-4913.

54. Mamajanov, I.; Engelhart, A. E.; Bean, H. D.; Hud, N. V., DNA and RNA in Anhydrous Media: Duplex, Triplex, and G-Quadruplex Secondary Structures in a Deep Eutectic Solvent. *Angew. Chem. Int. Ed.* **2010**, *49*, 6310-6314.

55. Lannan, F. M.; Mamajanov, I.; Hud, N. V., Human Telomere Sequence DNA in Water-Free and High-Viscosity Solvents: G-Quadruplex Folding Governed by Kramers Rate Theory. *J. Am. Chem. Soc.* **2012**, *134*, 15324-15330.

56. Jou, F.-Y.; Freeman, G. R., Temperature and Isotope Effects on the Shape of the Optical Absorption Spectrum of Solvated Electrons in Water. *J. Phys. Chem.* **1979**, *83*, 2383-2387.

57. Elkins, M. H.; Williams, H. L.; Neumark, D. M., Dynamics of Electron Solvation in Methanol: Excited State Relaxation and Generation by Charge-Transfer-to-Solvent. *J. Chem. Phys.* **2015**, *142*, article no. 234501.

58. Crespo-Hernández, C. E.; Kohler, B., Influence of Secondary Structure on Electronic Energy Relaxation in Adenine Homopolymers. *J. Phys. Chem. B* **2004**, *108*, 11182-11188.

59. Chen, J.; Kohler, B., Ultrafast Nonradiative Decay by Hypoxanthine and Several Methylxanthines in Aqueous and Acetonitrile Solution. *Phys. Chem. Chem. Phys.* **2012**, *14*, 10677-10682.

60. van Stokkum, I. H. M.; Larsen, D. S.; van Grondelle, R., Global and Target Analysis of Time-Resolved Spectra. *Biochim. Biophys. Acta Bioenergetics* **2004**, *1657*, 82-104.

61. Snellenburg, J. J.; Laptenok, S. P.; Seger, R.; Mullen, K. M.; van Stokkum, I. H. M., Glotaran: A Java-Based Graphical User Interface for the R Package TIMP. *Journal of Statistical Software* **2012**, *49*, 1-22.

62. Skowron, D. J.; Zhang, Y.; Beckstead, A. A.; Remington, J. M.; Strawn, M.; Kohler, B., Subnanosecond Emission Dynamics of AT DNA Oligonucleotides. *ChemPhysChem* **2016**, *17*, 3558-3569.

63. Crespo-Hernández, C. E.; Cohen, B.; Hare, P. M.; Kohler, B., Ultrafast Excited-State Dynamics in Nucleic Acids. *Chem. Rev.* **2004**, *104*, 1977-2019.

64. Takaya, T.; Su, C.; de La Harpe, K.; Crespo-Hernández, C. E.; Kohler, B., UV Excitation of Single DNA and RNA Strands Produces High Yields of Exciplex States Between Two Stacked Bases. *Proc. Natl. Acad. Sci. U.S.A.* **2008**, *105*, 10285-10290.

65. Steenken, S.; Jovanovic, S. V.; Bietti, M.; Bernhard, K., The Trap Depth (in DNA) of 8-Oxo-7,8-dihydro-2'-deoxyguanosine as Derived from Electron-Transfer Equilibria in Aqueous Solution. *J. Am. Chem. Soc.* **2000**, *122*, 2373-2374.

66. Steenken, S.; Jovanovic, S. V., How Easily Oxidizable is DNA? One-Electron Reduction Potentials of Adenosine and Guanosine Radicals in Aqueous Solution. *J. Am. Chem. Soc.* **1997**, *119*, 617-618.

67. Liu, Z.; Tan, C.; Guo, X.; Kao, Y.-T.; Li, J.; Wang, L.; Sancar, A.; Zhong, D., Dynamics and Mechanism of Cyclobutane Pyrimidine Dimer Repair by DNA Photolyase. *Proc. Natl. Acad. Sci. USA* **2011**, *108*, 14831-14836.

68. Adamo, C.; Barone, V., Toward Reliable Density Functional Methods Without Adjustable Parameters: The PBE0 Model. *J. Chem. Phys.* **1999**, *110*, 6158-6170.

69. Tomasi, J.; Mennucci, B.; Cammi, R., Quantum Mechanical Continuum Solvation Models. *Chem. Rev.* **2005**, *105*, 2999-3093.

70. Zhao, Y.; Truhlar, D. G., Density Functionals with Broad Applicability in Chemistry. *Acc. Chem. Res.* **2008**, *41*, 157-167.

71. Scalmani, G.; Frisch, M. J.; Mennucci, B.; Tomasi, J.; Cammi, R.; Barone, V., Geometries and Properties of Excited States in the Gas Phase and in Solution: Theory and Application of a Time-Dependent Density Functional Theory Polarizable Continuum Model. *J. Chem. Phys.* **2006**, *124*, article no. 94107.

72. Culp, S. J.; Cho, B. P.; Kadlubar, F. F.; Evans, F. E., Structural and Conformational Analyses of 8-Hydroxy-2'-Deoxyguanosine. *Chem. Res. Toxicol.* **1989**, *2*, 416-422.

73. Jayanth, N.; Ramachandran, S.; Puranik, M., Solution Structure of the DNA Damage Lesion 8-Oxoguanosine from Ultraviolet Resonance Raman Spectroscopy. *J. Phys. Chem. A* **2009**, *113*, 1459-1471.

74. Karunakaran, V.; Kleinermanns, K.; Improta, R.; Kovalenko, S. A., Photoinduced Dynamics of Guanosine Monophosphate in Water from Broad-Band Transient Absorption Spectroscopy and Quantum-Chemical Calculations. *J. Am. Chem. Soc.* **2009**, *131*, 5839-5850.

75. Zhang, Y.; Dood, J.; Beckstead, A.; Chen, J.; Li, X.-B.; Burrows, C. J.; Lu, Z.; Matsika, S.; Kohler, B., Ultrafast Excited-State Dynamics and Vibrational Cooling of 8-Oxo-7,8-dihydro-2 '-deoxyguanosine in D2O. *J. Phys. Chem. A* **2013**, *117*, 12851-12857.

76. Cohen, B.; Hare, P. M.; Kohler, B., Ultrafast Excited-State Dynamics of Adenine and Monomethylated Adenines in Solution: Implications for the Nonradiative Decay Mechanism. *J. Am. Chem. Soc.* **2003**, *125*, 13594-13601.

77. Zhang, Y.; Improta, R.; Kohler, B., Mode-Specific Vibrational Relaxation of Photoexcited Guanosine 5 '-Monophosphate and its Acid Form: a Femtosecond Broadband Mid-IR Transient Absorption and Theoretical Study. *Phys. Chem. Chem. Phys.* **2014**, *16*, 1487-1499.

78. Lu, Z.; Beckstead, A. A.; Kohler, B.; Matsika, S., Excited State Relaxation of Neutral and Basic 8-Oxoguanine. *J. Phys. Chem. B* **2015**, *119*, 8293-8301.

79. Onidas, D.; Markovitsi, D.; Marguet, S.; Sharonov, A.; Gustavsson, T., Fluorescence Properties of DNA Nucleosides and Nucleotides: A Refined Steady-State and Femtosecond Investigation. *J. Phys. Chem. B* **2002**, *106*, 11367-11374.

80. Changenet-Barret, P.; Gustavsson, T.; Improta, R.; Markovitsi, D., Ultrafast Excited-State Deactivation of 8-Hydroxy-2 '-deoxyguanosine Studied by Femtosecond Fluorescence Spectroscopy and Quantum-Chemical Calculations. *J. Phys. Chem. A* **2015**, *119*, 6131-6139.

81. Shukla, M. K.; Leszczynski, J., Electronic Spectra, Excited State Structures and Interactions of Nucleic Acid Bases and Base Assemblies: a Review. *J. Biomol. Struct. Dyn.* **2007**, *25*, 93-118.

82. Zhang, Y.; Dood, J.; Beckstead, A. A.; Li, X.-B.; Nguyen, K. V.; Burrows, C. J.; Improta, R.; Kohler, B., Photoinduced Electron Transfer in DNA: Charge Shift Dynamics Between 8-Oxo-Guanine Anion and Adenine. *J. Phys. Chem. B* **2015**, *119*, 7491-7502.

83. Gould, I. R.; Moser, J. E.; Armitage, B.; Farid, S., Electron-Transfer Reactions in the Marcus Inverted Region: Charge Recombination vs. Charge Shift Reactions. *J. Am. Chem. Soc.* **1989**, *111*, 1917-1919.

84. Remington, J. M.; Philip, A. M.; Hariharan, M.; Kohler, B., On the Origin of Multiexponential Fluorescence Decays from 2-Aminopurine-Labeled Dinucleotides. *J. Chem. Phys.* **2016**, *145*, article no. 155101.

85. Wan, C.; Fiebig, T.; Schiemann, O.; Barton, J. K.; Zewail, A. H., Femtosecond Direct Observation of Charge Transfer Between Bases in DNA. *Proc. Natl. Acad. Sci. U. S. A.* **2000**, *97*, 14052-14055.

86. Kuimova, M. K.; Dyer, J.; George, M. W.; Grills, D. C.; Kelly, J. M.; Matousek, P.; Parker, A. W.; Sun, X. Z.; Towrie, M.; Whelan, A. M., Monitoring the Effect of Ultrafast Deactivation of the Electronic Excited States of DNA Bases and Polynucleotides Following 267 nm Laser Excitation Using Picosecond Time-Resolved Infrared Spectroscopy. *Chem. Commun.* **2005**, *9*, 1182-1184.

87. Santoro, F.; Barone, V.; Improta, R., Influence of Base Stacking on Excited-State Behavior of Polyadenine in Water, Based on Time-Dependent Density Functional Calculations. *Proc. Natl. Acad. Sci. USA* **2007**, *104*, 9931-9936.

88. de La Harpe, K.; Crespo-Hernández, C. E.; Kohler, B., Deuterium Isotope Effect on Excited-State Dynamics in an Alternating GC Oligonucleotide. *J. Am. Chem. Soc.* **2009**, *131*, 17557-17559.

89. Sobolewski, A. L.; Domcke, W., Ab Initio Studies on the Photophysics of the Guanine-Cytosine Base Pair. *Phys. Chem. Chem. Phys.* **2004**, *6*, 2763-2771.

90. Perun, S.; Sobolewski, A. L.; Domcke, W., Role of Electron-Driven Proton-Transfer Processes in the Excited-State Deactivation Adenine-Thymine Base Pair. *J. Phys. Chem. A* **2006**, *110*, 9031-9038.

91. Abo-Riziq, A.; Grace, L.; Nir, E.; Kabelac, M.; Hobza, P.; de Vries, M. S., Photochemical Selectivity in Guanine-Cytosine Base-Pair Structures. *Proc. Natl. Acad. Sci. USA* **2005**, *102*, 20-23.

92. Schwalb, N. K.; Temps, F., Ultrafast Electronic Relaxation in Guanosine is Promoted by Hydrogen Bonding with Cytidine. *J. Am. Chem. Soc.* **2007**, *129*, 9272-9273.

93. Schwalb, N. K.; Michalak, T.; Temps, F., Ultrashort Fluorescence Lifetimes of Hydrogen-Bonded Base Pairs of Guanosine and Cytidine in Solution. *J. Phys. Chem. B* **2009**, *113*, 16365-16376.

94. Roettger, K.; Marroux, H. J. B.; Grubb, M. P.; Coulter, P. M.; Boehnke, H.; Henderson, A. S.; Galan, M. C.; Temps, F.; Orr-Ewing, A. J.; Roberts, G. M., Ultraviolet Absorption Induces Hydrogen-Atom Transfer in G center dot C Watson-Crick DNA Base Pairs in Solution. *Angew. Chem. Int. Ed.* **2015**, *54*, 14719-14722.

95. de La Harpe, K.; Crespo-Hernández, C. E.; Kohler, B., The Excited-State Lifetimes in a G•C DNA Duplex are Nearly Independent of Helix Conformation and Base-Pairing Motif. *ChemPhysChem* **2009**, *10*, 1421-1425.

96. Wagner, J. R.; Hu, C. C.; Ames, B. N., Endogenous Oxidative Damage of Deoxycytidine in DNA. *Proc. Natl. Acad. Sci. USA* **1992**, *89*, 3380-3384.

97. Yanagawa, H.; Ogawa, Y.; Ueno, M.; Sasaki, K.; Sato, T., A Novel Minimum Ribozyme with Oxidoreductive Activity. *Biochemistry* **1990**, *29*, 10585-10589.

98. Yanagawa, H.; Ogawa, Y.; Ueno, M., Redox Ribonucleosides: Isolation and Characterization of 5-Hydroxyuridine, 8-Hydroxyguanosine, and 8-Hydroxyadenosine from Torula Yeast RNA. *J. Biol. Chem.* **1992**, *267*, 13320-13326.

99. Thiviyanathan, V.; Somasunderam, A.; Volk, D. E.; Gorenstein, D. G., 5-Hydroxyuracil Can Form Stable Base Pairs with All Four Bases in a DNA Duplex. *Chem. Commun.* **2005**, *3*, 400-402.

100. Thiviyanathan, V.; Somasunderam, A.; Volk, D. E.; Hazra, T. K.; Mitra, S.; Gorenstein, D. G., Base-Pairing Properties of the Oxidized Cytosine Derivative, 5-Hydroxy Uracil. *Biochem. Biophys. Res. Commun.* **2008**, *366*, 752-757.

101. Kuepfer, P. A.; Leumann, C. J., Synthesis, Base Pairing Properties and Trans-Lesion Synthesis by Reverse Transcriptases of Oligoribonucleotides Containing the Oxidatively Damaged Base 5-Hydroxycytidine. *Nucleic Acids Res.* **2011**, *39*, 9422-9432.

102. Cockell, C. S.; Horneck, G., The History of the UV Radiation Climate of the Earth-Theoretical and Space-Based Observations. *Photochem. Photobiol.* **2001**, *73*, 447-451.

103. Liang, M.-C.; Hartman, H.; Kopp, R. E.; Kirschvink, J. L.; Yung, Y. L., Production of Hydrogen Peroxide in the Atmosphere of a Snowball Earth and the Origin of Oxygenic Photosynthesis. *Proc. Natl. Acad. Sci. USA* **2006**, *103*, 18896-18899.

104. Gilbert, W., Origin of Life: The RNA World. *Nature* **1986**, *319*, 618-618.

105. Cech, T. R.; Bass, B. L., Biological Catalysis by RNA. *Annu. Rev. Biochem* **1986**, *55*, 599-629.

106. Johnston, W. K.; Unrau, P. J.; Lawrence, M. S.; Glasner, M. E.; Bartel, D. P., RNA-Catalyzed RNA Polymerization: Accurate and General RNA-Templated Primer Extension. *Science* **2001**, *292*, 1319-1325.

107. Reader, J. S.; Joyce, G. F., A Ribozyme Composed of Only Two Different Nucleotides. *Nature* **2002**, *420*, 841-844.

108. La Francois, C. J.; Jang, Y. H.; Cagin, T.; Goddard, W. A.; Sowers, L. C., Conformation and Proton Configuration of Pyrimidine Deoxynucleoside Oxidation Damage Products in Water. *Chem. Res. Toxicol.* **2000**, *13*, 462-470.

109. Steenken, S., Electron-Transfer-Induced Acidity/Basicity and Reactivity Changes of Purine and Pyrimidine Bases: Consequences of Redox Processes for DNA Base Pairs. *Free Rad. Res. Commun.* **1992**, *16*, 349-379.

110. LaFrancois, C. J.; Fujimoto, J.; Sowers, L. C., Synthesis and Characterization of Isotopically Enriched Pyrimidine Deoxynucleoside Oxidation Damage Products. *Chem. Res. Toxicol.* **1998**, *11*, 75-83.

111. Suen, W.; Spiro, T. G.; Sowers, L. C.; Fresco, J. R., Identification by UV Resonance Raman Spectroscopy of an Imino Tautomer of 5-Hydroxy-2'-deoxycytidine, a Powerful Base Analog Transition Mutagen with a Much Higher Unfavored Tautomer Frequency Than That of the Natural Residue 2'-Deoxycytidine. *Proc. Natl. Acad. Sci. USA* **1999**, *96*, 4500-4505.

112. Rueda, M.; Luque, F. J.; López, J. M.; Orozco, M., Amino-Imino Tautomerism in Derivatives of Cytosine: Effect on Hydrogen-Bonding and Stacking Properties. *J. Phys. Chem. A* **2001**, *105*, 6575-6580.

113. Lukmanov, T.; Ivanov, S. P.; Khamitov, E. M.; Khursan, S. L., Relative Stability of Keto-Enol Tautomers in 5,6-Substituted Uracils: Ab Initio, DFT and PCM Study. *Computational and Theoretical Chemistry* **2013**, *1023*, 38-45.

114. Lu, Z.; Beckstead, A. A.; Kohler, B.; Matsika, S., Excited State Relaxation of Neutral and Basic 8-Oxoguanine (vol 119, pg 8293, 2015). *J. Phys. Chem. B* **2016**, *120*, 597-597.

115. Schreier, W. J.; Schrader, T. E.; Koller, F. O.; Gilch, P.; Crespo-Hernández, C. E.; Swaminathan, V. N.; Carell, T.; Zinth, W.; Kohler, B., Thymine Dimerization in DNA is an Ultrafast Photoreaction. *Science* **2007**, *315*, 625-629.

116. Kuimova, M. K.; Cowan, A. J.; Matousek, P.; Parker, A. W.; Sun, X. Z.; Towrie, M.; George, M. W., Monitoring the Direct and Indirect Damage of DNA Bases and Polynucleotides by Using Time-Resolved Infrared Spectroscopy. *Proc. Natl. Acad. Sci. USA* **2006**, *103*, 2150-2153.

117. Banyasz, A.; Douki, T.; Improta, R.; Gustavsson, T.; Onidas, D.; Vaya, I.; Perron, M.; Markovitsi, D., Electronic Excited States Responsible for Dimer Formation upon UV Absorption Directly by Thymine Strands: Joint Experimental and Theoretical Study. *J. Am. Chem. Soc.* **2012**, *134*, 14834-14845.

118. Cohen, B.; Crespo-Hernández, C. E.; Kohler, B., Strickler-Berg Analysis of Excited Singlet State Dynamics in DNA and RNA Nucleosides. *Faraday Discuss.* **2004**, *127*, 137-147.

119. Blancafort, L.; Cohen, B.; Hare, P. M.; Kohler, B.; Robb, M. A., Singlet Excited-State Dynamics of 5-Fluorocytosine and Cytosine: An Experimental and Computational Study. *J. Phys. Chem. A* **2005**, *109*, 4431-4436.

120. Gustavsson, T.; Bányász, Á.; Lazzarotto, E.; Markovitsi, D.; Scalmani, G.; Frisch, M. J.; Barone, V.; Improta, R., Singlet Excited-State Behavior of Uracil and Thymine in Aqueous Solution: A Combined Experimental and Computational Study of 11 Uracil Derivatives. *J. Am. Chem. Soc.* **2006**, *128*, 607-619.

121. Keane, P. M.; Wojdyla, M.; Doorley, G. W.; Watson, G. W.; Clark, I. P.; Greetham, G. M.; Parker, A. W.; Towrie, M.; Kelly, J. M.; Quinn, S. J., A Comparative Picosecond Transient Infrared Study of 1-Methylcytosine and 5 '-dCMP That Sheds Further Light on the Excited States of Cytosine Derivatives. *J. Am. Chem. Soc.* **2011**, *133*, 4212-4215.

122. Singh, J. S., FT-IR and Raman Spectra, Ab Initio and Density Functional Computations of the Vibrational Spectra, Molecular Geometries and Atomic Charges of Uracil and 5-Halogenated Uracils (5-X-uracils; X = F, Cl, Br, I). *Spectrochimica Acta Part a-Molecular and Biomolecular Spectroscopy* **2014**, *117*, 502-518.

123. Singh, J. S., FT-IR and Raman Spectra, Ab Initio and Density Functional Computations of the Vibrational Spectra, Molecular Geometries and Atomic Charges of Uracil and 5-Methyluracil (Thymine). *Spectrochimica Acta Part a-Molecular and Biomolecular Spectroscopy* **2015**, *137*, 625-640.

124. Steenken, S., Purine Bases, Nucleosides, and Nucleotides: Aqueous Solution Redox Chemistry and Transformation Reactions of Their Radical Cations and e- and OH Adducts. *Chem. Rev.* **1989**, *89*, 503-520.

125. Hare, P. M.; Crespo-Hernández, C. E.; Kohler, B., Internal Conversion to the Electronic Ground State Occurs via Two Distinct Pathways for Pyrimidine Bases in Aqueous Solution. *Proc. Natl. Acad. Sci. USA* **2007**, *104*, 435-440.

126. Salet, C.; Bensasson, R.; Becker, R. S., Triplet Excited States of Pyrimidine Nucleosides and Nucleotides. *Photochem. Photobiol.* **1979**, *30*, 325-329.

127. Strickler, S. J.; Berg, R. A., Relationship Between Absorption Intensity and Fluorescence Lifetime of Molecules. *J. Chem. Phys.* **1962**, *37*, 814-822.

128. Malone, R. J.; Miller, A. M.; Kohler, B., Singlet Excited-state Lifetimes of Cytosine Derivatives Measured by Femtosecond Transient Absorption. *Photochem. Photobiol.* **2003**, *77*, 158-164.

129. Nachtigallova, D.; Lischka, H.; Szymczak, J. J.; Barbatti, M.; Hobza, P.; Gengeliczki, Z.; Pino, G.; Callahan, M. P.; de Vries, M. S., The Effect of C5 Substitution on the Photochemistry of Uracil. *Phys. Chem. Chem. Phys.* **2010**, *12*, 4924-4933.

130. Zgierski, M. Z.; Fujiwara, T.; Kofron, W. G.; Lim, E. C., Highly Effective Quenching of the Ultrafast Radiationless Decay of Photoexcited Pyrimidine Bases by Covalent Modification: Photophysics of 5,6-Trimethylenecytosine and 5,6-Trimethyleneuracil. *Phys. Chem. Chem. Phys.* **2007**, *9*, 3206-3209.

131. Matsika, S., Radiationless Decay of Excited States of Uracil through Conical Intersections. *J. Phys. Chem. A.* **2004**, *108*, 7584-7590.

132. Teimoory, F.; Loppnow, G. R., Resonance Raman Intensities Demonstrate that C5 Substituents Affect the Initial Excited-State Structural Dynamics of Uracil More than C6 Substituents. *ChemPhysChem* **2016**, *17*, 1349-1355.

133. Blancafort, L.; Migani, A., Water Effect on the Excited-State Decay Paths of Singlet Excited Cytosine. *J. Photochem. Photobiol., A* **2007**, *190*, 283-289.

134. Canuel, C.; Mons, M.; Piuzzi, F.; Tardivel, B.; Dimicoli, I.; Elhanine, M., Excited States Dynamics of DNA and RNA Bases: Characterization of a Stepwise Deactivation Pathway in the Gas Phase. *J. Chem. Phys.* **2005**, *122*, article no. 074316.

135. Gut, I. G.; Wood, P. D.; Redmond, R. W., Interaction of Triplet Photosensitizers with Nucleotides and DNA in Aqueous Solution at Room Temperature. *J. Am. Chem. Soc.* **1996**, *118*, 2366-2373.

136. Nielsen, L. M.; Hoffmann, S. V.; Nielsen, S. B., Electronic Coupling Between Photo-Excited Stacked Bases in DNA and RNA Strands with Emphasis on the Bright States Initially Populated. *Photochem. Photobiol. Sci.* **2013**, *12*, 1273-1285.

137. Closs, G. L.; Miller, J. R., Intramolecular Long-Distance Electron Transfer in Organic Molecules. *Science* **1988**, *240*, 400-447.

138. Cockell, C. S.; Knowland, J., Ultraviolet Radiation Screening Compounds. *Biological Reviews of the Cambridge Philosophical Society* **1999**, *74*, 311-345.

139. Proteau, P. J.; Gerwick, W. H.; Garcia-Pichel, F.; Castenholz, R., The Structure of Scytonemin, an Ultraviolet Sunscreen Pigment from the Sheaths of Cyanobacteria. *Experientia* **1993**, *49*, 825-9.

140. Castenholz, R. W.; Garcia-Pichel, F., Cyanobacterial Responses to UV-Radiation. *Ecol. Cyanobacteria* **2000**, 591-611.

141. Karsten, U.; Sawall, T.; Hanelt, D.; Bischof, K.; Figueroa, F. L.; Flores-Moya, A.; Wiencke, C., An Inventory of UV-Absorbing Mycosporine-Like Amino Acids in Macroalgae from Polar to Warm-Temperate Regions. *Bot. Mar.* **1998**, *41*, 443-453.

142. Dunlap, W. C.; Shick, J. M.; Yamamoto, Y., Sunscreens, Oxidative Stress and Antioxidant Functions in Marine Organisms of the Great Barrier Reef. *Redox Rep.* **1999**, *4*, 301-306.

143. Dieser, M.; Greenwood, M.; Foreman, C. M., Carotenoid Pigmentation in Antarctic Heterotrophic Bacteria as a Strategy to Withstand Environmental Stresses. *Arctic Antarctic and Alpine Research* **2010**, *42*, 396-405.

144. Nienow, J. A.; McKay, C. P.; Friedmann, E. I., The Cryptoendolithic Microbial Environment in the Ross Desert of Antarctica: Light in the Photosynthetically Active Region. *Microbial Ecology* **1988**, *16*, 271-289.

145. Staehelin, J.; Harris, N. R. P.; Appenzeller, C.; Eberhard, J., Ozone Trends: A Review. *Reviews of Geophysics* **2001**, *39*, 231-290.

146. Foreman, C. M.; Cory, R. M.; Morris, C. E.; SanClements, M. D.; Smith, H. J.; Lisle, J. T.; Miller, P. L.; Chin, Y.-P.; McKnight, D. M., Microbial Growth Under Humic-Free Conditions in a Supraglacial Stream System on the Cotton Glacier, Antarctica. *Environmental Research Letters* **2013**, *8*, article no. 35022..

147. Margalith, P. Z., *Pigment Microbiology*. Chapman and Hall: London, 1992.

148. Konzen, M.; De Marco, D.; Cordova, C. A. S.; Vieira, T. O.; Antonio, R. V.; Creczynski-Pasa, T. B., Antioxidant Properties of Violacein: Possible Relation on its Biological Function. *Biorg. Med. Chem.* **2006**, *14*, 8307-8313.

149. Cao, W.; Chen, W.; Sun, S.; Guo, P.; Song, J.; Tian, C., Investigating the Antioxidant Mechanism of Violacein by Density Functional Theory Method. *Journal of Molecular Structure-Theochem* **2007**, *817*, 1-4.

150. Antonio, R. V.; Creczynski-Pasa, T. B., Genetic Analysis of Violacein Biosynthesis by Chromobacterium Violaceum. *Genetics and Molecular Research : GMR* **2004**, *3*, 85-91.

151. Otterstedt, J.-E. A., Photostability and Molecular Structure. *J. Chem. Phys.* **1973**, *58*, 5716-5725.

152. Mendes, A. S.; de Carvalho, J. E.; Duarte, M. C. T.; Duran, N.; Bruns, R. E., Factorial Design and Response Surface Optimization of Crude Violacein for Chromobacterium Violaceumi Production. *Biotechnol. Lett* **2001**, *23*, 1963-1969.

153. Rodrigues, A. L.; Goecke, Y.; Bolten, C.; Brock, N. L.; Dickschat, J. S.; Wittmann, C., Microbial Production of the Drugs Violacein and Deoxyviolacein: Analytical Development and Strain Comparison. *Biotechnol. Lett* **2012**, *34*, 717-720.

154. Wang, H.; Wang, F.; Zhu, X.; Yan, Y.; Yu, X.; Jiang, P.; Xing, X.-H., Biosynthesis and Characterization of Violacein, Deoxyviolaceiri and Oxyviolacein in Heterologous Host, and Their Antimicrobial Activities. *Biochem. Eng. J.* **2012**, *67*, 148-155.

155. Rettori, D.; Duran, N., Production, Extraction and Purification of Violacein: an Antibiotic Pigment Produced by Chromobacterium Violaceum. *World Journal of Microbiology & Biotechnology* **1998**, *14*, 685-688.

156. Sanchez, C.; Brana, A. F.; Mendez, C.; Salas, J. A., Reevaluation of the Violacein Biosynthetic Pathway and its Relationship to Indolocarbazole Biosynthesis. *ChemBioChem* **2006**, *7*, 1231-1240.

157. Dias, L. C.; Neto, J. D. D.; Rettori, D.; Duran, N., Semiempirical INDO/S Study on the Absorption Spectrum of Violacein. *Journal of Molecular Structure-Theochem* **2002**, *580*, 85-90.

158. Wang, H.; Jiang, P.; Lu, Y.; Ruan, Z.; Jiang, R.; Xing, X.-H.; Lou, K.; Wei, D., Optimization of Culture Conditions for Violacein Production by a New Strain of Duganella sp B2. *Biochem. Eng. J.* **2009**, *44*, 119-124.

159. Hebert, P.; Baldacchino, G.; Gustavsson, T.; Mialocq, J. C., Photochemistry of an Unsymmetrical Polymethine-Cyanine Dye: Solute Solvent Interactions and Relaxation Dynamics of LDS-751. *J. Photochem. Photobiol., A* **1994**, *84*, 45-55.

160. Lide, D. R., *Handbook of Chemistry and Physics*. 84th ed.; CRC Press: Boca Raton, **2004**.

161. Fogg, E. T.; Hixson, A. N.; Thompson, A. R., Densities and Refractive Indexes for Ethylene Glycol-Water Solutions. *Anal. Chem.* **1955**, *27*, 1609-1611.

162. Hoyt, L. F., New Table of the Refractive Index of Pure Glycerol at 20 degrees C. *Ind. Eng. Chem.* **1934**, *26*, 329-332.

163. Middleton, C. T.; Cohen, B.; Kohler, B., Solvent and Solvent Isotope Effects on the Vibrational Cooling Dynamics of a DNA Base Derivative. *J. Phys. Chem. A* **2007**, *111*, 10460-10467.

164. Terazima, M., Vibrational Relaxation from Electronically Photoexcited States in Solution Studied by the Acoustic Peak Delay Method: Hydrogen Bonding Effect to Betaine-30. *Chem. Phys. Lett.* **1999**, *305*, 189-196.

165. Miyata, R.; Kimura, Y.; Terazima, M., Intermolecular Energy Transfer from the Photo-Excited Molecule to Solvent: Malachite Green. *Chem. Phys. Lett.* **2002**, *365*, 406-412.

166. Stratt, R. M.; Maroncelli, M., Nonreactive Dynamics in Solution: The Emerging Molecular View of Solvation Dynamics and Vibrational Relaxation. *J. Phys. Chem.* **1996**, *100*, 12981-12996.

167. Horng, M. L.; Gardecki, J. A.; Papazyan, A.; Maroncelli, M., Subpicosecond Measurements of Polar Solvation Dynamics: Coumarin 153 Revisited. *J. Phys. Chem.* **1995**, *99*, 17311-17337.

168. Rosspeintner, A.; Lang, B.; Vauthey, E., Ultrafast Photochemistry in Liquids. In *Annual Review of Physical Chemistry, Vol 64*, Johnson, M. A.; Martinez, T. J., Eds. 2013; Vol. 64, pp 247-271.

169. Duxbury, D. F., The Photochemistry and Photophysics of Triphenylmethane Dyes in Solid and Liquid-Media. *Chem. Rev.* **1993**, *93*, 381-433.

170. Litvinenko, K. L.; Webber, N. M.; Meech, S. R., Internal Conversion in the Chromophore of the Green Fluorescent Protein: Temperature Dependence and Isoviscosity Analysis. *J. Phys. Chem. A* **2003**, *107*, 2616-2623.

171. Imamoto, Y.; Kuroda, T.; Kataoka, M.; Shevyakov, S.; Krishnamoorthy, G.; Liu, R. S. H., Photoisomerization by Hula Twist: 2,2 '-Dimethylstilbene and a Ring-Fused Analogue. *Angew. Chem. Int. Ed.* **2003**, *42*, 3630-3633.

172. Vengris, M.; van Stokkum, I. H. M.; He, X.; Bell, A. F.; Tonge, P. J.; van Grondelle, R.; Larsen, D. S., Ultrafast Excited and Ground-State Dynamics of the Green Fluorescent Protein Chromophore in Solution. *J. Phys. Chem. A* **2004**, *108*, 4587-4598.

173. Liu, R. S. H.; Asato, A. E., Photochemistry of Polyenes.22. The Primary Process of Vision and the Structure of Bathorhodopsin: A Mechanism for Photoisomerization of Polyenes. *Proc. Natl. Acad. Sci. USA* **1985**, *82*, 259-263.

174. Sharafy, S.; Muszkat, K. A., Viscosity Dependence of Fluorescence Quantum Yields. *J. Am. Chem. Soc.* **1971**, *93*, 4119-4125.

175. Murphy, S.; Sauerwein, B.; Drickamer, H. G.; Schuster, G. B., Spectroscopy of Cyanine Dyes in Fluid Solution at Atmospheric and High Pressure: The Effect of Viscosity on Nonradiative Processes. *J. Phys. Chem.* **1994**, *98*, 13476-480.

176. Jehlicka, J.; Edwards, H. G. M.; Nemec, I.; Oren, A., Raman Spectroscopic Study of the Chromobacterium Violaceum Pigment Violacein Using Multiwavelength Excitation and DFT Calculations. *Spectrochimica Acta Part a-Molecular and Biomolecular Spectroscopy* **2015**, *151*, 459-467.

177. Garcia-Pichel, F.; Wingard, C. E.; Castenholz, R. W., Evidence Regarding the UV Sunscreen Role of A Mycosporine-Like Compound in the Cyanobacterium Gleoecapsa sp. *Applied and Environmental Microbiology* **1993**, *59*, 170-176.

178. Staleva, H.; Zeeshan, M.; Chabera, P.; Partali, V.; Sliwka, H.-R.; Polivka, T., Ultrafast Dynamics of Long Homologues of Carotenoid Zeaxanthin. *J. Phys. Chem. A* **2015**, *119*, 11304-11312.

179. Ilagan, R. P.; Christensen, R. L.; Chapp, T. W.; Gibson, G. N.; Pascher, T.; Polivka, T.; Frank, H. A., Femtosecond Time-Resolved Absorption Spectroscopy of Astaxanthin in Solution and in Alpha-Crustacyanin. *J. Phys. Chem. A* **2005**, *109*, 3120-3127.

180. Asker, D.; Awad, T. S.; Beppu, T.; Ueda, K., Isolation, Characterization, and Diversity of Novel Radiotolerant Carotenoid-Producing Bacteria. *Methods in molecular biology (Clifton, N.J.)* **2012**, *892*, 21-60.

181. Clauditz, A.; Resch, A.; Wieland, K.-P.; Peschel, A.; Goetz, F., Staphyloxanthin Plays a Role in the Fitness of Staphylococcus Aureus and its Ability to Cope with Oxidative Stress. *Infection and Immunity* **2006**, *74*, 4950-4953.

182. Genereux, J. C.; Barton, J. K., Mechanisms for DNA Charge Transport. *Chem. Rev.* **2010**, *110*, 1642-1662.

183. Kawai, K.; Majima, T., Hole Transfer Kinetics of DNA. *Acc. Chem. Res.* **2013**, *46*, 2616-2625.

184. Steckl, A. J., DNA - A New Material for Photonics? *Nature Photonics* **2007**, *1*, 3-5.

185. Pinheiro, A. V.; Han, D.; Shih, W. M.; Yan, H., Challenges and Opportunities for Structural DNA Nanotechnology. *Nature Nanotechnology* **2011**, *6*, 763-772.

186. Lee, C.-H.; Ezra, F. S.; Kondo, N. S.; Sarma, R. H.; Danyluk, S. S., Conformational Properties of Dinucleoside Monophosphates in Solution: Dipurines and Dipyrimidines. *Biochemistry* **1976**, *15*, 3627-39.